PROCESSING OF SiC WHISKER REINFORCED REACTION BONDED SILICON NITRIDE COMPOSITES

Laurence Gavoret

Department of Mining and Metallurgical Engineering
McGill University
Montreal, Canada.

October 1992

A thesis submitted to the Faculty of
Graduate Studies and Research
in partial fulfilment of the
requirements for the degree of
Master of Engineering

Processing of RBSN composites

ABSTRACT

Due to the problems associated with conventional sintering of whisker reinforced Si_3N_4 composites such as whisker bridging, reaction bonding is being studied as an alternative way to produce such composites. The major advantages of Reaction-Bonded Silicon Nitride (RBSN) over other densification methods such as hot-pressing or sintering lies in the ability to form complex final shapes without diamond machining. Negligible shrinkage of the compacts occurs during the nitridation, resulting in near-net shape RBSN components.

In the present study, the production of green compacts with homogeneous reinforcement distribution was investigated; parameters include viscosity measurements, pH adjustment and consolidation methods (isostatic pressing and slip casting). The nitridation of the Si/SiCw compacts was monitored by a microbalance system which recorded the weight gain during the reaction. Kinetics of nitridation and a study of complete nitridation were carried out . The nitridation process is very sensitive to a change in temperature-time schedule and green density whereas whisker content does not significantly influence the nitridation.

A low modulus of rupture value was measured (~190MPa) due to low nitrided densities (~75%) and the presence of low density regions associated with whisker bundles.

RESUME

L'élaboration du composite Nitrure de Silicium (Si_3N_4) renforcé par des whiskers en Carbure de Silicium (SiC) a été réalisée par "Reaction Bonding". Ce procédé permet d'éviter certains problèmes liés au frittage des composites à whiskers, tels que, par exemple, la formation de ponts de whiskers. De plus, un des importants avantages du "Reaction Bonding" par rapport aux autres procédés de densification comme le frittage ou le pressage à chaud est qu'il conduit à la fabrication sans usinage de pièces composites complexes. En effet, la pièce composite ne change pas de dimension pendant la nitruration, ce qui rend possible la production directe de pièces à contours nets.

Différentes méthodes de compaction, telles que le pressage isostatique et le "slip-casting" ont été utilisées pour la fabrication des compacts bruts Si/SiCw. Une distribution homogène des whiskers a été obtenue grâce à des mesures systématiques de viscosité et un ajustement du pH des mixtures avant "slip-casting". La nitruration de ces compacts a été contrôlée par un système de four couplé à une microbalance, permettant l'enregistrement continu du changement de poids de l'échantillon pendant la réaction. Il a ainsi éte possible d'étudier la cinétique de nitruration et la nitruration complète de différents compacts contenant 0 à 30% de whiskers. Le procédé de nitruration s'est avéré très sensible à tout changement de programme Température-Temps et de densité des compacts bruts. Par contre, les whiskers ne semblent pas influencer de manière significative le comportement du Silicium à la nitruration. Le composite élaboré possède un faible module de rupture (~109MPa), ceci étant probablement dû à son importante porosité (25% densité théorique) mais aussi à de petites régions à faible densité, associées à la présence de paquets de whiskers agglutinés.

ACKNOWLEDGEMENTS

I would like to express my sincere gratitude and appreciation to Professor M.D. Pugh for his inspiring supervision, and his continued interest and encouragement throughout the course of this work.

I also wish to especially thank Professor R.A.L. Drew for his support.

Special thanks go to A. Luganov and A. De Ciccio for their significant help in the fulfilment of experiments and analysis.

I would like to thank D. Muscat, A. Hadian and C. Edovas for their assistance and their helpful suggestions as well as M. Entezarian and Y. Baik.

I would also like to thank all of the members of the Ceramic research group for their helpfulness and team-like disposition. My fellow office associates, and particularly E. Benguerel and Th. Lebeau, are also acknowledged for their invaluable help in alleviating the tensions of research work.

TABLE OF CONTENTS

LIST OF FIGURES

LIST OF TABLES

LIST OF SYMBOLS

k_{II}: Linear rate constant of section II of the thermogravimetric curve

t_0: Starting time of a run

t_I: Time at the end of section I

t_{II}: Time at the end of section II

t_{III}: Time at the end of section III

Δt_I: Duration of section I

Δt_{III}: Duration of section III

1 INTRODUCTION

In the last few decades, ceramists have been increasingly asked to develop new materials with high reliability and performances, making necessary the use of new processing technologies. Understanding the mechanisms which control the processing of a ceramic as well as its behavior under stress is of crucial importance to better monitor and optimize the properties of finished components. A millennial technique, as ceramic manufacturing was yesterday, today becomes a leading science which influences the development of the materials of the future.

Technical or advanced ceramics, as opposed to ceramics for household or traditional uses, play a more and more important role in the technology of today and tomorrow, because of their electrical, magnetic, optical superconducting, thermal and thermo-mechanical properties.

Amongst the different kinds of ceramics, the thermo-mechanical ceramics are drawing growing attention because of their potential use at temperatures higher than those at which common metals, alloys and superalloys can be used (Table 1.1)(1,2,3).

	Maximum temperature of use (°C)
Silicon carbide	1400
Silicon nitride	1400
Zirconia-Alumina	1200
Zirconia-Mullite	1000
Aluminium Titanate	800
Nickel based superalloy HA 8077	1150
Nickel based superalloy IN 100	1050
Cobalt based superalloy MAR M609	1050

Table 1.1: Maximum use temperature of some ceramics and superalloys (1)

In Figure 1.1, a general outline of the possible fields of applications of several materials versus temperature is presented. As shown in this Figure, applications at temperatures higher than 1400ºC demand the use of materials other than metals: ie. composites with a ceramic matrix(4).

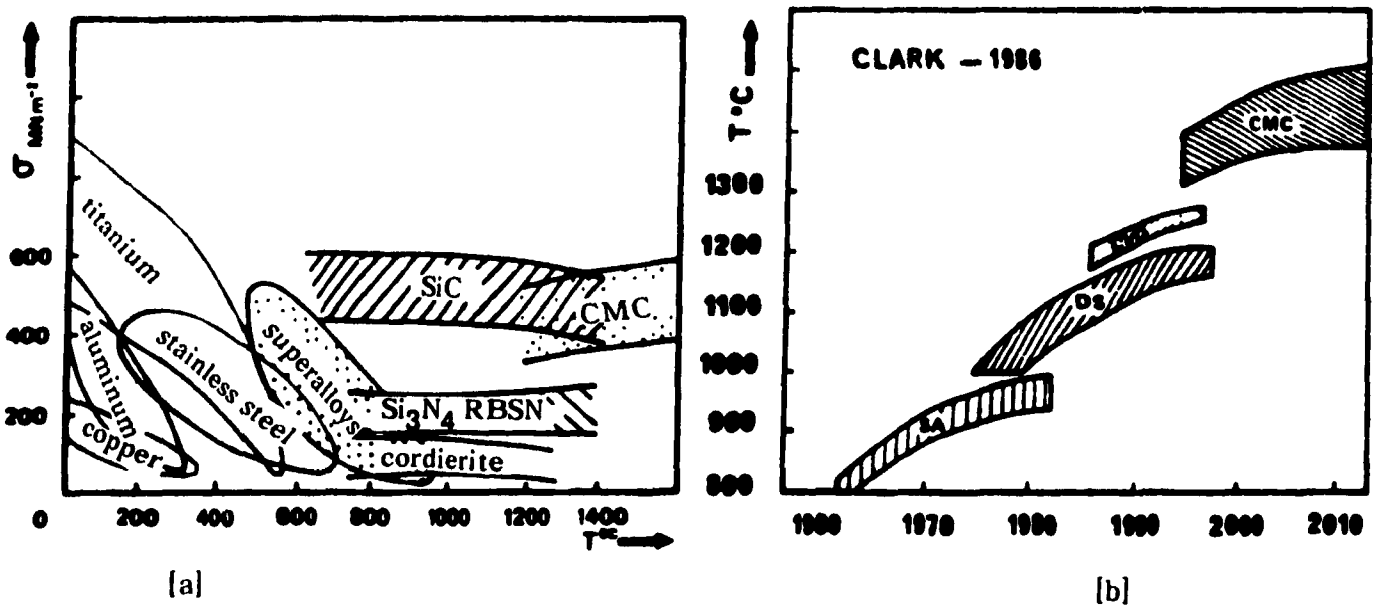

[a] [b]

Fig 1.1: [a] Mechanical properties at high temperature and
[b] Evolution of thermo-mechanical materials since 1960 (4)
(SA: Superalloys, DS: materials fabricated by direct solidification, CVD: materials with thermal coatings, CMC: Ceramic Matrix Composites)

This great interest in thermo-mechanical ceramics is probably due to the oil crisis of the 70's: improving the efficiency of thermal engines by increasing the working temperature and by reducing as much as possible the thermal losses in the cooling circuits became imperative. For example, with the gas turbine engine of a car fitted with a thermal exchanger, 27% of the fuel consumption can be saved if the

temperature at the gas entrance in the turbine is about 1400ºC, compared to the standard temperature of 600ºC.

However, it is still difficult to know exactly the real and effective use of ceramics even in the 1992 car industry. It is likely, however that effective developments will still require ten more years for application in common cars and that ceramic components will be only used for a few parts in present cars. Nissan, for example, has developed a sports car named "Fairlady", with a 2 litre engine fitted with a silicon nitride turbocharger. This turbocharger maintains the off-gases of the engine at nearly 900ºC and its density is 3.2 instead of 8.2 g/cm^3 as for a metallic turbocharger; consequently, this leads to lower centrifugal forces in rotating components and the lower inertia permits higher accelerations. In addition, the Si_3N_4 component shows better corrosion and erosion resistance.

In consequence, materials which can withstand temperatures higher than the currently used superalloys are necessary for more powerful and efficient engines. Some ceramics can indeed, withstand high temperatures, but they are known to be brittle, (non-ductile), vulnerable to very small defects and have non-homogeneous characteristics. However, the brittle character of ceramics should not necessarily be considered as damning: glass, for instance, has taken a very important role in our environment thereby proving that it is possible for human beings to live with brittle materials and even to use them in cars. The brittle character of ceramics has to be taken into account, especially in the design of components. The required strength, and assembly route have to be envisioned and obviously, it is not conceivable to substitute a metallic component by an identically shaped ceramic part.

Examples of some advanced ceramics are presented in Table 1.2. Evident advantages of ceramics are that they are composed of elements having low cost with large available quantities of raw material. In addition, they are usually lighter than metals or superalloys.. The weight savings for a gas turbine engine of 130 HP

can be up to 50%: 300 kg for a turbine engine made with classical material and 150 kg for a turbine engine made with ceramics(5). Other advantages offered by engineering ceramics include improved oxidation and corrosion resistance, high hardness and good wear resistance(6).

	Maximum temperature of use (ºC)
Silicon carbide	1400
Silicon nitride	1400
Zirconia-Alumina	1200
Zirconia-Mullite	1000
Aluminium Titanate	800
Nickel based superalloy HA 8077	1150
Nickel based superalloy IN 100	1050
Cobalt based superalloy MAR M609	1050

Table 1.2: Different types of ceramics (6)

Nevertheless, in order to be used, a thermo-mechanical ceramic has to meet several criteria, which will depend on the working conditions in place. Specific thermal properties to resist thermal shock, sufficient mechanical resistance at room temperature as well as at high temperature, the highest possible toughness, stable mechanical properties which do not change with time and environment, and a good repeatability of the characteristics of the compound are properties on which these

criteria are based.

The material under consideration in the present study is silicon nitride (Si_3N_4). Different forms of silicon nitride can be manufactured depending on their processing route. Thus, dense Si_3N_4 made by Hot-pressing, sintering or Hot Isostatic Pressing is among the leading contenders in advanced heat engine applications. However, "high-tech" equipment is usually necessary to produce dense and strong ceramics like these. The high cost of such equipment and the difficulty of diamond machining components with complex final shapes are two major disadvantages which limit the use of such ceramics.

Another type of silicon nitride ceramic can be produced through the reaction-forming process. In this method, the ceramics increase in mass during firing by reaction with either a gas or a liquid phase. These bodies differ from sintered and pressure-densified ceramics, in that negligible shrinkage occurs during densification

Reaction Bonded Silicon Nitride (RBSN) is made by reaction of compacted silicon powder with nitrogen gas to form solid silicon nitride. The advantages of reaction bonding over hot-pressing and sintering methods lie in the ability to form complex final shapes to close dimensional shrinkages without diamond machining, and the low cost of raw materials and manufacturing equipment. However, due to the way in which RBSN is formed, it contains ~ 20% residual porosity, resulting in limited strength and toughness. Nonetheless, enhanced mechanical reliability has been achieved in the recent development of a new class of structural materials based on whisker and fiber reinforcement called "Ceramic-Matrix Composites" (CMC's). Large gains in fracture strength and toughness are possible in these types of materials. Therefore, by adding some whiskers in the starting silicon powder, silicon nitride composites can be produced by reaction bonding.

The objective of this work was to combine the two techniques of reaction

bonding and whisker reinforcement to produce RBSN composites reinforced by silicon carbide (SiC) whiskers.

The following chapter reviews the background science of silicon nitride including its chemical and physical properties and its fabrication and engineering properties. Then, the reaction bonding process is introduced and the thermodynamics and kinetics of nitridation are discussed. Finally, theoretical mechanisms of whisker reinforcement and the influence of different parameters on the processing route of RBSN composites are presented.

Based on the literature review, a number of objectives were chosen and these will be presented in Chapter 3.

The results of this research, which is divided into two main sections; kinetics of nitridation and effects of selected parameters on complete nitridation, are then presented and discussed in Chapter 5.

2 LITERATURE SURVEY

The potential of advanced ceramics as components in heat engines and thermomechanical applications has been widely reported over the past 25 years (1,2) and significant progress has been made in their development.

The last few years has seen the development of a new class of structural materials based on fibre and whisker reinforcement.

Tremendous efforts have been made to develop this new science and, as a result, a large quantity of data has been generated and an understanding of the fundamentals regarding processing has been established. The properties of these new materials, factors that determine their mechanical properties and ways of improving them have been the topic of numerous publications.

The aim of this chapter is to review the work carried out on this subject to date. An overview of the basic concepts of Silicon Nitride ceramics is briefly presented before moving onto the preparation and properties of Reaction Bonded Silicon Nitride. Finally, whisker-reinforcement of this ceramic and the processing technology used will be presented as will the resulting microstructural mechanical properties of the ceramic composites thus formed.

2.1 SILICON NITRIDE

Silicon nitride is not a naturally occurring compound. It is synthetically formed by the combination of silicon and nitrogen. Silicon nitride was first produced by heating silicon tetrachloride in an ammonia atmosphere at high temperature (3). Subsequent work went on to form silicon nitride by the direct nitridation of silicon and by carbothermal reduction of silica (4,5,6).

In the early 1950's, the potential of silicon nitride as a useful ceramic material for engineering applications was realized and since this time, extensive research has been carried out on the characterization and processing of this nitride ceramic.

The aim of this section is to outline the more important aspects of the compound's crystal structure and properties. The different fabrication processes of silicon nitride ceramics will then be presented and compared. The major advantages of the reaction bonding process will be pointed out.

2.1.1 CRYSTAL STRUCTURE OF SILICON NITRIDE

Silicon nitride occurs in two crystalline phases designated α-Si_3N_4 and β-Si_3N_4, having density values 3.185 and 3.196 g/cm^3 respectively (7). Both phases are chemically identical and have hexagonal unit cells, but the c-dimension of the α-Si_3N_4 unit cell is twice that of β-Si_3N_4 (8). Both structures comprise of Si_3N_4 tetrahedra in which the four N atoms are arranged tetrahedrally around a central Si atom. The tetrahedra are joined in a three-dimensional network by sharing corners as shown in Fig 2.1.

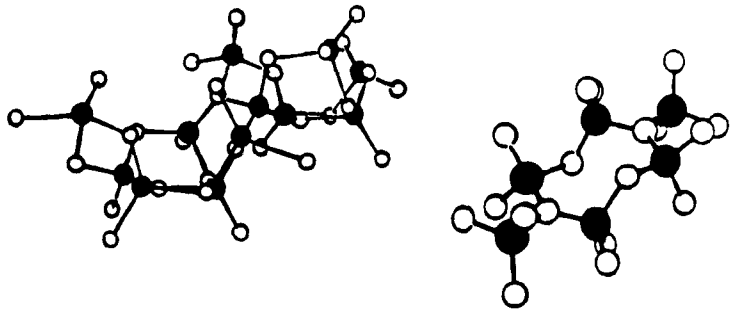

Fig 2.1: Structural formulae (7) for
(a) α-Si_3N_4 (b) β-Si_3N_4

The β structure consists of Si_6N_8 layers, alternating in the sequence ABAB, whereas α consists of $Si_{12}N_6$ planes in a sequence ABCD, where CD are mirror inverted layers of AB.

The α structure is more strained than the β-Si_3N_4 structure which probably implies that it forms under more constrained or sterically hindered conditions. Both phases may be synthesized over a wide range of temperatures. However, the α phase becomes increasingly unstable at higher temperatures. It has been argued that the α- and β- are respectively low and high temperature polymorphs of silicon nitride (9), with α-Si_3N_4 being formed on nitriding silicon at temperatures between 1200-1400ºC and the β-phase at temperatures above the melting point of silicon (1410ºC). This may be in conflict with free energy and density arguments. (High temperature phases are usually less dense).

It was also proposed (10) that the α-phase is further stabilized by the presence of oxygen in the structure, to form an oxynitride having a compositional range between $Si_{11.4}N_{15}O_{0.3}$ and $Si_{12}N_{15}O_{0.5}$. This was suggested due to the observed variation in unit cell dimensions and other factors (11). However, this hypothesis was shown to be incorrect (12,13) since α and β powders have been produced which do not contain any oxygen.

The mechanism by which the different crystallographic forms are produced is not fully understood, but it has been suggested by experimental evidence that high β-phase containing materials are favoured by the presence of liquid phases and that α-Si_3N_4 forms from vapor phase reactions (15). The reactions are slow and easily influenced by many variables (time, environment). The reaction forming α and β Si_3N_4 are, at the very least, in kinetic competition. Possible reaction routes and their associated thermodynamics and implied kinetics will be discussed later in this review.

The characteristic morphology of α-Si_3N_4 is dependent on the growth conditions and ranges from equiaxed crystals to very fine whiskers, whereas, β-Si_3N_4 consists of well-formed acicular crystals grown in a liquid (16).

2.1.2 PROPERTIES

According to Pauling (17), the bonding in Si_3N_4 can be estimated to be 70% covalent. Due to the rigid nature and directionality of the covalent bond, Si_3N_4 is a hard, strong material with a high decomposition temperature, high strength even at high temperatures and with a low thermal expansion coefficient. It is brittle like most ceramics; low in density and a good conductor of heat compared to other refractory ceramics. This combination of thermomechanical properties makes it a leading contender for high temperature applications.

Pure Si_3N_4 should be transparent but due to impurities such as Fe, Al and Ca, the commercial material appears grey.

Si_3N_4 is inert, being resistant to most corrosive environments except for hydrofluoric acid and molten alkali salts.

PROPERTIES	DENSE Si_3N_4	RBSN
CRYSTAL STRUCTURE	α: c/a=0.70 β: c/a =0.37	
DECOMPOSITION TEMPERATURE (°C)	1920	
THEORETICAL DENSITY (g/cm^3)	α = 3.168-3.188 β = 3.19-3.202	
RELATIVE DENSITY	90-100% th.	70-88% th.
THERMAL EXP. COEFF. ($/10^6$ °C)	2.9-3.6	
THERMAL COND. (W/mK)	15-56	4-30
SPECIFIC HEAT (J/kg °C)	700	
MICROHARDNESS (VICKERS, GPa)	16-22	
YOUNG'S MOD.(GPa)	300-330	120-220
FLEXURAL STRENGTH (MPa)	400-950	150-350
FRACTURE TOUGHNESS ($MPa.m^{1/2}$)	3.4-8.2	1.5-2.8

Table 2.1: Physical properties of RBSN and dense Si_3N_4

As shown in table 2.1, the properties of Si_3N_4 depend strongly on the extent of densification of the material. The following section reviews the different fabrication processes of Si_3N_4.

2.1.3 PROCESSING OF Si_3N_4 CERAMICS

During the past ten years, technological investigations have mainly concentrated on two types of Si_3N_4: dense Si_3N_4, which can be produced by hot-pressing, sintering or hot-isostatic pressing, and porous Si_3N_4 produced by reaction bonding of silicon powder compacts. The first type involves the sintering of a Si_3N_4 powder compact using pressure, be it external (hot-pressing), by the presence of a liquid phase, or both. The second is the direct nitridation of a silicon powder compact, to form Reaction Bonded Silicon Nitride (RBSN).

2.1.3.1 Sintering

Two methods have been developed to sinter Si_3N_4: pressing, which includes Hot-Pressing and Hot-Isostatic Pressing (HIPing) and sintering, which includes pressureless sintering and gas pressure sintering.

PRESSING: The silicon nitride powder is usually mixed with a suitable sintering aid, for example MgO, and pressed at high temperature (1500-1800ºC). The simultaneous application of high pressure and temperature results in densification by liquid phase sintering (18,19,20).

Fully dense Si_3N_4 with good mechanical properties may be produced using this technique, however the major disadvantage is the high cost of equipment and the fact that only simple symmetrical shapes may be produced by hot-pressing; complex shapes require extensive post-pressing diamond machining.

SINTERING: In the pressureless sintering method, Si_3N_4 powder compacts containing liquid-forming additives (MgO, Y_2O_3) are densified at high temperature

(1800ºC) under a nitrogen atmosphere. The capillary pressure created by the presence of the liquid phase is used as the driving force for fast diffusion (21,22). In the gas pressure sintering method, the partial pressure of nitrogen is increased above atmospheric, resulting in reduced decomposition and higher densities.

Furnace design is much simpler and cheaper than in that requiring external pressure. However, in pressureless sintering, the starting powders must be ultra-fine to provide the thermodynamic driving force for densification and a close control of the partial pressure of the reactants in the sintering atmosphere is necessary to avoid dissociation of Si_3N_4 and loss of sintering additives.

2.1.3.2 Reaction Bonding

The starting material is a silicon powder compact which can be machined into complex shapes. Nitridation occurs at temperatures between 1250-1450ºC (15,23,24). The result is a porous Si_3N_4 matrix (~20% porosity), however, in contrast to hot pressed silicon nitride, complex RBSN components can be readily manufactured to close dimensional tolerances due to negligible shrinkage during nitridation. In addition, the starting material for reaction bonding is silicon powder which is readily available and relatively cheap in comparison to the ultrafine silicon nitride powders required for hot-pressing and sintering. In addition, since no liquid-phase forming sintering aids are used in this method, the RBSN has a very low creep rate due to the absence of glassy, grain boundary phases.

From this, it is clear that although the residual porosity and lengthy reaction times are disadvantages, the reaction bonding process does have some advantages when compared to sintering and hot pressing routes.

The main purpose of the present work is to investigate the feasibility of reinforcing the porous RBSN with SiC whiskers. This entails an analysis of the effect of whisker additions on the nitridation process and a subsequent optimization of the reaction kinetics. The formation mechanism, the kinetics of nitridation and the influence of different parameters on the reaction bonding process are reviewed in the following section.

2.2 RBSN

The reaction between silicon and nitrogen has been extensively studied and numerous reviews have summarized and refined a large body of information (25).

The aim of this section is to explain the mechanism of formation of RBSN based on the literature. The influence of different parameters such as powder properties, processing conditions and densification is considered in some detail.

2.2.1 THERMOCHEMISTRY

Silicon nitride can be formed from its elements according to the following equations:

$$3Si(s) + 2N_2(g) = Si_3N_4(s)$$
$$\Delta G = -723 + 0.315T \text{ kJmol}^{-1}$$
$$3Si(l) + 2N_2(g) = Si_3N_4(s)$$
$$\Delta G = -874 + 0.405T \text{ kJmol}^{-1}$$
$$3Si(g) + 2N_2(g) = Si_3N_4(s)$$
$$\Delta G = -2080 + 0.757T \text{ kJmol}^{-1}$$

The thermodynamic relationships are derived from the basic data generated by Phelke and Elliott(26).

The reactions are strongly exothermic and careful control is required during nitridation to prevent the melting of silicon. From Fig 2.2, showing the equilibrium nitrogen pressure as a function of temperature, it can be seen that the dissociation temperature, i.e the temperature at which the equilibrium nitrogen pressure is 1 atm, is about 1900ºC (27). This graph presents the minimum nitrogen pressure which must be maintained around the nitride at any temperature, to prevent dissociation.

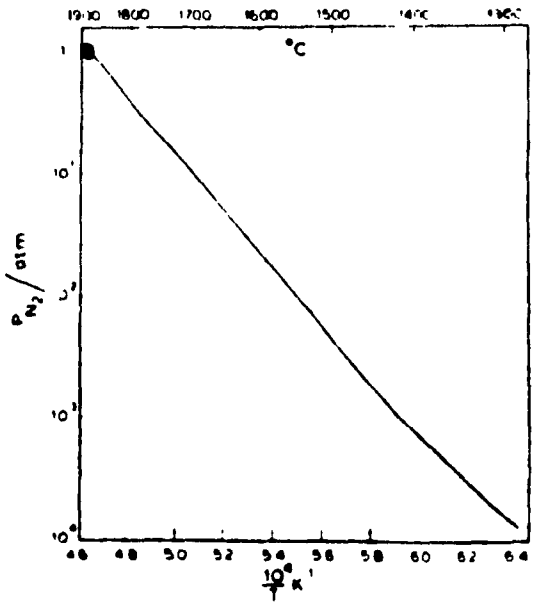

Fig 2.2: Equilibrium vapor pressure of N_2 over Si_3N_4 (27)

2.2.2 FORMATION OF RBSN FROM A GAS OR A LIQUID PHASE

RBSN is formed by heating a silicon powder compact in a nitrogen atmosphere between 1250 and 1450ºC where the three reactions presented above can occur, depending on the temperature.

NO SOLID STATE REACTION

For several reasons, it has generally been viewed that a true "solid state" reaction probably does not take place(25). In reaction bonded silicon nitride, the overall dimensions of the powder compact do not change to any great extent during the reaction even though the volume of solid increases by 22%. This means, therefore, that as the reaction progresses into a particle, Fig 2.3, solid material is not uniformly pushed outward, i.e it only forms in "open" space.

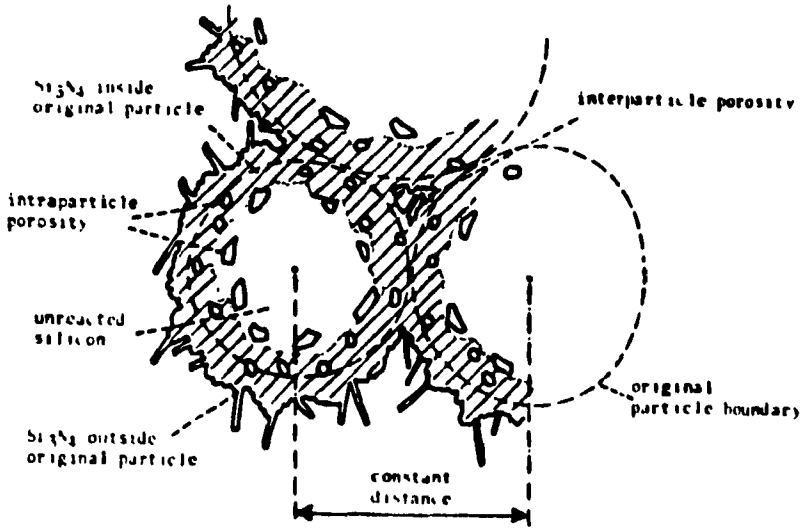

Fig 2.3: Schematic representation of silicon particle reacting with nitrogen (25)

Thus, reaction leading to particle formation must be accompanied by the creation of space. Therefore, silicon must be transported out of the particle, to the surface either, as a liquid or vapor. If porosity proceeds the reaction product, then a surface reaction site is created on which the reaction can occur. After a thin product layer has formed it can thicken only if silicon is transported to the reaction site and therefore the silicon is almost certainly either liquid or gas. A new surface is created and the process repeated.

Further evidence for excluding a "solid state" reaction during the nitridation process is the fact that it is known that nitrogen does not dissolve in solid silicon (28).

2.2.2.1 Formation of α-Si_3N_4

FEASIBILITY OF A GAS STATE REACTION:

Although it is generally agreed that α-Si_3N_4 phase results from the reaction of gases (10,29), a detailed understanding of why a strained structure arises from a gas reaction, where the reactants have the highest degree of freedom, is lacking.

Up to now, the only suggestion (30) is that Si-N complexes have difficulty in adopting the β-Si_3N_4 structure when they are formed in the gaseous state.

Furthermore, N_2 gas is very unreactive and a true gaseous reaction seems unlikely. The standard values of energy and heat of dissociation are:

$$N_2 \rightarrow 2N \qquad \Delta G = 946.76\ kJmol^{-1}$$

$$\Delta H = 912.46\ kJmol^{-1}$$

The reaction between silicon monoxide and nitrogen according to the following equation:

$$3SiO(g)+2N_2(g) \rightarrow Si_3N_4(s)+3/2O_2(g)$$

is also often discussed concerning the formation of the α phase (10,29).
The ΔG° of this reaction is positive under standard conditions but many parameters, such as the presence of hydrogen in the nitriding gas for example, can influence the partial pressure of SiO and O_2 and thus the equilibrium constant of this equation.

THERMODYNAMIC REACTION PATH leading to α-Si_3N_4:

Fig 2.4 illustrates a possible route for α phase formation (25). In the initial stages, silicon may react with molecular nitrogen during the dissociation process to form α-Si_3N_4 nuclei. As the reaction proceeds, silicon will volatilize and react with molecular nitrogen, on a convenient surface.

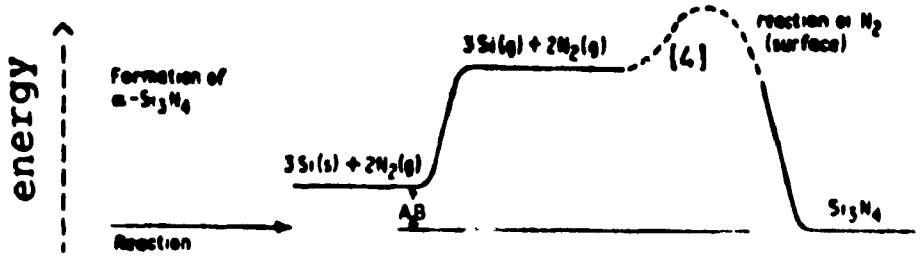

Fig 2.4: Thermodynamic reaction paths leading to α-Si_3N_4 (25)

2.2.2.2 Formation of β-Si_3N_4

FEASIBILITY OF A LIQUID STATE REACTION:

The role that liquid silicon may play in the formation of β-Si_3N_4 has been the subject of some research (31,32). Very often β-Si_3N_4 is seen as angular "spikes" (Fig 2.5) which grow from the edge of a grain towards the interior.

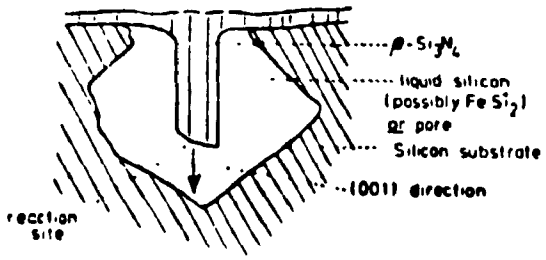

Fig 2.5: β-Si_3N_4 growing as a faceted "spikes" (25)

The reaction site is probably at the end of the spike (32,33),thus extending its length in the fast growing c-direction.

Boyer and Moulson (34) have suggested that nitrogen diffuses through a liquid, often $FeSi_2$.

Jennings and Richman (31), have proposed the possibility that nitrogen diffuses down the large channels which exist in the c-direction of the β-Si_3N_4 structure. Thermodynamic data however, suggest that this process would be slow.

THERMODYNAMIC REACTION PATHS leading to β-Si_3N_4:

Table 2.2 presents some thermodynamic data.

Process	Pre-exponential $cm^2\ sec$	Activation energy ($kJ\ mol^{-1}$) (per mole to form Si_3N_4)	Free energy change change of reaction ($kJ\ mol^{-1}$)
A Reaction with solid silicon (probably a mixture of diffusion of nitrogen in Si_3N_4 and surface reaction in pores)		652 661 418	−193 at 1683 K
B Reaction with liquid silicon (diffusion of nitrogen in liquid)	~ 3.22×10^{-6} (at 1683 K)	460	−192 at 1683 K
C Reaction with gaseous silicon			−805 at 1683 K
D Diffusion of nitrogen in β-Si_3N_4	1×10^{19} 6.8×10^{6}	777 776	
E Diffusion of nitrogen in α-Si_3N_4	1.2×10^{-13}	233	
F Diffusion of silicon in silicon	9×10^{3}	495	
G Dissociation of Si-N bond		435	
H Dissolve Si_3N_4 in silicon ($\alpha \rightarrow \beta$ Si_3N_4 transformation)		690 (1698–1823 K)	
I Sublimation of Si_3N_4			740

Table 2.2: Thermodynamic data (25)

Three thermodynamic possibilities concerning reaction paths which lead to β-Si_3N_4 are proposed by Jennings (25) in Fig 2.6. The reaction progresses from left to right along the three different paths indicated. Energy changes, relative to the starting silicon material, are represented by the height of the curve. The dotted lines indicates that the activation energies are not known.

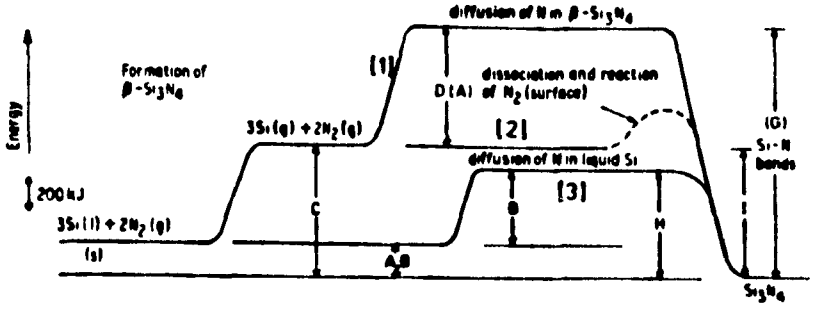

Fig 2.6: Thermodynamic reaction paths leading to β-Si_3N_4 (25)

The reaction will proceed most rapidly along the available path with lowest energy.

Initial formation of Si_3N_4 is represented by curve 2, where nitrogen dissociates and then reacts on the silicon surface.

Diffusion through the β-Si_3N_4, path 1, requires a large amount of energy and growth will be slow.

In the presence of melted silicon or a $FeSi_2$ liquid phase, the reaction follows path 3. This has the lowest activation energy and therefore the fastest kinetics.

2.2.2.3 The reactive nitrogen

Before the nitridation reaction begins, gaseous nitrogen is in contact with the surface of the solid silicon particles. As the temperature is increased, the reaction can begin and either nitrogen gas molecules dissociate to atomic nitrogen and then combine with silicon or silicon moves to combine with a near-by diatomic nitrogen molecule.

Since a solid state reaction is unlikely to occur, the silicon must be mobile when it takes part in the reaction; it is either in the liquid or gas state.

If nitrogen is atomic (active nitrogen) and therefore completely mobile when the reaction occurs, the more symmetrical and naturally bonded β-Si_3N_4 structure may be obtained (30).

Certain environments, including high temperatures and low pressures in N_2 gas, contribute to the formation of atomic nitrogen.

The large diatomic nitrogen molecule must dissociate before it can dissolve and diffuse through liquid silicon. Diffusion requires the formation of atomic nitrogen and, in β-Si_3N_4, the channels in the c-direction are only large enough to transport a nitrogen atom (27).

If molecular nitrogen enters into the reaction process, the higher steric hindrance may result in the more strained α-Si_3N_4 structure being produced (30).

Active atomic nitrogen can easily be removed either by the presence of oxygen impurities or through lower temperatures. In fact, most reaction conditions discourage the formation of large quantities of atomic nitrogen and thus molecular gas reactions appear to predominate in the reaction bonding process (15,35,36).

In general, the formation of each of the two phases is governed by particular and separate reaction mechanisms. The reactions, which are easily influenced by many parameters, are slow. For example, the presence of previously formed silicon nitride is probably very important. The reactions leading to the formation of α- and β-Si_3N_4 are in kinetic competition. Because of the complexity of this system, full details of all of the reactions are still lacking. Nevertheless, a model for the formation of RBSN from a silicon compact has been established and is presented in the following section.

2.2.3 MODEL OF RBSN DEVELOPMENT IN THE SILICON COMPACT

By correlating the developing microstructure with kinetic rate data, a reaction model has been proposed as shown in Fig 2.7 (37,38).

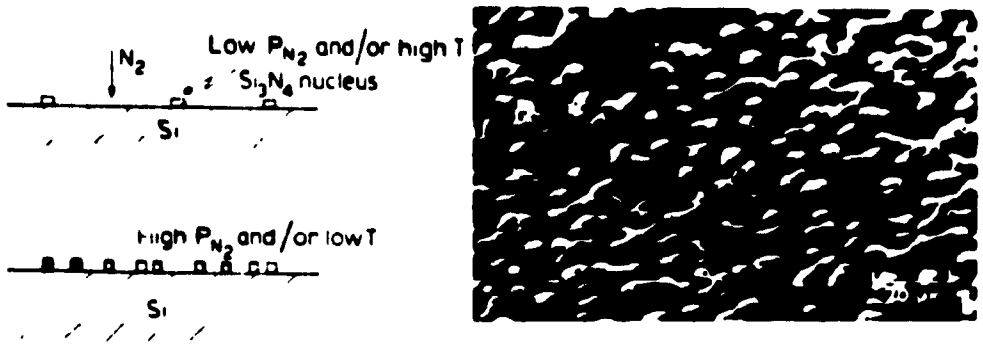

(i) Formation of Si_3N_4 nuclei on Si surface areal density of nuclei increases as p_{N_2} increases and T decreases

(ii) Nuclei grow laterally and vertically Si supplied to growth sites by combination of surface diffusion and evaporation. Rate of arrival of nitrogen to growth site determines reaction rate for $p_{N_2} < 1$ atm, at least.

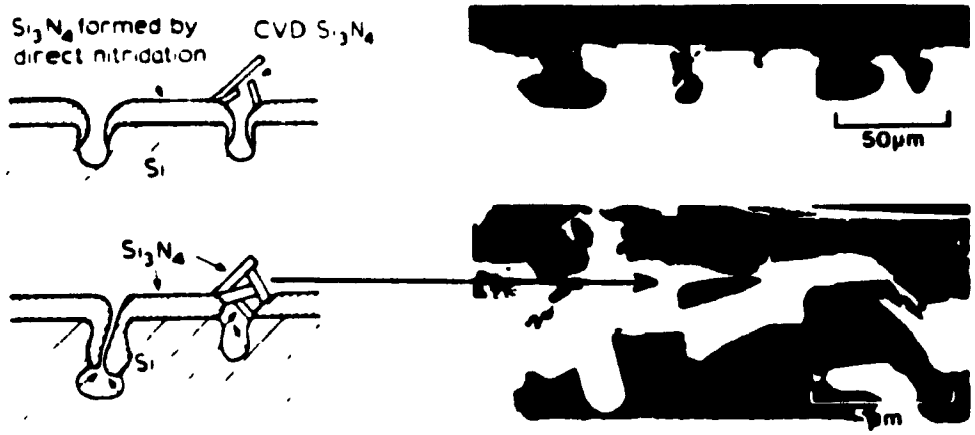

(iii) As free Si surface area decreases, surface diffusion distances increase and so direct nitridation slows Reaction of Si in the vapour state to form a complex which subsequently condenses, continues 'Zero' reaction rate when reactants effectively separated

Fig 2.7: Stages through the course of reaction between Si and N_2 (15)

The first stage involves the formation of Si_3N_4 nuclei on the surface of the silicon particle followed by their growth, thought to occur through the reaction between chemisorbed nitrogen and silicon, the latter arriving at the reaction site by a combination of surface diffusion and an evaporation - condensation process.

2.2.3.1 Initial surface reaction

It is believed that when there is no substantial oxide layer on the surface of the silicon particle, the initial reaction is a nucleation and growth process (37). Silicon nitride nuclei are formed on the surface of the silicon particle through chemisorption. In fact, unreactive nitrogen molecules probably begin to dissociate only once adsorbed on a surface. Small Si_3N_4 crystals form and as the reaction proceeds they gradually cover the entire surface (Fig 2.8).

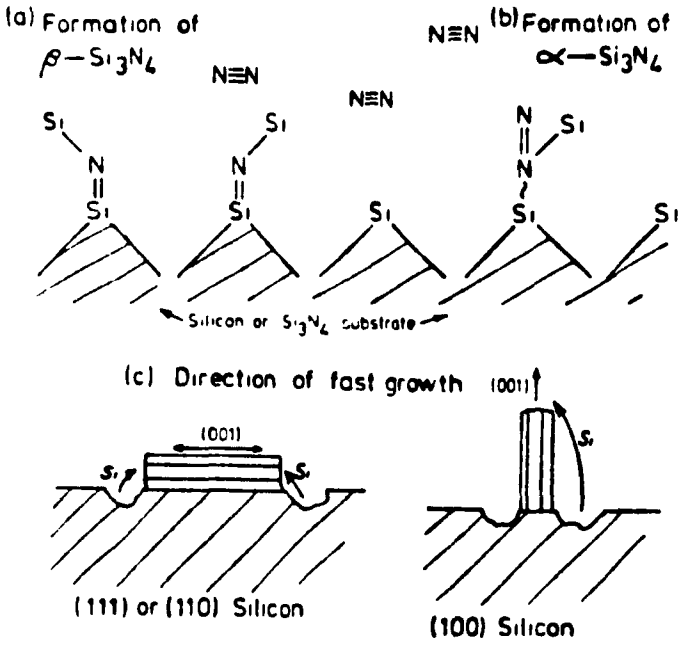

Fig 2.8: Formation of initial Si_3N_4 layer (25)
[a] nuclei of β-Si_3N_4 form as dissociated nitrogen reacts and [b] α-Si_3N_4 form as molecular nitrogen reacts. The orientation of nuclei depends on substrate orientation.
[c] the nuclei grow in the z-direction

X ray evidence has shown that the formation of nuclei of Si_3N_4 is most likely epitaxial (25).

Continued Si_3N_4 formation occurs on the available surfaces. After nucleation, Si_3N_4 particles grow. It is probable that silicon nitride has a very strong tendency to grow in the c-direction, and therefore crystals having high aspect ratios will form (39). Indeed poisoning or inhibition of growth in other directions by impurities such as iron or oxygen, may enhance this effect, a process which may be particularly important during the growth of long α-Si_3N_4 needles (Fig 2.9). In fact, many of these whiskers have a spherical origin, frequently containing impurities such as iron which form lower melting point phases; for example, $FeSi_2$ (1208°C) (31,40).

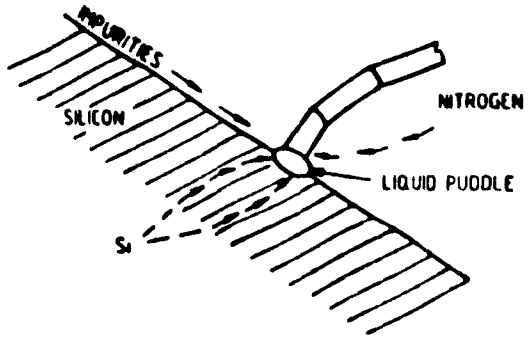

Fig 2.9: Formation of α-needles (31)

Silicon is transported, to the nuclei, through evaporation-condensation or surface diffusion from the vicinity of the nuclei. With increasing growth of the nuclei, a dense silicon nitride layer is formed.

2.2.3.2 Continued reaction

At this point, additional space must be created before the "inner product" can form. Pores are generated in the areas where silicon has evaporated. It seems improbable that the large silicon atom, much larger than nitrogen, can diffuse through Si_3N_4 and in these newly formed pores, the nitrogen which has diffused in, reacts with silicon or silicon monoxide in the gas phase (Fig 2.10).

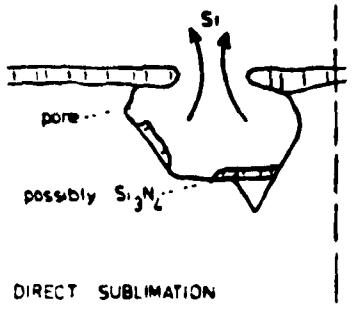

Fig 2.10: Formation of porosity (25)

As the reaction front progresses into the silicon, nitrogen must be transported to the reaction site. Because of the volume expansion occurring during this reaction, the newly formed pores can be completely refilled with nitride. If silicon melts, then space for reaction product is created and the nitrogen can diffuse relatively easily through the large hexagonal tunnels in β crystals (Fig 2.11).

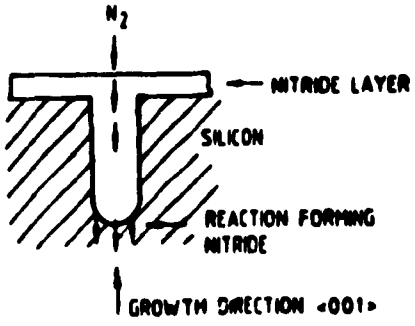

Fig 2.11: Growth of β-spikes into a silicon grain by diffusion of nitrogen down the hexagonal tunnels in Si_3N_4 to the end of the spike where reaction occurs (31).

2.2.3.3 Rate limits

If the reaction occurs outside the boundaries of the silicon, space is not a problem. Silicon must simply be transported to the reaction site which is probably the rate determining step. Pore growth is limited by the rate at which silicon escapes.

If a silicon surface is directly exposed to nitrogen i.e if there is a large opening into a pore, then the rate at which the reaction front advances will be equal to the rate at which porosity develops. This situation may occur when pores form faster than Si_3N_4 layers. If, however, nitrogen must be transported through the nitride layer, (nitrogen has no solubility in solid silicon (28)) the reaction rate will be limited by nitrogen diffusion which is much slower than the chemical reaction.

In the case of a liquid state reaction in molten Si or $FeSi_2$, the solubility of nitrogen in liquid is fairly high (28). Fig 2.12 illustrates some diffusion data from which it can be seen that diffusion of nitrogen in Si_3N_4 is, indeed, a slow step compared to that of nitrogen in the liquid silicon (32,41,42,43).

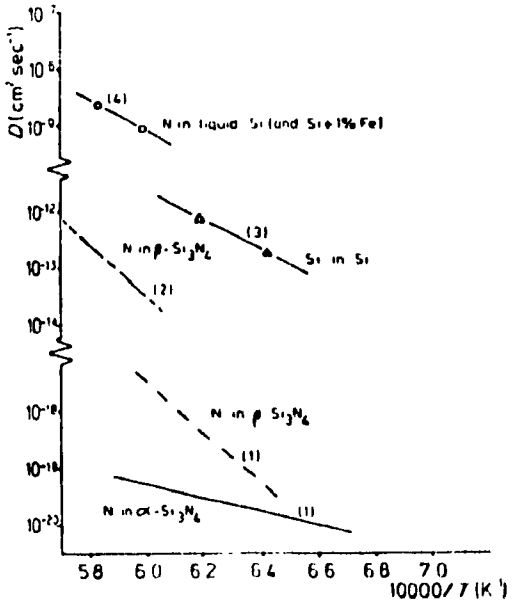

Fig 2.12: Diffusion coefficients relevant to the transport of silicon or nitrogen, curve [1] from (42), [2] from (41), [3] from (43) and [4] from (32)

2.2.4 KINETICS OF NITRIDATION

From the preceding discussion, it can be seen that the overall kinetics of the nitridation of silicon is the sum of separate kinetics for α- and β-Si_3N_4 formation and further, the reaction rate and associated kinetics forming either phase can change with changing conditions, such as temperature.

The complexity of the system leads to numerous theories. The aim of this section is to present different possible laws describing the nitridation kinetics.

A schematic of the general mechanisms is proposed by Sheldon and Haggerty (44). The nitriding mechanism is divided into different steps; an induction period, the nitrogen adsorption on the surface; the nucleation and growth of Si_3N_4 crystals; the formation of the α- and β-Si_3N_4 and the final reaction period where the nitriding rate asymptotically approaches zero.

Fig 2.13 presents typical thermogravimetric analysis curves on which the kinetic study is based. The induction period in samples (B) and (C) is clearly observed.

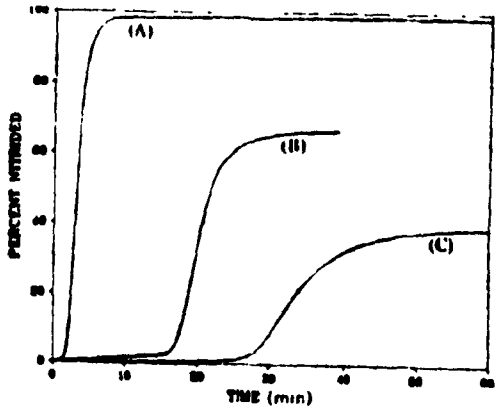

Fig 2.13: Thermogravimetric data, for dry pressed samples at 1250º (44)

(A): as-synthesized Si powder

(B): Si powder dispersed in methanol

(C): Si powder with ~30% of an oxygen monolayer

2.2.4.1 Induction period and adsorption of nitrogen

As shown in Fig 2.13, initially there is an induction period, where only a very small amount of nitridation occurs. The silicon particles are usually covered by a thin silica layer. The induction period corresponds to the disruption of this silicon oxide layer, initiating nitridation The disruption of the silica layer exposes the underlying Si and allows the adsorption of the N_2 and then Si_3N_4 particles nucleate on the Si surface. The induction period corresponds to a nucleation time lag.

The small weight gain during the induction period corresponds to a very slow continuing reaction of nitrogen with the silicon surface, beyond the adsorption of a nitrogen monolayer at lower temperature (15,44).

The kinetics of the initial step can be described by the N_2 gas adsorption on the silicon surface. This adsorption can only be accomplished through the breaking of silicon-silicon bonds and by a rearrangement of the silicon crystal structure to form several atom layers of amorphous silicon nitride Si-N (25,44).

Billy (45) proposed a constant reaction rate of adsorbed species with time and pressure. The duration of this induction period depends strongly on the presence of the silica layer on the surface of the silicon particle.

2.2.4.2 Nucleation and growth

The nucleation step can be described as the formation of crystalline Si_3N_4 from the amorphous Si-N. Surface diffusion and evaporation-condensation processes allow the growth of the nuclei and the formation of the "outer" nitride layer.

Fig 2.14 presents a schematic of reaction kinetics showing three regimes (15). The first stage has a linear relationship with time. The initial part of the curve has been described by the equation:

$$\Delta M/A = k_l t \quad (37)$$

k_l is the linear rate constant which has been shown to be approximately proportional to N_2 pressure, and t is the elapsed time, indicating that the development of the reaction product does not affect the rate at which it is formed, at the beginning of the nitriding process.

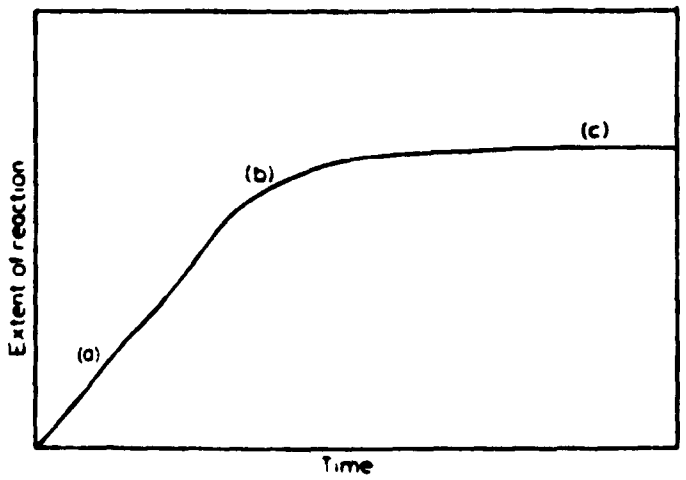

Fig 2.14: Schematic of reaction kinetics showing three regimes (15)

This curve however does not show the induction period typical of most reaction bonding processes.

2.2.4.3 Formation of the α- and β-Si_3N_4

After the initial stages, it has been suggested that the product now acts as a partial barrier to the transport of reactants since the rate decreases as more nitride is formed.

Numerous investigations have attempted to explain this step of the nitriding mechanism (31,46,47) and computer simulation and theoretical models are proposed in the literature.

Jennings and Richman (31) superposed two independent reaction rates, corresponding to the separate kinetics of the formation of α- and β-Si_3N_4 respectively.

α-Si_3N_4 MATTE FORMATION:

The formation of α-matte is related to the diffusion of the reactants through the nitride layer and this is assumed to be the rate-controlling step, with the important parameters being the diffusion coefficient, the particle radius, the reaction time and temperature.

β-Si_3N_4 FORMATION:

The development and growth of the β-spikes into the silicon grains suggests that the product is formed at the inner tip of the spike (i.e the point penetrating into the silicon grains) (Fig 2.11). Nitrogen must therefore adsorb on the opposite end of the spike (i.e at the particle surface) and then diffuse down through the length of the spike through the hexagonal tunnels to reach the silicon-silicon nitride interface. This β-phase will continue to grow as long as there is room for expansion inside the silicon grain i.e where molten silicon exists.

2.2.4.4 The final step

With the closure of all channels in the nitride layer, the rate decreases and the reaction effectively stops. Kinetic data in the decreasing rate region have been described (37) by the self-blocking channel model of Evans (48), who deduced the following asymptotic rate law:

$1-(\Delta M/\Delta M_f) = \exp(-k_a t)$

ΔM: weight gain, ΔM_f: final weight gain

k_a: asymptotic rate constant

The final step often occurs before a complete conversion of all the silicon into silicon nitride. This results from either the lack of any Si-vapor interface due to the difficulty of nitrogen penetration through the thick nitride layer or to the lack of space for expansion.

From the last two sections, the importance of processing parameters such as temperature, starting powder characteristics and gas pressure and nature is evident and the effects of these factors is presented in the next section.

2.2.5 INFLUENCE OF DIFFERENT PARAMETERS

The influence of several variables on the final product has been summarized by Jennings and is presented in Table 2.3 (25). A brief explanation is given for each reaction variable. However only those pertaining to the present study will be discussed below.

2.2.5.1 Influence of silicon starting powder properties

GRAIN SIZE:

As the specific surface area of the starting silicon powder increases (with decreasing grain size), the degree of reaction at low temperatures is increased. This results in significant decrease in the total time of reaction as well as to a decrease in the required final temperature (49).

The various possible courses of the reaction lead to large differences in the microstructure of the final Si_3N_4. For example, with a fine or coarse starting powder, different amounts of α-modification occur. The increase in α-modification with fine powders can be explained by the fact that its higher specific surface is more favorable for silicon evaporation than that of a coarse powder and since the α-phase is obtained through a gaseous reaction, as explained previously, higher α-modification results (50). The higher specific surface area is also important since more silicon is initially available for reaction before the particle surfaces are completely surrounded by Si_3N_4 and the reaction is slowed or stopped and therefore a higher conversion may be obtained.

In addition, for a constant density, the pore distribution in a silicon compact increases with increasing grain size of the silicon starting powder (51). The final micropore size distribution of the RBSN samples after nitridation seems to be dependent on the micropore structure of the initially green compacts (51,52).

For these reasons, the grain size of the silicon starting powder is an important parameter in the reaction bonding process. However, not only do the

Reaction variable		Influence on product	Influence on kinetics and final % reacted	Outline of an explanation
Time		Early reaction produces high α/β-Si_3N_4	Reaction rate decreases with time	Oxygen associated with surface encourages α-Si_3N_4 As reaction proceeds silicon is sealed
Low temperature (< 1350° C)		High α/β-Si_3N_4 Fine structure	Slow reaction rate Small % reacted	Thin nitride layers covers surface
		(Comparing with above)	(Comparing with above)	
Medium temperature (1350–1410° C)		Texture becomes coarser with increasing temperature Pore size increases	Extends linear kinetics Increases rate Increases % reacted	Encourages diffusion and volatization of silicon and formation of porosity
High temperature (> 1410° C, Si melting)		Strongly encourages β-Si_3N_4 formation Coarsens structure	Increases % reacted	Presence of liquid encourages fast diffusion of nitrogen and allows silicon to flow to and from reaction site
Surface area		α/β-Si_3N_4 increases with increasing surface	Reaction rate increases with increasing surface Increases % reacted	Oxygen associated with surface encourages α-Si_3N_4 Surface reaction may involve molecular nitrogen Reaction proceeds further before underlying silicon is sealed
Pressure (medium temperature)		Texture becomes finer with increasing pressure	Early linear rate increases with increasing pressure High pressure reduces % reacted, i.e. linear rate terminates sooner	High pressure increases nucleation rate High pressure encourages product to form rapidly over entire surface
Flowing gas may influence concentration of impurities, i.e. oxygen may be removed	Oxygen	Increases α/β-Si_3N_4	Little change in kinetics Initial dormant period is lengthened	Discourages reduction of initial silica layer Increases SiO but this may not react Discourages the formation of atomic nitrogen
	Hydrogen	Increases α/β-Si_3N_4 Texture becomes finer	Increases kinetics Shortens initial dormant period Increases % reacted	Encourages reduction of silica layer Encourages reaction of SiO Discourages atomic nitrogen
Iron		Increases β-Si_3N_4 at high temperature	Increases % reacted Shortens dormant period	Encourages reduction of silica layer Encourages melting and fast diffusion of nitrogen Encourages atomic nitrogen
Flowing nitrogen atmosphere		Encourages clean porosity	Not clear	Removes silicon Encourages porosity Removes or introduces impurities
Heating rate		Various heating rates appear to alter α/β Si_3N_4	Not clear	Early reaction influences later reaction

Table 2.3: Influence of reaction variables on the product (25)

particle size distribution and the fineness have a strong influence on the resulting Si_3N_4 product, the chemical characteristics of the initial Si-powder are important as well.

IMPURITIES:

Many of the impurities in technical silicon powder, such as iron, aluminum, calcium, carbon or oxygen, can affect the course of nitridation and therefore also effect the microstructural characteristics and development. The influence of iron has been intensively studied (40,53,54) because it is commonly present as a contaminant impurity during processing and also it has somewhat beneficial effects.

Iron may act as an inert catalyst, increasing the diffusion rate of silicon or alternatively it may provide voids, pores, and channels for diffusing atoms via the formation of liquid phase Fe_xSi_y compounds. It may also act as an oxygen depleter by either dissolving surface oxide barriers (SiO_2) or by combining directly to form iron-suboxides (55).

THE REMOVAL OF THE SiO_2 LAYER: Because of the thermodynamic instability of silicon with oxygen, silicon powder particles always contain SiO_2 layers on their surfaces.

For thin SiO_2 layers, SiO_2 can react with silicon to form gaseous SiO and in this fashion, be eliminated during the nitridation process at least to a certain extent. Thicker SiO_2 layers (>20nm) can on the other hand, considerably reduce the overall degree of reaction (50).

Boyer (55) has confirmed that Fe first induces the volatization of the native oxide layer on each particle prior to nitridation.

Atkinson and Moulson (37) suggested that the Fe might assist this process by facilitating the oxidation of Si, through enhanced oxygen ion mobility in the SiO_2. Boyer (54,55) developed this theme by suggesting that Fe devitrified the amorphous silica film, leading to its disruption. The resulting exposure of the underlying Si would then be subject to the equilibrium: $SiO_2 + Si = 2SiO$.

LIQUID PHASE Fe_xSi_y: It is known that metals reduce the melting temperature of silicon and this in turn promotes the formation of a liquid phase such as $FeSi_2$. Microstructural observations have shown that the β-phase grows into $FeSi_2$, known from the Fe-Si phase diagram (56,57) to be liquid at the reaction temperature (T~1400ºC).

In summary, it is believed that the presence of Fe can:

- catalyze the removal of the native SiO_2 oxide film surrounding the silicon particles by converting it to SiO,
- promote the growth of β-Si_3N_4 in liquid $FeSi_2$ (proportionally to the amount of Fe present in the powder).

The various processes are shown schematically in Fig 2.15.

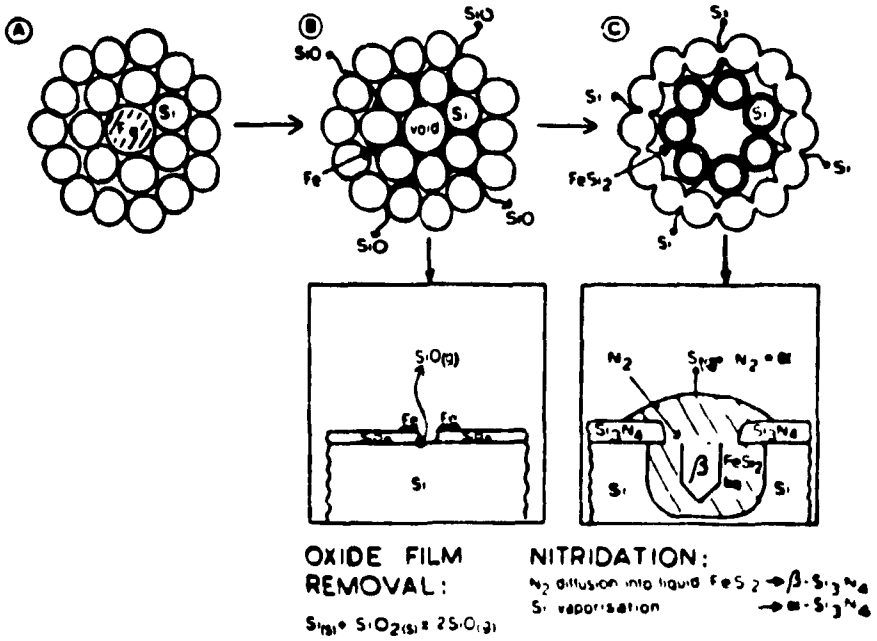

Fig 2.15: Schematic of role of Fe in nitridation behavior (54)

Thus, it is evident that the effect of additions of Fe on the rate of reaction is important (Fig 2.16)

However, large iron particles are detrimental as they can form iron silicides at ~1210ºC which melt out to form large pores.

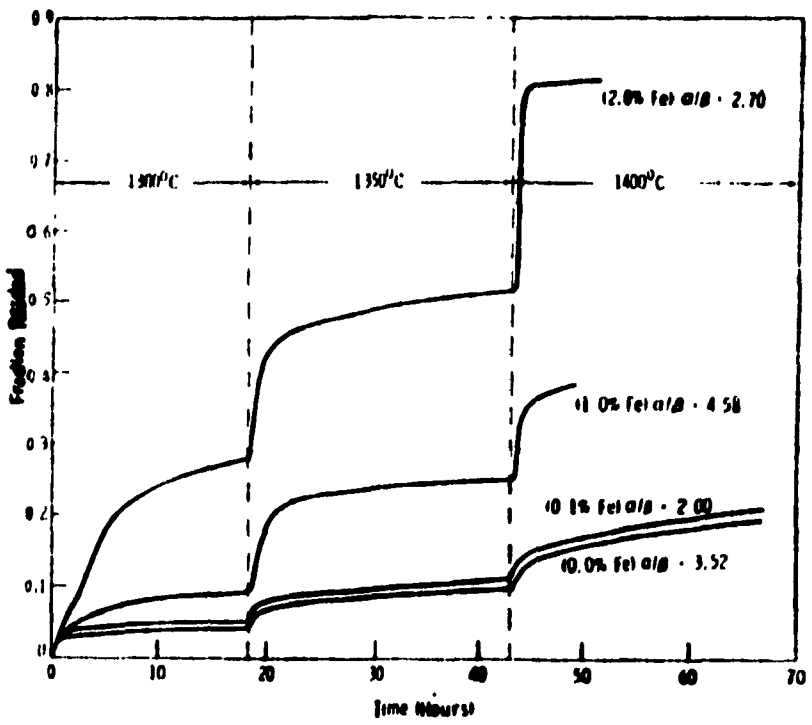

Fig 2.16: Effect of Fe additions on the rate of reaction of Si (99.95%) powder compacts with N_2 (40).

ADDITION OF Si_3N_4:

It has been observed (38) that the addition of some α- Si_3N_4 powder dispersed in the starting silicon powder improves the nitridation reaction between Si and N_2. It is suggested that the amount of pore closure occurring in the compact as the nitridation reaction proceeds is reduced by the addition of silicon nitride powder to the silicon powder. Here the silicon nitride serves as an ideal chemically inert filler.

In addition, it is believed that Si_3N_4 can prevent sintering of Si during nitridation by keeping the Si particles apart as well as by acting as a heat sink during the exothermal nitridation reaction (38).

It is hoped that a similar beneficial effect will be seen by the addition of other "inert" filler materials such as SiC whiskers as is planned in the experimental stage of this work.

2.2.5.2 Influence of processing conditions

TEMPERATURE-TIME PROGRAM:

The reaction between silicon and nitrogen to form silicon nitride is an exothermic process. If the temperature-time program is not carefully monitored, the heat generated during this reaction may lead to overheating which results in an uncontrollable reaction (37,40). Reaction rates which are too rapid may lead to local overheating and therefore to local melting of Si.

In Fig 2.17 the fraction of Si converted versus time for different heating cycles is presented (40). The very rapid weight gain at 1400ºC shown in part (a) results from selfheating of the sample due to the exothermicity of the nitridation reaction. The sample shown in Fig 2.17b was heated to a higher temperature than the one in Fig 2.17a (without melting of unreacted silicon). A comparison of microstructures shows that large voids (black area) arising from melting of unreacted silicon are present in the overheated sample. The effect of the heating rate during nitridation on the microstructure of the final product is thus crucial and must be addressed. A fine grained microstructure, usually associated with good mechanical properties, will be obtained only through careful nitridation with an appropriate temperature-time program (58,59).

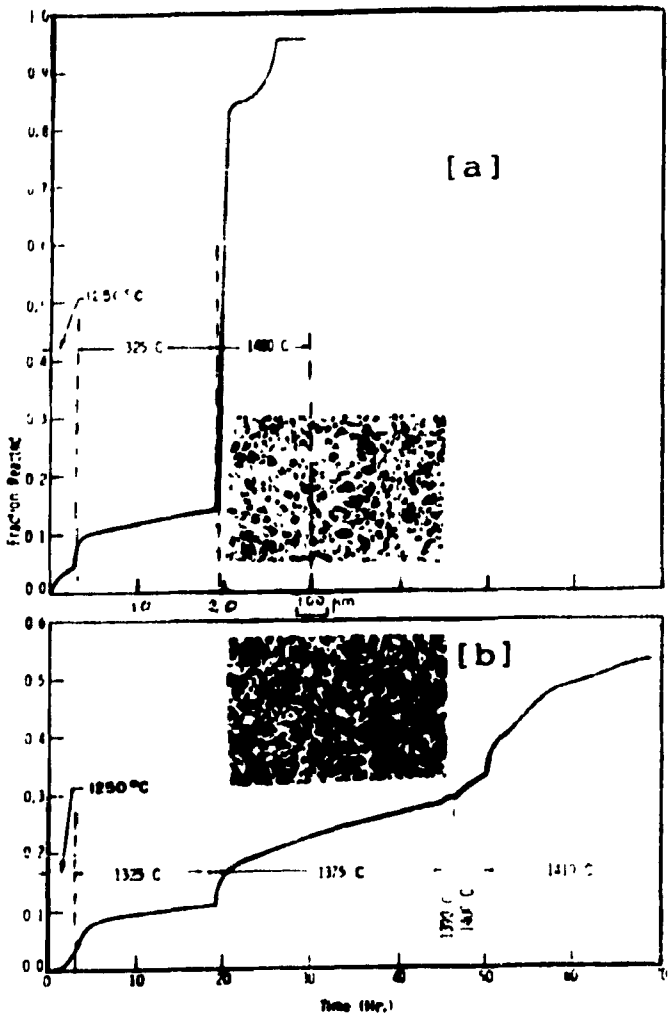

Fig 2.17: Fraction of high purity (99.99%) silicon powder compacts reacted versus time for different heating cycles (40).

GAS COMPOSITION:

The composition and pressure of the nitriding gas can also influence the course of the reaction and thus influence the microstructural development and the resulting mechanical properties.

EFFECT OF O2: Few investigations have focused on the effect of oxygen in the nitriding gas (15). However, Messier and Wong (60) suggest that even extremely low levels of O_2 can significantly retard the rate and degree of nitriding. The considerable effect of small amounts of O_2 on the nitridation kinetics, however, awaits theoretical explanation.

THE ROLE OF H_2: It has been proposed that the function of hydrogen is primarily to accelerate the rate of reduction of the native silica film on the silicon particles (61) by the reaction:

$$SiO_2(s) + H_2(g) \rightarrow H_2O(g) + SiO(g)$$

$$\Delta G^{\circ}_{1643^{\circ}K} = 226\ kJmol^{-1}$$

The speed with which this can be achieved determines to a large extent the surface area of silicon available for evaporation and the eventual rate of formation of silicon nitride by reaction of silicon atoms transported via the vapor phase.

GAS PRESSURE:

As can be expected, decreasing the nitrogen partial pressure in the nitridation reaction strongly reduces the reaction rate (50). This automatically lengthens the time required to achieve a complete degree of reaction. It has been suggested that at high nitrogen partial pressure, many Si_3N_4 nuclei are formed at the silicon surface which results in a homogeneous, finegrained microstructure with small pores (37). At low nitrogen pressures, by contrast, a relatively small amount of Si_3N_4 nuclei are formed at the silicon surface. Silicon then evaporates and precipitates on or diffuses to, these nuclei.

STATIC OR FLOWING NITROGEN:

Although the flow rate of nitrogen gas around silicon compacts during nitriding has been shown to influence the strength of the resulting silicon nitride, its exact role has not been fully explained.

It has been reported by Jones and Lindley (35,36) that under flow conditions, notably weaker silicon nitride is produced as compared to material produced under "static" conditions at all equivalent degrees of conversion. In addition, a higher proportion of β-Si_3N_4 is present in material prepared under "flow" conditions. Jennings (25) however suggested that under flow condition, impurities could be swept away from the reaction sites. As previously discussed, most impurities discourage the formation of active nitrogen and therefore slow the formation of β-Si_3N_4. If

however, they are swept away by the N_2 flow, the possibility of formation of β-Si_3N_4 is increased.

Another role suggested for flowing N_2 is to remove the silicon vapor which forms and lower its partial pressure; this will encourage pore formation and therefore a coarse product will be obtained, thus explaining the reduced mechanical strength of Si_3N_4 prepared under "flow" conditions.

2.2.6 PROPERTIES OF RBSN

Typical property values for commercial RBSN will be given in this section. The effect of the green Si compact characteristics on these properties are predictable and will be briefly discussed.

In addition, the aim of the following section is to deal with those properties required of structural high temperature ceramics, for example high temperature strength, creep-resistance and oxidation resistance.

2.2.6.1 Typical properties values

Table 2.4 presents some typical values for commercial reaction-bonded silicon nitride.

Density	2.35-2.6 Mgm^{-3}
Porosity	26-18%
Bend strength (25°C)	160 MPa
Weibull modulus	15
Young's modulus (25°C)	170 GPa
Thermal expansion coefficient	2-3 $x10^{-6}$ $°K^{-1}$
Thermal conductivity	10-15 $Wm^{-1}°K^{-1}$
Specific heat capacity	1100 $Jkg^{-1}°K^{-1}$
Thermal Shock Resistance (ΔT downshock)	600°K

Table 2.4: Typical values for commercial RBSN

Careful control during the preparation of high-grade, well blended, optimized size range, silicon powders to ensure a good packing density and the absence of large voids can lead to reaction-bonded silicon nitride with four-point bend strengths of better than 300 MPa. Normal commercial densities are in the 2.4 $g.m^{-3}$ range and bend strengths are of the order of 160 MPa at 25ºC.

INFLUENCE OF FINAL POROSITY:

It has been observed (62-65) that the properties of RBSN are strongly dependent on the final porosity in nitrided samples. In fact, Jones and Lindley (62) have observed a linear relationship between the developing bend strength of the ceramic during nitridation and the partially nitrided compact density (Fig 2.18).

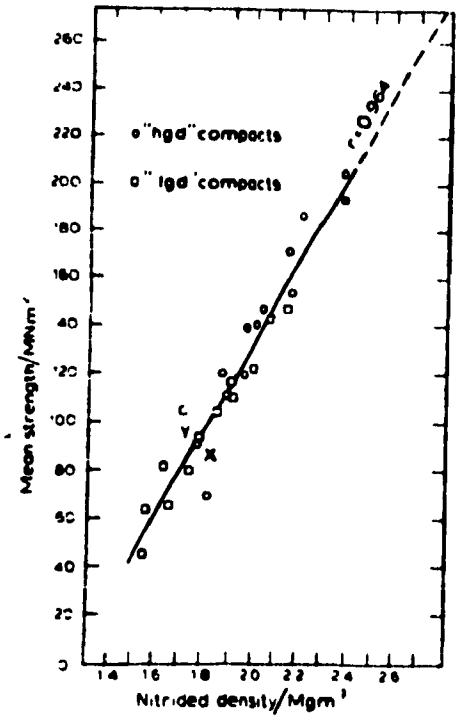

Fig 2.18: Strength versus nitrided density for high (hgd) and low (lgd) green density compacts (62)

In addition, the creep rate of RBSN strongly depends on the open porosity and the pore size distribution (63-65); as porosity increases so does the creep rate.

Furthermore, oxidation of RBSN varies depending on the total porosity, the pore size and the pore size distribution (64). There is a competition between formation of a protective oxide layer over the external surfaces and internal oxidation along pores and grain boundaries, until the pores are completely filled with oxides (50). Nevertheless, this oxidation depends on the ambient oxygen partial pressure (64,65). At low oxygen partial pressure (< 10^2 Pa at 1300ºC), active oxidation occurs according to the following equation:

$$2Si_3N_4(s) + 3O_2(g) = 6SiO(g) + 4N_2(g)$$

Some silicon is released in the form of SiO gas, leading to a decrease in the sample weight. At relatively high oxygen partial pressures, when passive oxidation occurs, a protective layer of silica is formed on the surface according to the reaction:

$$Si_3N_4 + 3O_2(g) = 3SiO_2(s) + 2N_2(g).$$

Some silicon oxynitride (Si_2ON_2) could thermodynamically be formed but would be further oxidized to silica.

THERMOMECHANICAL PROPERTIES:

Variation of Modulus of Rupture, creep and oxidation resistance versus time or temperature have been investigated by many authors (66,67,68) as they represent important properties in engineering applications. Fig 2.19 compares the modulus of rupture for different types of silicon nitride as a function of temperature.

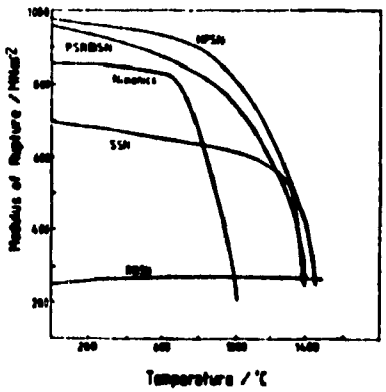

Fig 2.19: Variation of MOR with temperature for silicon nitride (66,67)

The modulus of rupture of RBSN materials is relatively low but remains almost constant even at high temperature (1400ºC).

In addition, creep resistance under relatively low stress at high temperature is an important property for RBSN products. The creep strain for different ceramics tested under a compressive stress of 238 MNm^{-2} at 1350ºC in air is presented in Fig 2.20.

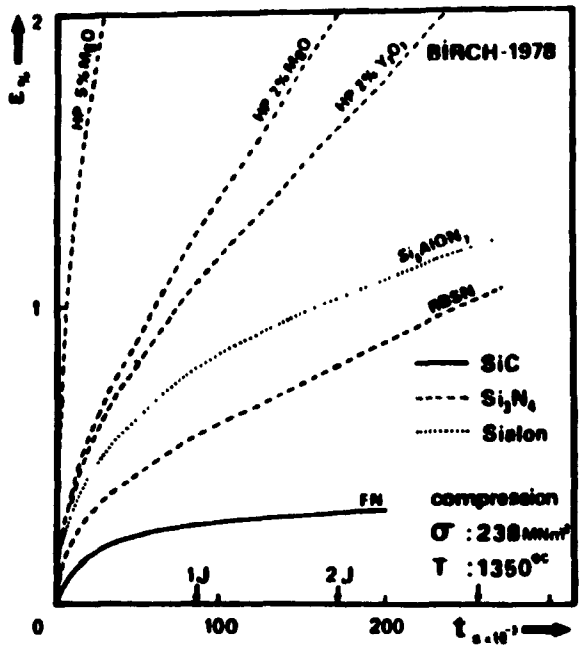

Fig 2.20: Creep strain versus time for different materials (T=1350ºC, σ=238MNm^{-2})(68)

The reduction in creep resistance and strength of dense silicon nitride at high temperatures is due to the presence of a continuous, glassy intergranular phase formed by the sintering aids used to promote liquid phase sintering. In RBSN materials which contain no additives, the creep rate is quite low and this property makes RBSN products attractive, for example, in gas turbine components.

The oxidation behavior of silicon nitride ceramics operating at elevated temperature in air is also an important factor. The oxidation of RBSN in air is significant even at temperatures around 900ºC and follows parabolic kinetics (69). At temperature in the range of 1100 to 1300ºC, formation of silica is notable on the

internal surface area of RBSN but the reaction rate is low since the oxygen has to penetrate into the compact. At higher temperature, external oxidation is rapid and the pores are quickly blocked with silica preventing further internal oxidation. This surface oxidation of RBSN can even lead to an improvement in strength due to the blunting of surface cracks and pores.

2.2.6.2 Improvement of RBSN

Due to the way in which it is formed, RBSN contains ~20% residual porosity resulting in limited strength and oxidation resistance. Several attempts have been made to reduce this residual porosity or to improve the mechanical properties of this material. Thus, it has been suggested that a post-sintering of the RBSN compact in nitrogen after the reaction bonding process could reduce porosity and increase bend strength and oxidation resistance (70).

The process of post-sintering RBSN integrates the attractive advantages of both reaction-bonding and sintering. High density values can be reached with this process and therefore the properties of RBSN are improved, however the necessary additions of sintering additives reintroduce the problem of a glassy intergranular phase.

Another way to improve the mechanical properties of RBSN may be to reinforce the material with short fibers or whiskers. The aim of the following section is to review the toughening mechanism of ceramics and to introduce the processing technology of such ceramic composites.

2.3 RBSN REINFORCED BY WHISKERS

Recent works (71,72,73) have shown that large gains in fracture strength and toughness are possible in Ceramic Matrix Composites and some of these toughening mechanisms have been identified.

2.3.1 THEORETICAL ASPECT OF WHISKER REINFORCEMENT

Whisker reinforcement can involve several toughening mechanisms. The mechanisms most applicable to advanced ceramics are summarized in this section.

When a crack is generated several behaviours are possible. First, the crack can be perturbed by the presence of whiskers and crack deflection occurs, causing a reduction in stress intensity (Fig 2.21) (74,75).

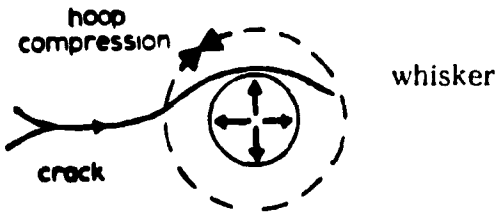

Fig 2.21: Crack deflection

If debonding along the whisker-matrix interface can take place, toughening by bridging is induced. Fig 2.22 shows a schematic of a bridging zone behind the crack (76). The magnitude of the toughening depends on the extent of debonding.

On the other hand, if the crack front is pinned at a whisker, the crack cannot advance until the whisker fails. The toughness then increases as the ratio of whisker radius to the spacing between whiskers increases. Thus, for a fixed radius, the toughness increases with volume fraction of whiskers (77,78).

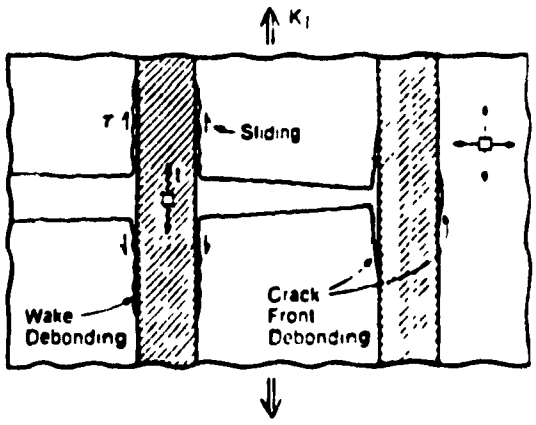

Fig 2.22: Schematic of a bridging zone (76)

In addition to the effect of whiskers, porosity can also play a role in crack propagation behavior. In a brittle material like RBSN ceramic, pores are larger than the Griffith minimum flaw size. Therefore, cracks keep propagating through the pores (79). Microcracking formed circumferentially around whiskers in the matrix has been noticed by Evans and Faber (74). With a narrow range of microcracks both in distribution and size, toughening is increased by 2 to 5 times of that without microcracking.

With crack deflection and microcracking, crack branching can commonly occur as shown in Fig 2.23 (79).

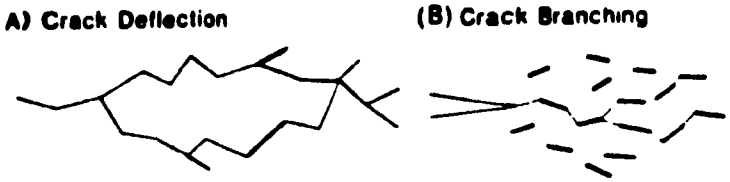

Fig 2.23: Crack branching

(A): illustrates the combination of crack branching with crack deflection and

(B): the combination of crack branching with microcracking.

This mechanism should substantially add to the fracture toughness. It is illustrated by the fact that since crack deflection or microcracking by themselves improve the fracture toughness having, for example two cracks, should indeed result in a higher level of fracture energy.

Increased toughness associated with whisker reinforcement is not always accompanied by an increase in flexural strength. It is a number of authors' experience that this is often a result of nonuniform distribution of whiskers in the composites (80). Regions of very high or low whisker content often act as the source of mechanical failure and yield lower strength composites than those achieved with uniform microstructures. Therefore, good dispersion of the reinforcing phase is essential.

The next section will deal with the processing technology of such ceramic composites.

2.3.2 PROCESSING TECHNOLOGY

The processing technology of ceramic composites can be divided into two parts: first, establishment of a stable suspension of the silicon powder and whiskers and secondly, compaction of the mixture before the nitridation.

2.3.2.1 Mixing and dispersion

Because advanced ceramic materials require starting powders of such small particle size, inter-particle attraction prohibits dry mixing of the powders. Suspension processing is therefore used and a colloidal slip is formed by adding Si powder and whiskers to a liquid, such as alcohol or water. To overcome the ever-present attractive forces between the particles, the slip is rendered stable by inducing repulsive forces such as, for example, electrostatic or steric forces (81).

ELECTROSTATIC FORCES: Solid surfaces immersed in water have the ability to adsorb ions dissolved in the water. These ions form an electric double layer (Fig 2.24). As two particles approach one another, their outer double layers overlap which results in a repulsive electrostatic force due to the similar charges. This force is counteracted by the attractive Van der Waals forces.

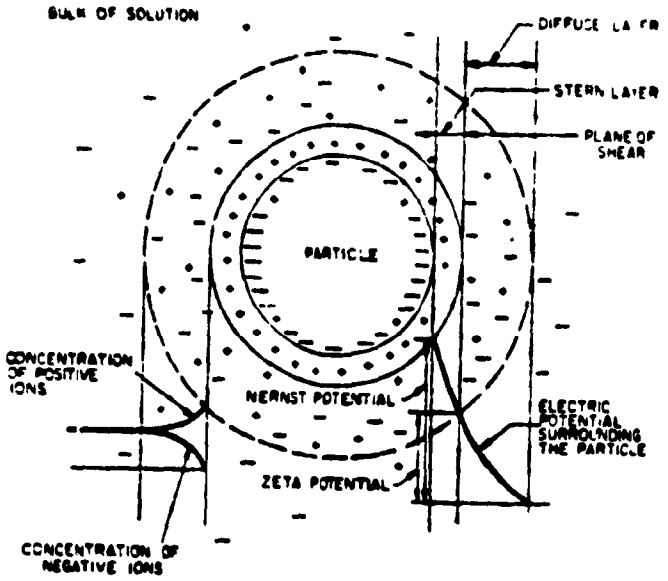

Fig 2.24: The electrostatic double layer (82)

Therefore, by altering the pH of the slip, dispersion of the slurry can occur. In the case of Si/SiCw particles in water, the silica layer around the particles and the whiskers can easily form silanol-groups leading to aggregation of the Si particles (83,84,85). A careful control of the pH of the slurry can avoid this flocculation.

2.3.2.2 Fabrication of the green compacts

The two most popular fabrication methods to produce green compacts are pressing and slip casting. For pressing, the slurry has to be dried and granulated, whereas in slip casting it is processed as a concentrated suspension.

In slip casting, a slip is poured into a dry plaster mold. At once, due to capillary forces, the water from the slip is drawn into the plaster. The slip adjacent to the plaster wall loses sufficient water to increase its yield point until it becomes firm and the plaster capillaries begin to fill. With increasing time, this flow process continues and the thickness of the firm wall increases while the plaster becomes wetter. The rate of casting, that is, the rate of increase of wall thickness, decreases with increasing time for two reasons: the first is that due to the everthickening layer, the diffusion of water becomes difficult, and the second is the lowered suction capacity of the plaster because its pores are filled with water (86).

The viscosity of a slip must be carefully controlled, for if it becomes too high, it will not fill the mold cleanly. It is desirable to have as low a water content as possible and still have sufficient fluidity. This makes it necessary to add deflocculants as described in the previous section.

2.3.2.3 Nitridation of the green whisker compact

The nitridation process of a silicon compact has been presented in section 2.2. In the case of Si/SiC whiskers compacts, the effect of whisker content has to be considered. Nevertheless, the nitridation of whisker-containing compacts occurs in nearly the same way as for the fabrication of pure RBSN.

In the literature, the majority of work on Si_3N_4 based composites has been done using hot-pressing as the consolidation method. The advantage of using the reaction bonding technique to produce composites is that no bridging of whiskers occurs during the nitridation, which is a common problem during the sintering of Si_3N_4 composites. Bridging of whiskers prohibits the shrinkage during sintering, therefore leading to a material with a high porosity and strength limiting defects.

In addition, since the processing temperature in reaction bonding (<1450ºC) is lower than in sintering (1800ºC), degradation of whiskers is less likely to occur (87).

The effect of whisker content on the mechanical properties of RBSN is presented in the following section.

2.3.3 MECHANICAL PROPERTIES

Most mechanical property characterization of RBSN composites has been carried out on fiber reinforced composites (88,89,90) as opposed to whisker reinforced.

Only a few investigations have been reported in the literature on the mechanical properties of RBSN reinforced by whiskers (91,92,93). The green and nitrided densities in the processing of these composites are presented in Fig 2.25.

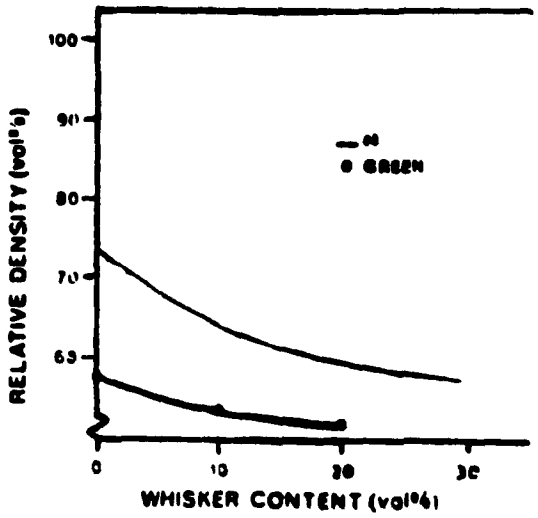

Fig 2.25: Relative density of green and nitrided samples versus whisker content (91)

Whiskers seem to hinder both consolidation in the pressing stage and densification during the nitriding stage (91).

It has been observed that both flexural strength and fracture toughness decrease slightly with whisker addition (91). No real explanation has been found for

the first parameter. The decrease of the fracture toughness has been explained by too strong a bond between fibers and matrix. No fiber pullout (corresponding to a high toughness composite) was observed by the authors. The strong bond might result from the fact that during the nitridation, SiC fibers served as growth sites for Si_3N_4 so that after nitridation the fibers were totally covered with Si_3N_4 and debonding or crack bridging were inhibited.

Some investigations have been carried out in RBSN reinforced by SiC particles (< 0.05μm) (94) but no improvement has been noted in comparing some mechanical properties between RBSN and the composites.

Moreover the whisker/matrix interface has also been considered in the literature: weak interface bonding results in shear failure as seen previously in section 2.3.1, whereas stronger bonding results in filament fracture which decreases toughness.

Some authors have studied the interface between the matrix and some SiC continuous-fibers coated with carbon (90,95). For a low carbon layer thickness, infiltration of the coating with silicon occurs. Infiltrated carbon does not provide for a delamination/crack deflection layer as pure carbon can. Thus, when silicon infiltration consumes the entire carbon layer, a lower strength and lower toughness composite results (91).

More results are necessary to fully understand the influence of whiskers since the mechanical properties of such composites are strongly dependent on the powder and whiskers characteristics but also on the nitriding process.

The aim of this research is to fabricate a whisker-reinforced RBSN composites using wet processing methods and to investigate any change in the nitridation process brought about by the addition of SiC whiskers to the silicon compacts and to correlate mechanical properties with the processing conditions.

3 OBJECTIVES

This work will be aimed at fulfilling the following objectives:

1) To define the optimum parameters for obtaining good dispersions of reinforcing phases (SiC whiskers) in silicon powder by wet processing.

2) To determine the best fabrication route for producing green compacts with homogeneous reinforcement distribution.

3) Study the effect of temperature and whisker content on kinetics of nitridation.

4) Analyse the effect of green density and whisker content on complete nitridation.

4) Measure the mechanical properties of RBSN composites and possibly determine strengthening mechanisms.

4 EXPERIMENTAL PROCEDURE

4.1 RAW MATERIAL CHARACTERIZATION

The Si powder used in this work is a fine grained and high purity powder[1]. The specifications of the powder (4C) are shown in Table 4.1 as are those for the SiC whiskers[2], which show aspect ratios ranging from 15-50, and an average diameter of 1 μm.

GRADE		Si POWDER, 4C	SiC whiskers
MORPHOLOGY		equiaxed	acicular
PARTICLE SIZE		d_{av} = 7μm	L/d = 15-50
SPEC. SURF. AREA		1.2 m^2/g	
PURITY	Fe	0.07%	
	Al	0.07%	
	Ca	0.01%	
	C	0.06%	
	O	0.2-0.7%	

Table 4.1: Specification of starting powder and whiskers

Fig 4.1 and 4.2 are scanning electron micrographs of the raw materials. Different weight percentages of whiskers (0%, 15%, and 30%) and 1wt% of Iron[3] in the form of a fine powder (6 μm) were added to the mixture.

[1]SICOMILL Grade 4C, Superior Graphite

[2]American Matrix Company

[3]AESAR

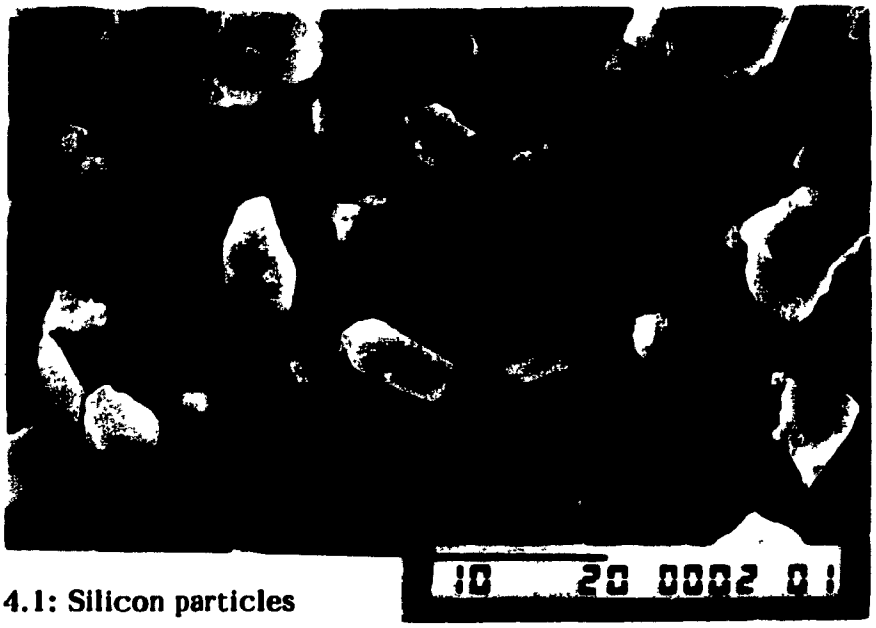

Fig 4.1: Silicon particles

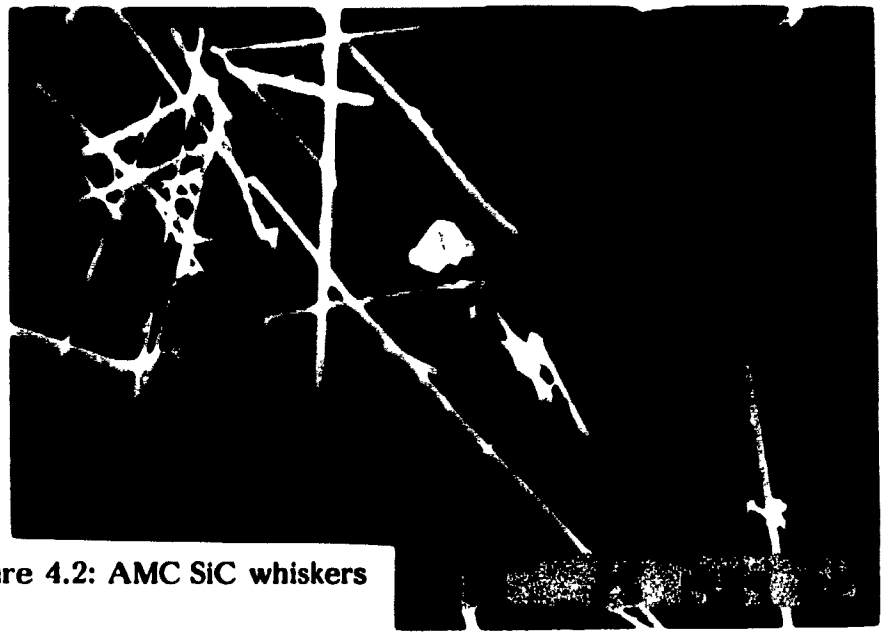

Figure 4.2: AMC SiC whiskers

Oxygen analysis was carried out on the Si powder by the "inert gas fusion" method[4] and a total of 0.5 weight percent was found. Based on the average size of the Si particles, this would indicate that each particle is surrounded by a silica layer of ~ 4nm (appendix 4.1). For this reason ~ 1% of Fe powder was added to all mixtures to help remove this oxide layer prior to nitridation.

---

[4] TC 136 LECO EF 100 electrode furnace and associated analyser, Elkem Metals, Niagara Falls, NY.

4.2 FABRICATION OF GREEN SAMPLES

4.2.1 POWDER MIXING AND DISPERSION

The Si powder was mixed with the whiskers in the wet state. Added to distilled water, the powder-whisker mix was attrition milled at a speed of 250 rpm for 30 minutes. The ratio of solid to liquid was 2:1 by weight. Silicon nitride milling media, having a diameter of ~5 mm, was used in the proportion of 2.5 times the weight of powder used.

After attrition milling, the colloidal suspension was then dispersed by pH adjustment. The pH of the slip was modified to between 1 and 10 by adding either NH_4OH or HCl. After mixing, the slip viscosity was measured at each pH value, at an operating speed of 500 rpm in a cone viscometer[5]. Fig 4.3 presents the procedure used for this dispersion method.

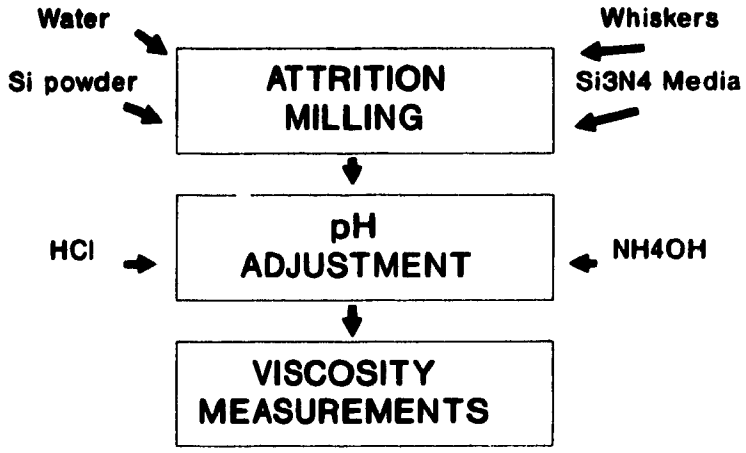

Fig 4.3: Processing route for attrition

[5]Model 115 Rheomet, Contraces, Zurich, Switzerland

4.2.2 FABRICATION OF GREEN COMPACTS

Several different methods were used to make compacts from the Si/SiC whiskers mixture as shown in Fig 4.4.

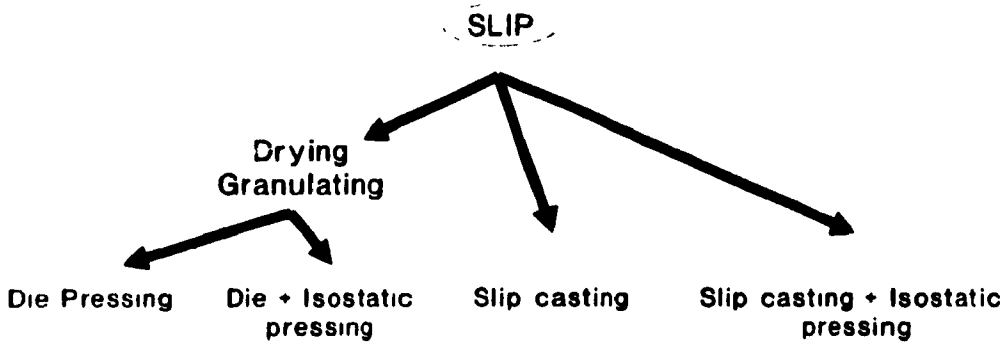

Fig 4.4: Processing route for fabricating green compacts

4.2.2.1 Slip casting

After attrition milling, the slip was cast into a plaster mould. The molds were made up following a standard procedure as outlined in appendix 4.2. Slip was continually added to form a solid cast. The resulting slip-cast compact had a circular cross section and dimensions of approx. 10 mm (dia) x 10 mm. Some compacts were subsequently isostatically pressed at 200-300 MPa.

4.2.2.2 Drying and pressing

In some cases, the powder/whisker mixture was dried and compacts made by conventional pressing techniques. First, the slip was dried in a microwave oven. The resulting large aggregates of dry powder and whiskers were then granulated through a 212 μm sieve so as to form a free flowing powder.

Two types of pressed compact were prepared: cylinders (ϕ=10mm, h=10mm) and bars (55x7x4 mm approx) using a die press at a pressure of ~5MPa.

Some compacts were then isostatically pressed at 200-340 MPa. The compacts were dried at 130ºC for 5 hours. Some hydrolysis of the samples was expected during the milling, slip casting and drying processes. On analysis, the oxygen content was found to have increased to 1.2%. Nevertheless, the percentage is still relatively low.

4.3 NITRIDATION

4.3.1 APPARATUS

The nitridation of silicon to silicon nitride is one which involves a theoretical weight gain of 67%. In fact, 3 moles of silicon are converted into 1 mole of Si_3N4 and the molecular weights of silicon and silicon nitride are respectively 84g and 140g; 1g of silicon will be converted into 1.67g of Si_3N_4, thus leading to a weight gain of 67% on complete conversion. If the original weight of silicon is known, it is thus possible to monitor the extent of the nitridation process by measuring the change in weight of the sample. In order to monitor this weight change, a thermogravimetric balance (TGB) furnace system was constructed which would allow the continuous monitoring of sample weight during nitridation in a flowing nitrogen atmosphere at temperatures in the range of 1400ºC. The TGB comprised of a Cahn Microbalance head attached by a sample lifting mechanism (which allowed the sample to be raised and lowered into the furnace once the system was evacuated) to a resistance-heated furnace. The apparatus is described more fully below.

4.3.1.1 Furnace

All nitriding experiments were carried out in a vertical tube furnace such as that shown schematically in Fig 4.5. The Al_2O_3 working tube diameter was 63.5 mm, with a hot zone length of ~ 100mm. Heating was by LaCr elements, with water cooled, brass O-ring fittings at each end. A vacuum pump was used to evacuate the system before flushing with nitrogen.

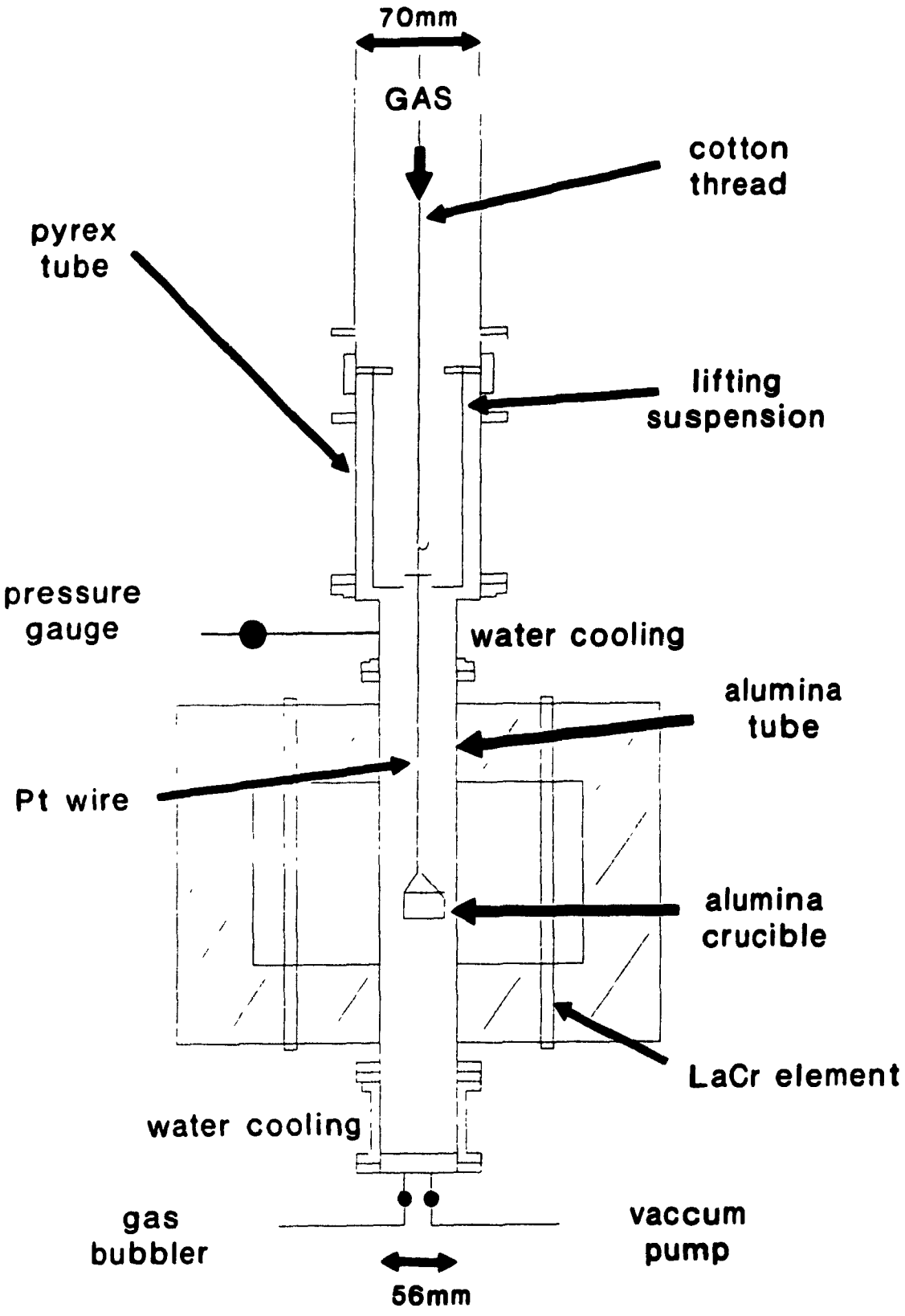

Fig 4.5: Nitriding furnace

The electromagnetic balance[6] was located above the furnace, permitting the weight of a sample suspended in the reaction zone to be continuously recorded. A schematic diagram of the system is shown in Fig 4.6.

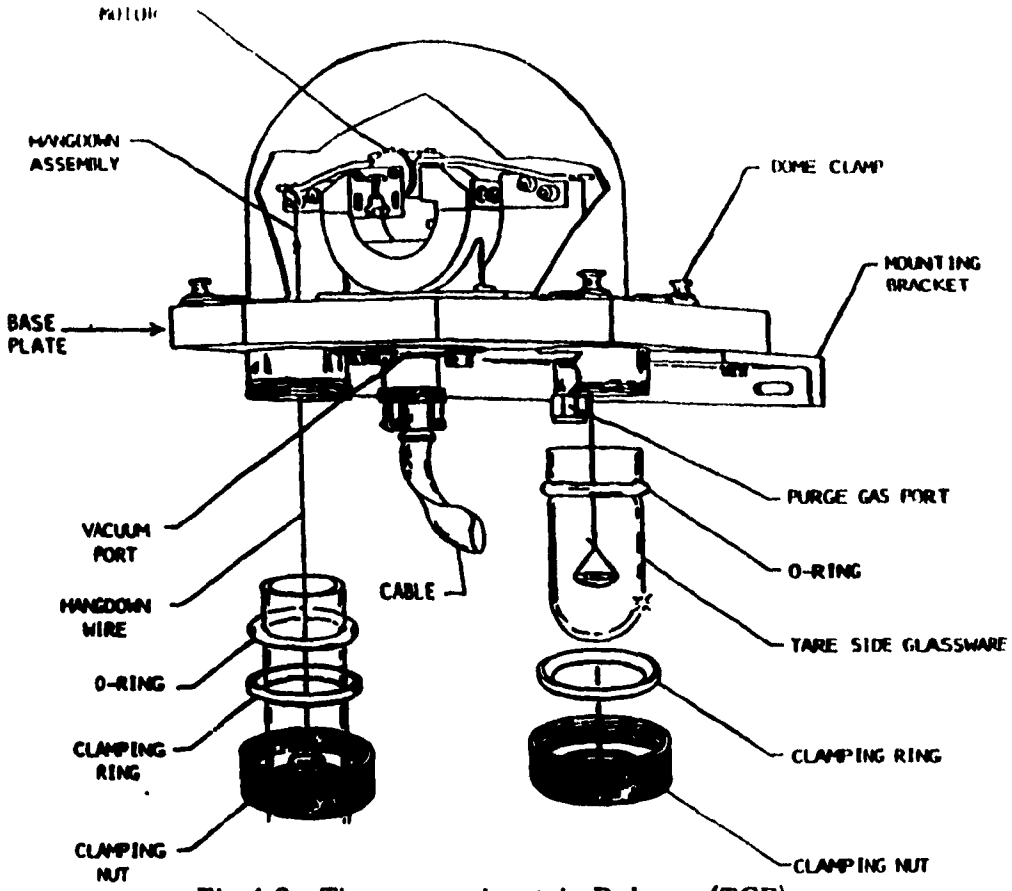

Fig 4.6: Thermogravimetric Balance (TGB)

Principle of the microbalance:

The D-100 series Cahn balance is a very sensitive weight measurement instrument, capable of measuring weight changes up to 100 grams and has a resolution of 1 microgram.

The weight unit is shown Fig 4.7: it may be described simply as a force to current converter.

---

[6]CAHN D-100, CAHN Instruments., California, USA

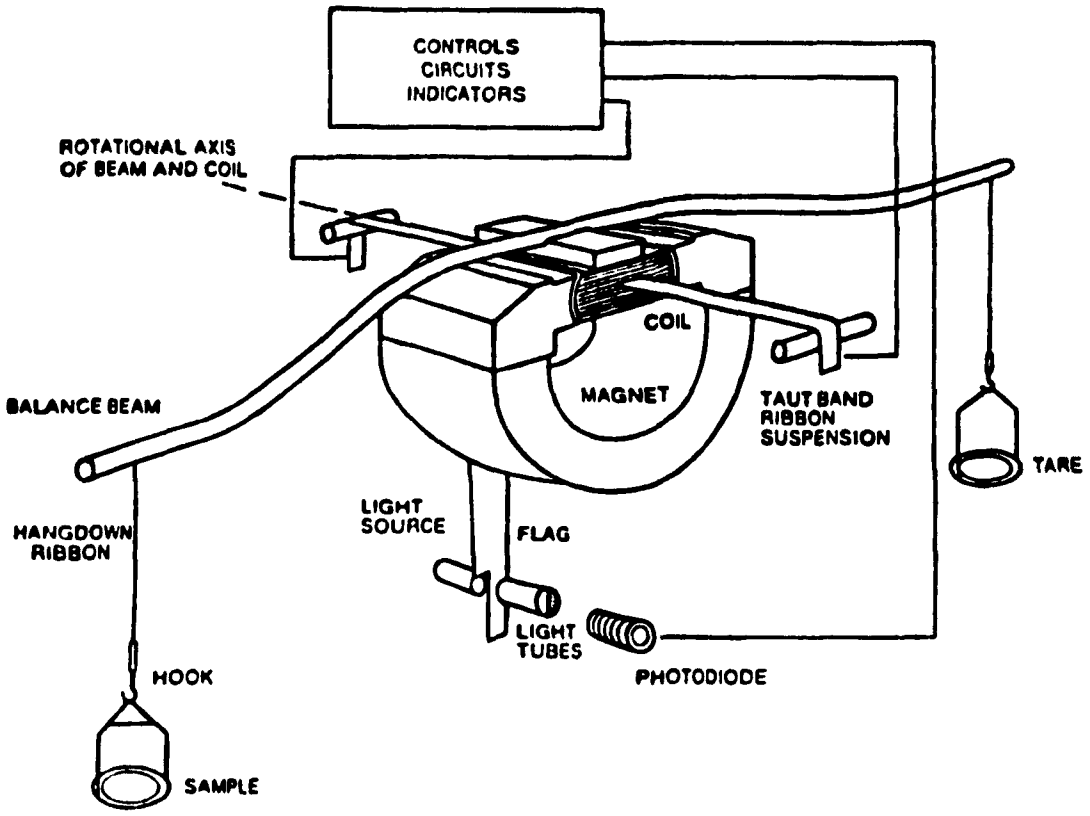

Fig 4.7: Detailed schematic of the microbalance

The sample whose weight is to be monitored is suspended from the sample (left) side of the beam (see Fig 4.7) which produces a force about the axis of rotation. An electric current then flows in the torque motor to produce a force about the same axis which is equal and opposite to the force produced from the sample. A greater force on the beam (weight gain) will require a greater opposite force from the torque motor. The current necessary to produce the required torque motor force is therefore a direct measure of the force on the beam, and thus the sample weight change.

The control unit processes the electrical signals from the weighing unit. These signals are converted into a digital form which can be recognized by a computer; the weight change then being recorded as a function of time. The

sampling time of the recording unit is variable but for the majority of the runs, this was set at 5 minutes.

4.3.1.2 Wire suspension and crucible

The silicon compact is somewhat difficult to suspend due to its reactivity with many metals at these temperatures (1400ºC). Several suspension systems were tried (Pt, Mo, BN, W) but reaction with SiO or Si vapor species resulted in erroneous readings. In fact, for example with a Mo suspension, a thin green film has been obtained on the surface of the compact during nitridation. Microanalysis of this film has shown traces of Mo, probably from a $MoSi_2$ or MoO_3 phases. The compact had gained some weight but X-ray analysis revealed only the presence of Si_2ON_2, possibly due to the difficulty for the nitrogen to penetrate through the thin film at the surface of the compact.

Thus an alumina suspension system which proved to be inert with respect to the silicon was used to suspend the compact. Platinum wire was used to suspend the Al_2O_3 crucible arrangement from the microbalance system (Fig 4.8). This Al_2O_3 crucible was made by slip casting. After presintering, the crucible was drilled with holes to allow unrestricted gas flow and the alumina hanging arms were fixed with alumina slip. Sintering was performed at 1500ºC for 5 hours.

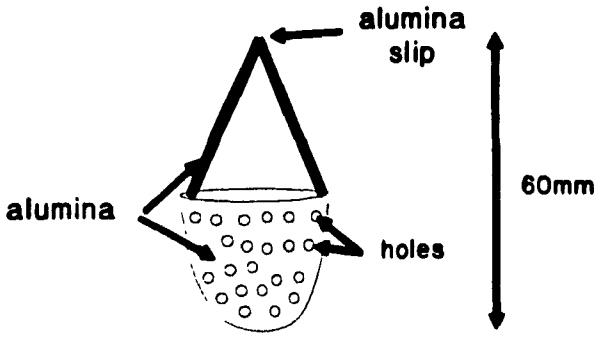

Fig4.8: Al_2O_3 crucible

4.3.2 EXPERIMENTAL CONDITIONS

4.3.2.1 Nitridation temperature-time cycle

Two different types of experiment were performed: (a) kinetic measurements at constant temperature and (b) complete nitridation.

Kinetic study: In this series of experiments, the sample was lowered into the furnace that was already at a specific constant temperature in the range of 1250 to 1415ºC. The sample weight gain as a function of time was recorded by the microbalance. The end of the test was taken to be the time at which the weight gain reached a plateau. This experiment was repeated at the following temperatures: 1315, 1340, 1365 and 1390ºC.

Complete nitridation: Based on the results obtained in the kinetic study described above, a temperature-time schedule was established as shown in Fig 4.9. This is similar to the type of nitridation schedules commonly seen in the literature which are necessary to ensure complete nitridation, however, these are not always generated from kinetic data as in the present study. In fact, the kinetic curve at a specific temperature has allowed the determination of the time necessary for each compact to reach the final plateau. Therefore, it has been possible to fix the duration of each temperature step in the nitridation schedule so that maximum conversion is achieved and the temperature is raised as soon as the conversion rate starts to decrease, since the same compact size has been used in both kinetic and complete nitridation experiments.

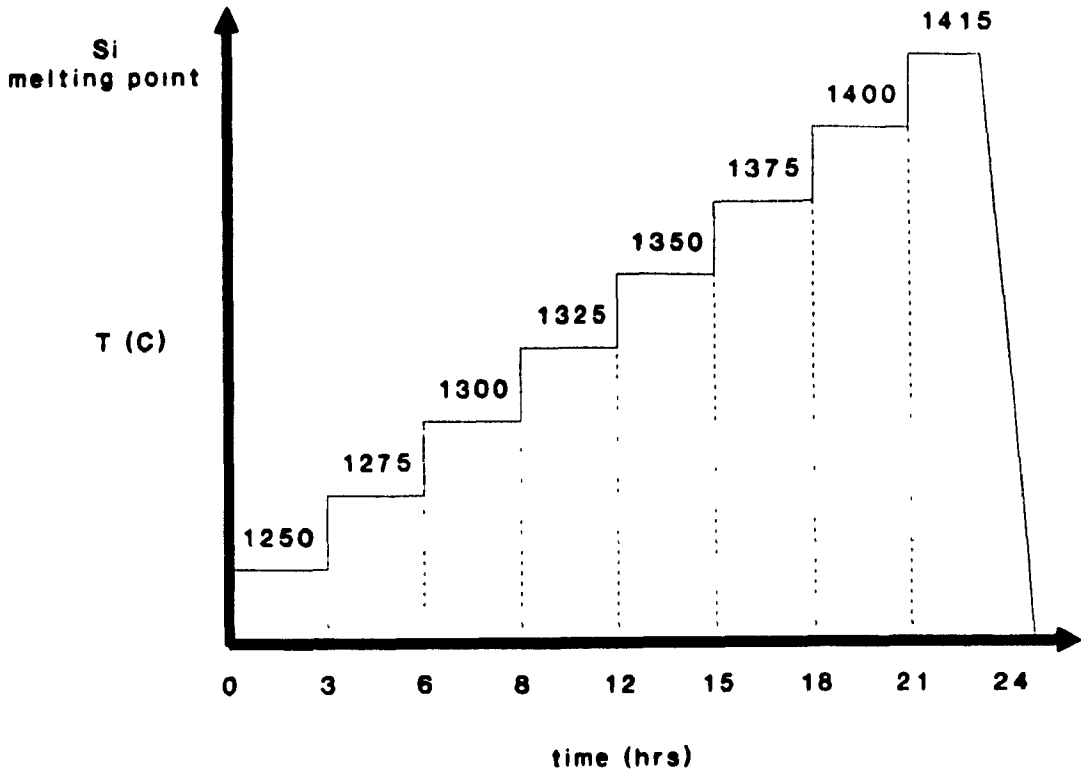

Fig 4.9: Nitridation temperature-time schedule

4.3.2.2 Gas flow and nature

Prior to each experiment, the TGB system was evacuated by rotary pump and flushed with nitrogen. After subsequent reevacuation, the system was backfilled with nitrogen.

All experiments were carried out using a high purity nitrogen gas flow. The pressure in the furnace remained slightly above atmospheric to avoid the entrance of oxygen in the furnace through possible leaks.

The gas flow was set at 3 l/min. The gas entered the sample crucible with a velocity of approximately 3.5 cm/min, but at high temperature, gas dilation occurs which can slightly modify this velocity. Table 4.2 presents the gas specification.

Nitrogen prepurified	
Maximum moisture	5 ppm
Ar	< 25 ppm
CO_2	< 1 ppm
H_2	< 1 ppm
O_2	< 5 ppm

ex. LINDE

Table 4.2: N_2 gas specification

Initially, H_2 containing gas mixtures (N_2 + 4% H_2) were used in an attempt to remove the silica layer, however, water was found to condense in cooler parts of the furnace probably due to oxygen contamination and this practice was discontinued. Iron powder was added to the initial material to fulfill the function of silica removal as discussed in section 2.2.5.

4.4 SAMPLE ANALYSIS AND CHARACTERIZATION

4.4.1 DENSITY MEASUREMENTS

The green density of the silicon compacts was measured by the Archimedean method by submersing the samples in mercury. These values are accurate to 0.03 g/cm^3. Nitrided densities were calculated from volumes and weights or measured by immersion in water.

4.4.2 α/β PHASE IDENTIFICATION

Phase identification was carried out by X-ray powder diffraction[7]. The samples were ground into powder and were then subjected to filtered Cu Kα radiation. For each of the α-Si_3N_4 and β-Si_3N_4 diffraction patterns, a single peak of the highest relative intensity was selected (Table 4.3).

	Angle 2θ selected
α-Si_3N_4 phase	27.1º (201)
β-Si_3N_4 phase	31.0º (200)

Table 4.3: Selection of diffraction peak

The percentage of α-Si_3N_4 was calculated as follows:

$$\%\alpha = \alpha/(\alpha+\beta) = I_{\alpha(201)}/(I_{\alpha(201)}+I_{\beta(200)})$$

$I_{\alpha(201)}$ corresponding to the net relative intensity (total intensity - background) of the (201) peak.

[7]Phillips X-ray diffractometer (APD1700)

4.4.3 MICROSTRUCTURAL CHARACTERIZATION

Polished samples were prepared by sectioning with a diamond cut off wheel followed by conventional mounting, grinding and diamond polishing. Optical microscopy was carried out in reflected light and after carbon coating the samples were then examined by Scanning Electron Microscopy[8]. Fracture surfaces were gold coated prior to SEM examination.

4.4.4 MECHANICAL MEASUREMENTS

Strength values were determined using four-point bending as shown in Fig 4.10.

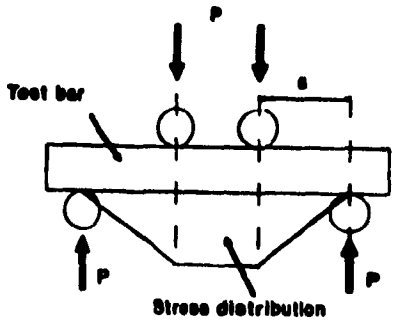

Fig 4.10: Four-point bending test

Test bars were 9.1mm x 2.5mm x 55mm in size and flat and parallel surfaces were made by grinding the samples with a 240 grit diamond wheel in the longitudinal direction followed by bevelling of the edges. A crosshead speed of 0.02 in/min was used for loading.

[8]Jeol 840 A

The MOR was calculated using the equation (70):

$$MOR = 3Pa / bd^3$$

P: load at fracture (N)

a: half the distance between the point loads (mm)

b: width (mm)

d: thickness (mm)

Hardness measurements were made on a polished specimen using a Vickers diamond indentor with a load of 20 kg.

5 RESULTS AND DISCUSSION

This research effort deals with the processing of an RBSN composite reinforced with SiC whiskers. In this section, results will be presented dealing with powder/whisker dispersion during the fabrication of the green compacts, as well as with the kinetics of nitridation and finally, with the resulting composite properties.

The influence of various parameters such as temperature, whisker content and green density on the nitridation behaviour will be discussed.

5.1 GREEN COMPACT CHARACTERIZATION

5.1.1 INFLUENCE OF pH AND WHISKER CONTENT ON THE COLLOIDAL DISPERSION

A study of the dispersion behaviour of the SiC whiskers in the Si powder slurry was carried out by obtaining viscosity measurements at 500 rpm. Slurries containing different whisker contents, ranging from a control sample with no whiskers, to up to 20 wt% were examined. For each composition, attrition milling and pH adjustment were used as the dispersion method, as previously described in section 4.2.1.

Figures 5.1 and 5.2 show viscosity versus pH for 4 different slurries ranging from 0 to 20% whisker weight content.

The curves show that for a given solids loading, initially the viscosities of the slips decrease slightly with increasing pH. After a minimum in viscosity is reached, a sharp increase occurs. Minimum flocculation is achieved when the slip is at the pH which corresponds to the minimum in viscosity because decreased flocculation increases the amount of liquid available in the slip for shear.

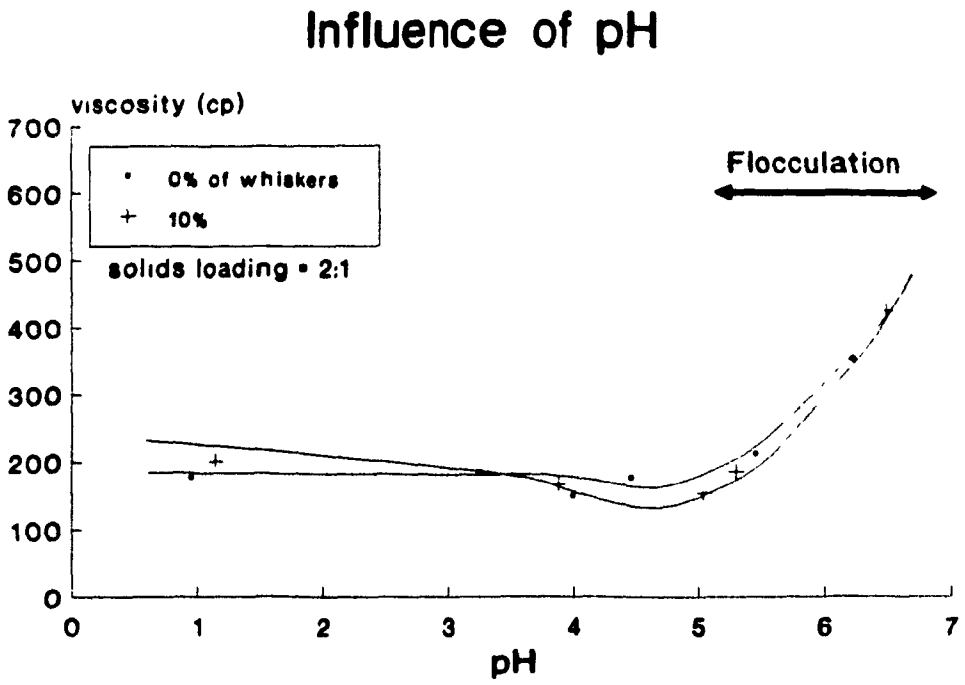

Fig 5.1: Viscosity vs pH for slurries containing 0 and 10 wt% of whiskers

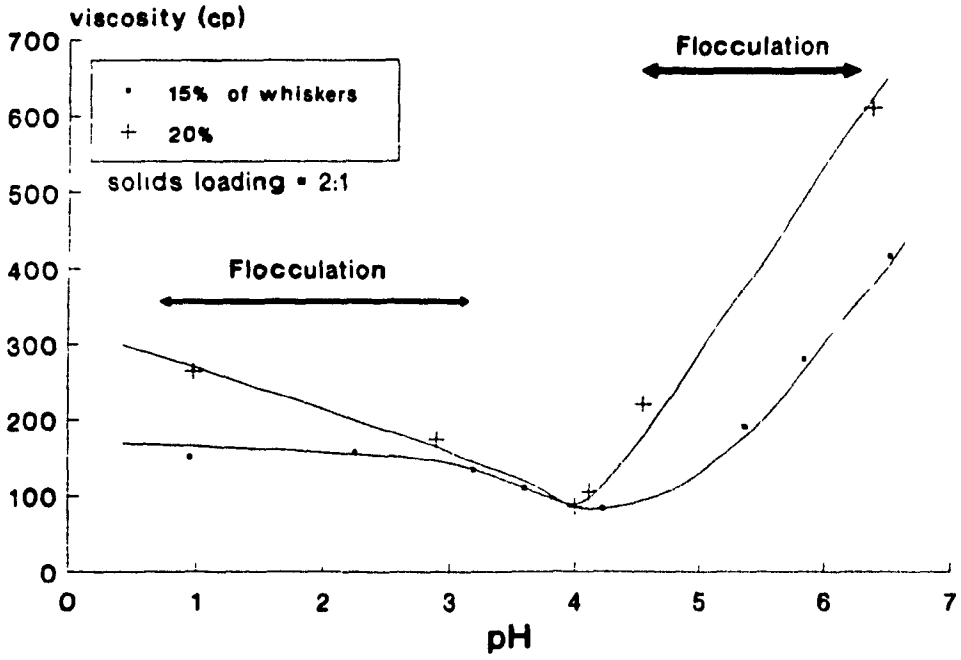

Fig 5.2: Viscosity vs pH for slurries containing
15 and 20 wt% of whiskers

In addition, Figure 5.1 shows the marginal effect of a whisker content of up to 10 weight percent on the viscosity. In fact, the two curves (0 and 10%) are very similar and the minimum viscosity is observed at pH=4.8.

The viscosity of the slurries containing more than 10% whiskers however, appears to be more sensitive to a change in pH, as shown in Figure 5.2. Flocculation occurs rapidly as the pH increases or decreases from the minimum viscosity value.

Both the surface chemistry and the surface area of the colloidal particles play an important role in the dispersion behaviour. The silica layer around the particles and the whiskers can easily form a silanol which could lead to aggregation of the colloidal particles. The high surface area of the whiskers allows this to occur easily, therefore flocculation of the slurry containing a high percentage of whiskers occurs rapidly as the pH changes from the minimum viscosity value.

A good dispersion of whiskers was obtained in the pH range of 4 to 5.

5.1.2 INFLUENCE OF pH AND WHISKER CONTENT ON THE GREEN DENSITY

Compacts were fabricated by slip casting the slurry previously used for viscosity measurements. The compacts were then characterized using green density measurements.

No significant changes in the relative densities of the compacts containing 0 to 15% whiskers were observed in the pH range of 4 to 5 (Fig 5.3), where deflocculation of the slip occurs. A relative density of ~53% was measured for the compacts containing 0 to 15% whiskers. For these compacts, the green density remains nearly constant with increasing pH and this means that the aggregates formed at a pH value outside the minimum range are small enough not to hinder the compaction during slip casting.

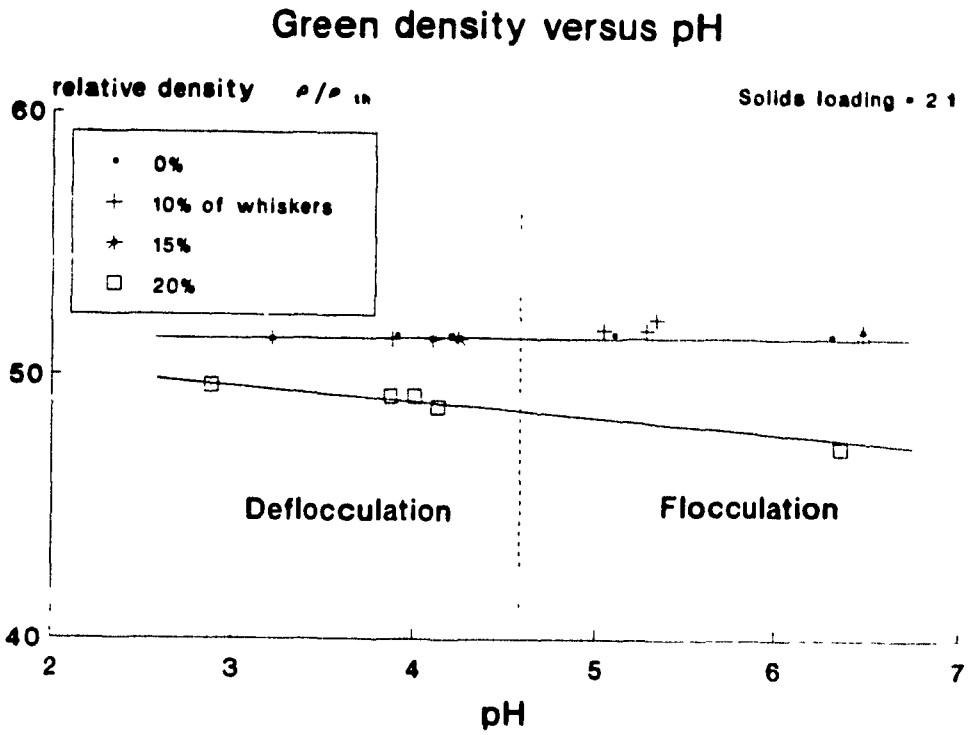

Fig 5.3: Relative density vs pH for slurries containing 0 to 20 wt% of whiskers

For compacts containing 20% whiskers, the green density decreased with increasing pH. Higher densities were observed at low pH where some flocculation occurs, possibly due to the presence of a bimodal aggregate size distribution, however, the variation in green density is actually very small, ranging over only 3%.

The relative densities of compacts prepared from a deflocculated slip (obtained at minimum viscosity) versus percentage of whiskers are given in Fig 5.4. In a dry powder/whisker mixture, packing would become more difficult with increasing whisker content process. However, in the present case, the very nature of the slip casting method, namely suction of the liquid, allows the percolation of powder between whisker bridges and thus, even with high whisker content of 20 wt%, the green density only decreases by 4%.

The effect of whiskers

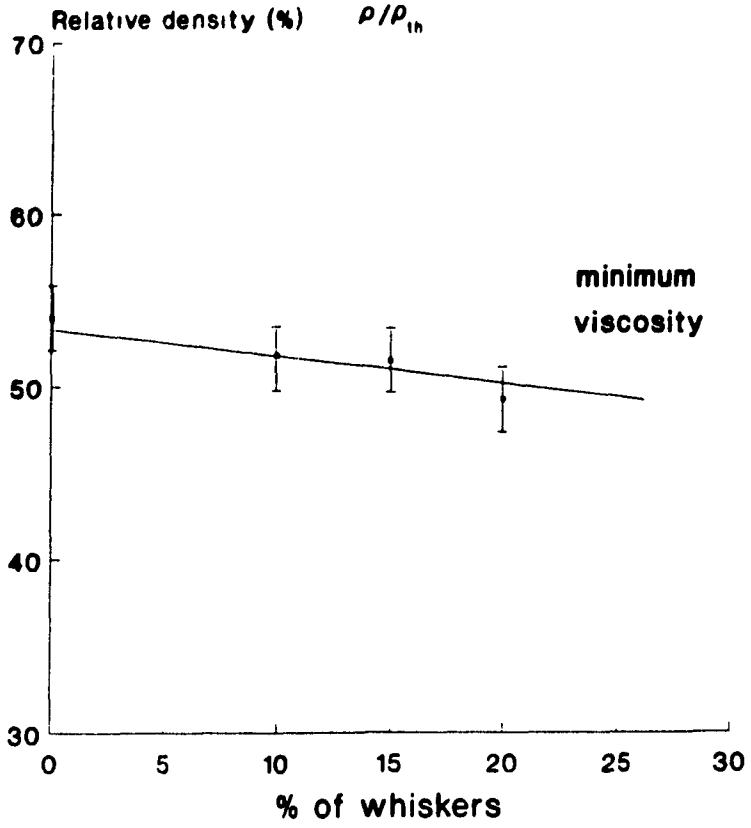

Fig 5.4: Relative density vs % of whiskers for slurries at minimum viscosity

5.1.3 MICROSTRUCTURAL EXAMINATION

An analysis of the microstructure of a fractured green surface (Fig 5.5) shows good dispersion of the whiskers in the powder for samples prepared from a deflocculated slip. A good dispersion of the whiskers was obtained in a 20% SiC whiskers compact fabricated at pH 4, whereas bundles of whiskers were observed in some areas in compacts fabricated at higher pH (Fig 5.6). Within the fracture surface, low density regions were observed, showing the uneven distribution of whiskers in the compact fabricated at even higher pH conditions (pH=10.6) (Fig 5.7). The presence of low density regions and whisker agglomerates are undesirable in the finished compact as they will be stress concentrators and possible flaw initiation sites.

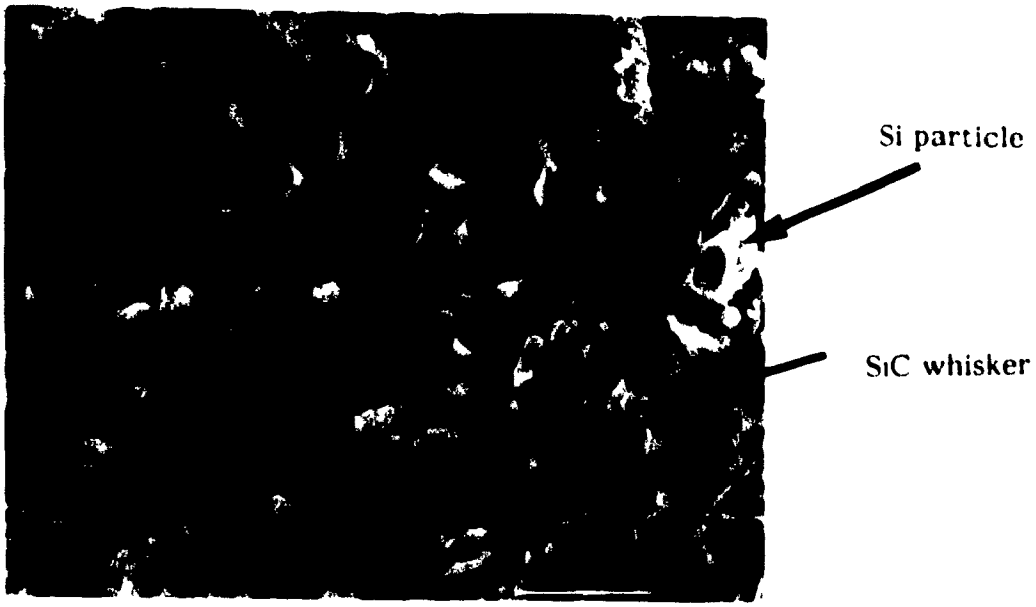

Fig 5.5: Fracture surface of a green(Si + 20% SiCw) compact (pH=4) showing a good dispersion of whiskers

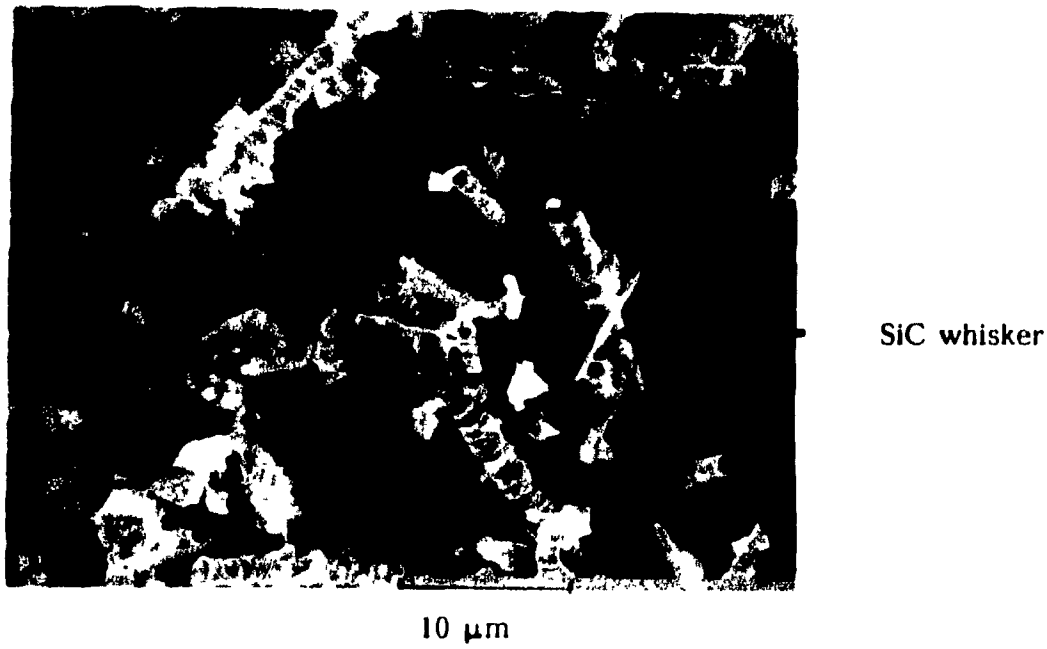

Fig 5.6: Fracture surface of a green (Si + 20% SiCw) compact (pH=6.5), showing a bundle of whiskers

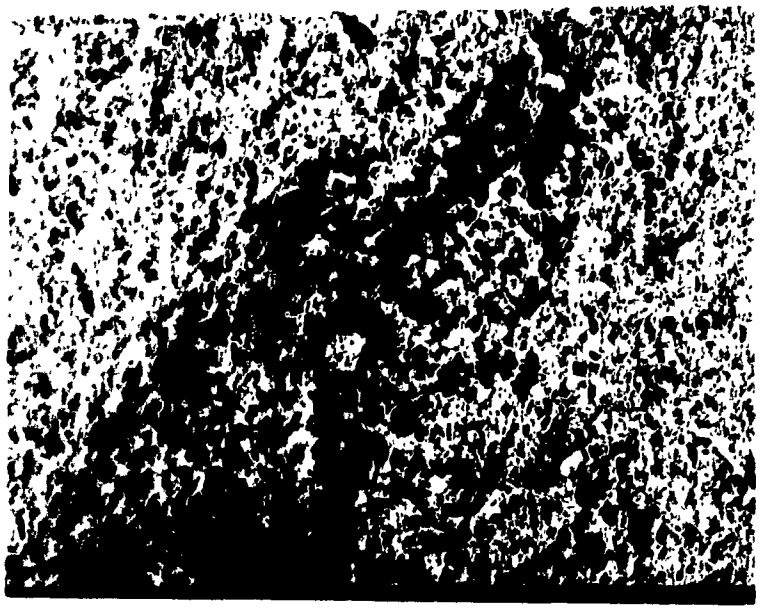

Fig 5.7: Fracture surface of a green (Si + 10% SiCw) compact (pH=10.5), showing a low density region

It is apparent that careful pH adjustment leads to a good dispersion of the whiskers in the green compact. All the nitrided samples were therefore fabricated under conditions of minimum viscosity. A kinetic study of the nitridation is presented in the following section.

5.2 KINETICS OF NITRIDATION

As discussed in the literature survey, it has been suggested that the overall kinetics of the Si_3N_4 formation are, in fact, the sum of different kinetic steps corresponding to several stages in the nitriding mechanism (27).

The kinetic study performed here was carried out by recording the weight gain of different compacts at fixed temperature under nitrogen gas flow as a function of time. Compacts containing 0% to 30 wt% whiskers were nitrided at a constant temperature, ranging from 1315ºC to 1390ºC. The kinetic study is based on the results obtained from the thermogravimetric curves (Fig 5.8, 5.9 and 5.10).

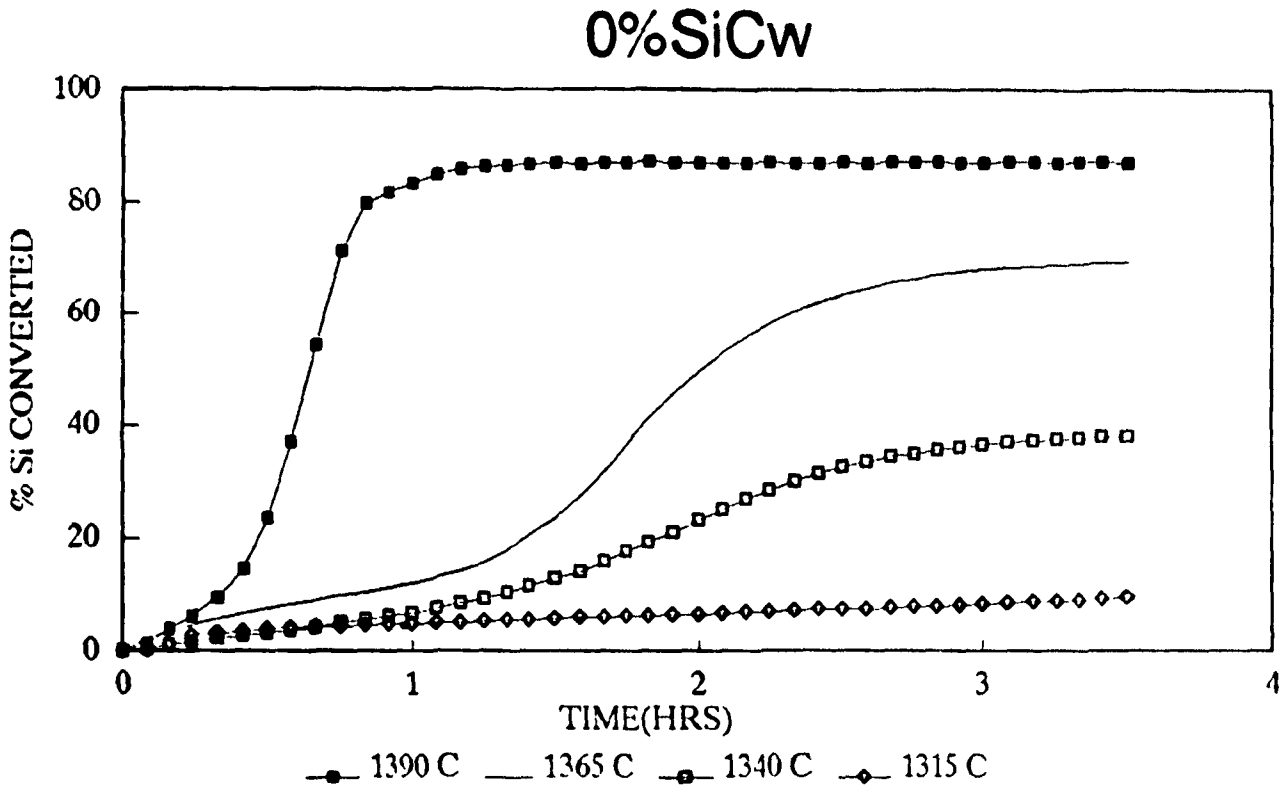

Fig 5.8: Thermogravimetric curve of the nitridation of 0% SiCw-compacts

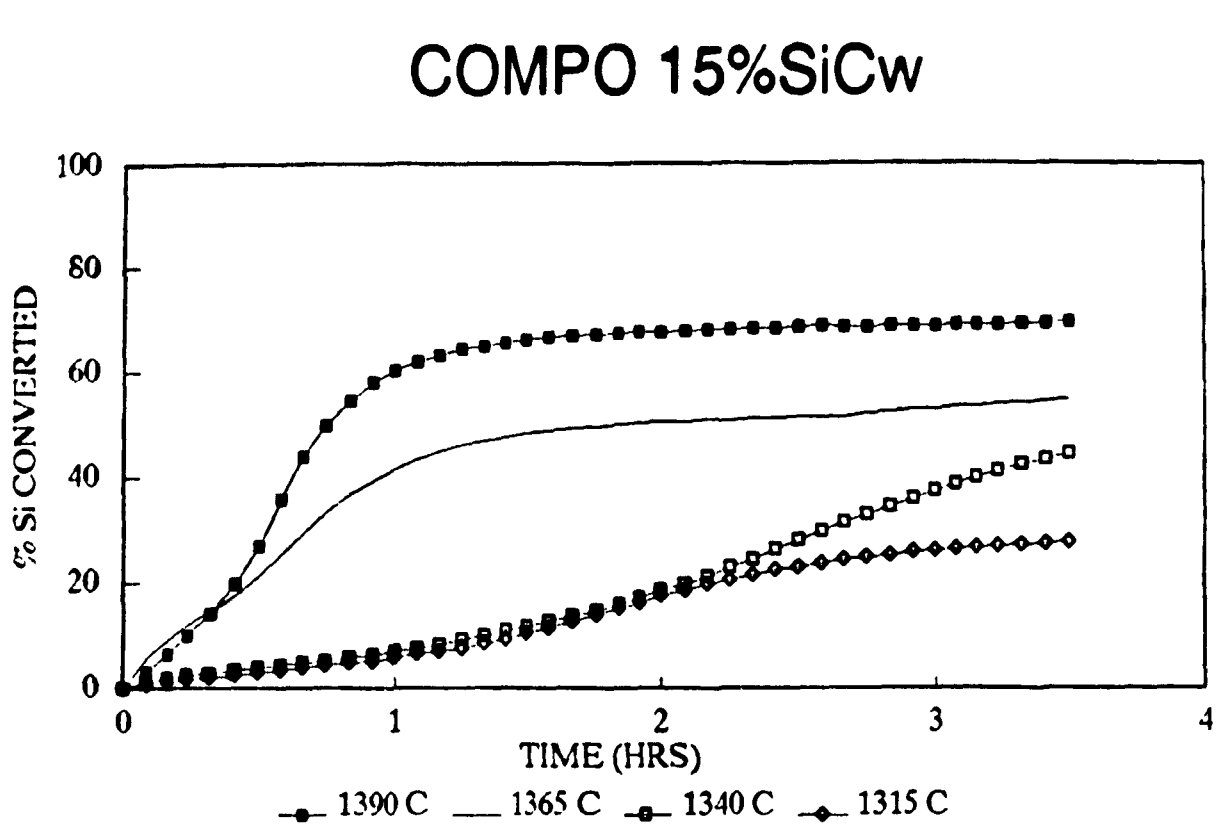

Fig 5.9: Thermogravimetric curve of the nitridation of 15% SiCw-compacts

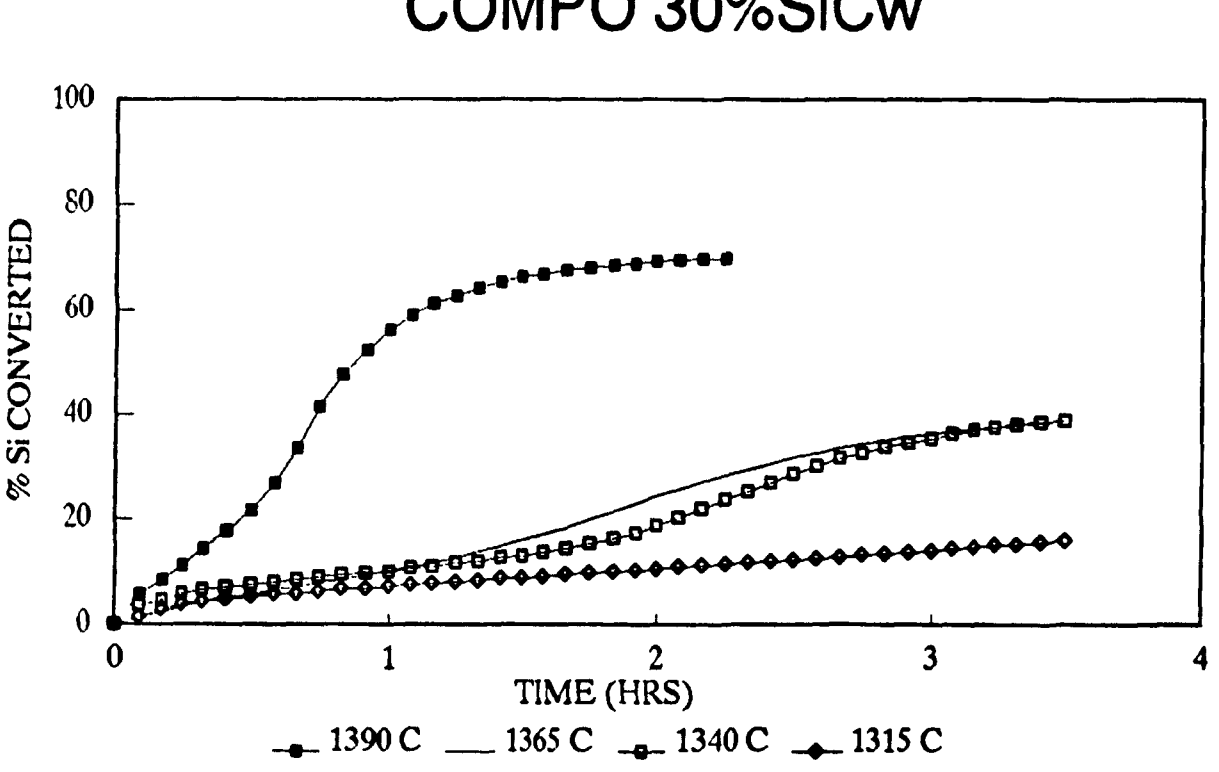

Fig 5.10: Thermogravimetric curve of the nitridation of 20% SiCw-compacts

The thermogravimetric curve can be divided into 3 major sections as shown in Fig 5.11.

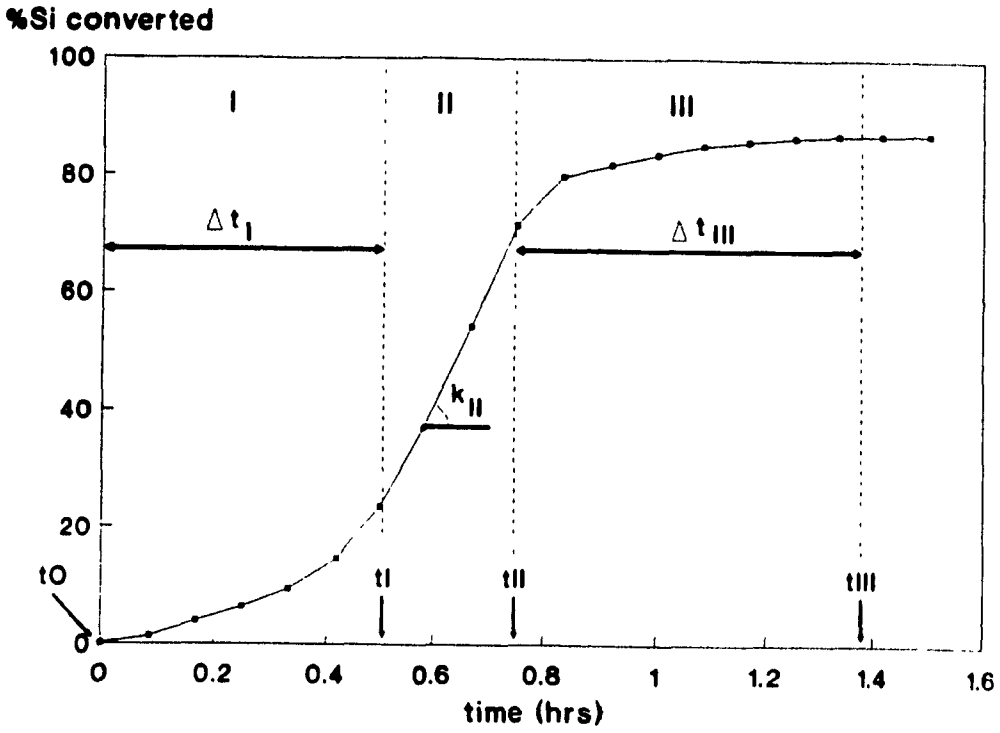

Fig 5.11: Schematic of a typical thermogravimetric curve

Section I corresponds to the induction period; the adsorption of nitrogen on the surface of the particles and the start of nucleation and growth of Si_3N_4 crystals. In this part, only a small amount of nitridation occurs. The duration of this part strongly depends on the presence or absence of a silica layer on the surface of the silicon particles which may vary from compact to compact and therefore, no kinetic analysis was carried out on section I of the curves.

The second section of the curve corresponds to the nucleation and growth of the Si_3N_4 crystals followed by the formation of α and β Si_3N_4. The weight gain is linear with respect to time and strongly depends on the temperature. This part of the curve can be described by the equation $\Delta M/A = k_{II}t$, where k_{II} is the linear rate constant (30).

The third section of the thermogravimetric curve corresponds to the final stage where the reaction rate decreases and eventually reaches zero.

As one can readily see from the curves (Fig 5.8-11) the conversion of silicon to silicon nitride occurs much more rapidly at higher temperature, whether whiskers are present or not. In addition, the final amount of silicon converted is higher for those samples nitrided at higher temperature (1390ºC). Samples nitrided at lower temperatures produce a lower yield of Si_3N_4 even at longer times.

In order to analyze these results more thoroughly, the thermogravimetric curves were differentiated. Derivatives of a thermogravimetric curve (Fig 5.12) allow for the determination of three kinetic parameters. In fact, these curves present a maximum denoted by (t_M,k_{II}), where k_{II} gives the value of the linear rate constant of section II. t_0 is the starting time of the run; t_I is defined as the time at which the derivative curve starts its raise to the maximum, t_{II} the time just after the maximum and t_{III} the time at which the derivative curve reaches zero. Thus, $\Delta t_I=t_I-t_0$ gives the duration of section I, k_{II} the linear rate constant describing section II and $\Delta t_{III}=t_{III}-t_{II}$ the duration of the final stage. These values were calculated for all the thermogravimetric runs obtained in the kinetic study and, in the following sections, the effects of temperature and percentage of whiskers on these three parameters will be presented and discussed.

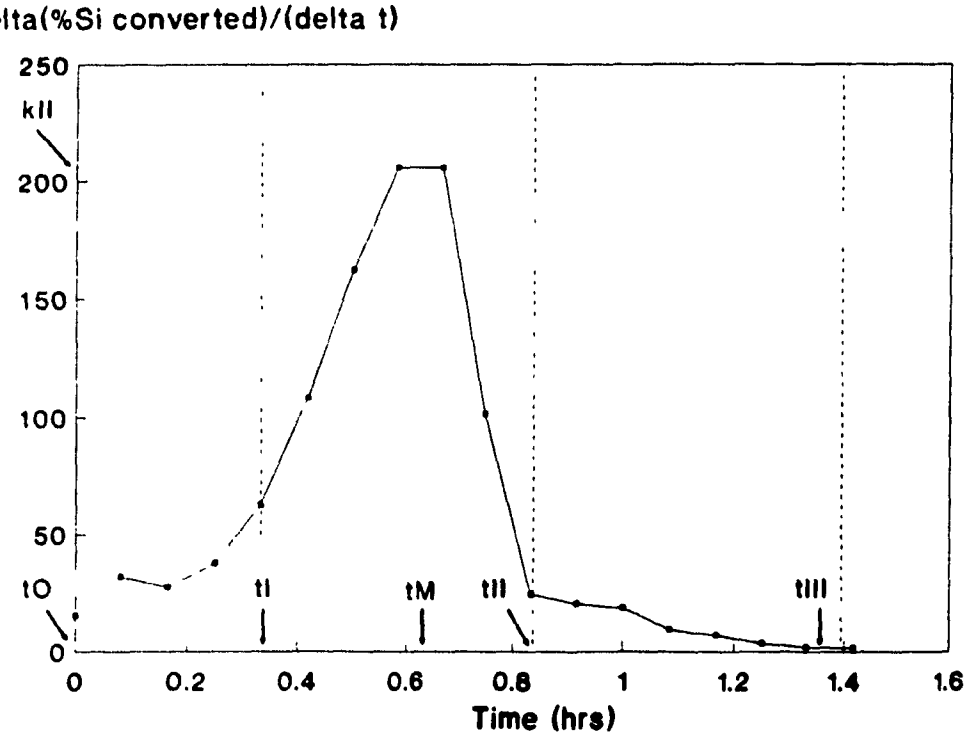

Fig 5.12: Derivative of a typical thermogravimetric curve

5.2.1 EFFECT OF TEMPERATURE

In order to gain an understanding of the effect of temperature on the reaction rates of RBSN whisker composites, it is necessary to establish the dependence of conversion of pure Si compacts on temperature.

Thus, this section will deal with this first, before discussing the effects of whisker additions on the nitridation.

Table 5.1 presents values of Δt_I, the duration of the induction period and the nucleation and growth of Si_3N_4 crystals. The duration of this period decreases from 1.35 to 0.4 hours on increasing the temperature from 1340ºC to 1390ºC.

In fact , it can be said that the removal of the SiO_2 layer is accelerated by an increase in temperature. SiO_2 can react with silicon to form gaseous SiO and in this way be eliminated during the nitridation process. The disruption of the amorphous silica film then leads to the direct exposure of the underlying Si. Nucleation and growth of Si_3N_4 can then easily occur.

T(ºC)	Δt_I(hrs)	k_{II}(%Siconv/min)	Δt_{III}(hrs)
1340	1.35	0.4	1.8
1365	1.3	0.9	1.75
1390	0.4	3.4	1

Table 5.1: Kinetic parameters

As shown in table 5.1, on increasing the temperature from 1340 to 1390ºC, the linear rate constant increases from 0.4 to 3.43% of silicon converted per minute. Increasing the temperature has the effect of accelerating the evaporation-condensation process and also of increasing nitrogen diffusion. At higher temperatures, the formation of β-Si_3N_4 occurs. It has been suggested that this reaction happens in the liquid state. The nitrogen diffuses through a liquid, often $FeSi_2$, or down the large channels which exist in the c-direction of the β-Si_3N_4 structure.

Table 5.1 presents values of Δt_{III}, which corresponds to the duration of the final conversion stage of the nitriding mechanism.

Considering only the effect of the temperature, the duration of the final stage decreases to 1 hour at 1390ºC, from 1.8 hours at 1340ºC.

At this point, a nitride layer exists and nitrogen must diffuse through the last pore channels or in the liquid phase. Thus, as diffusion is temperature dependent this decrease in the rate of conversion is expected. At 1390ºC, a liquid phase is present due to the exothermic nature of nitridation; the local temperature exceeds the melting point of Silicon (1410ºC)and thus the rate determining step is now diffusion through the liquid phase rather than the solid nitride phase, and as diffusion under these conditions is considerably higher, the value of Δt_{III} decreases.

5.2.2 EFFECT OF WHISKER CONTENT

Once the kinetic data for compacts containing only silicon were established, those for whisker-containing samples were obtained and these results are given in Table 5.2, 5.3 and 5.4 for different compacts ranging in whisker content from 0 to 30 wt%.

T(ºC)	0% SiCw	15% SiCw	30% SiCw
1340	1.35	1.7	1.7
1365	1.3	(0.8)	1.5
1390	0.4	0.4	0.5

Table 5.2: Kinetic time Δt_I (hrs)

At low temperature, higher values of Δt_I are obtained with increasing whisker content indicating that a longer induction period was required for these samples.

There are several possible explanations for this behavior: firstly, the diffusion of nitrogen through the pore channels could be hindered by the presence of the whiskers which may form a network in the structure, however the whiskers are very fine and may in fact be leading to a more open network. Secondly, the whiskers which are SiC, are, like the silicon powder, prone to surface oxidation and likely to be covered in a silica film (50). This may be responsible for increasing the induction period as more SiO_2 has to be removed before conditions (pN_2, pSiO) are suitable for nucleation/nitridation. In addition, these SiC whiskers may also provide sites for nucleation of Si_3N_4 particles/whiskers formed from the gaseous phase without providing material for the subsequent growth of these nuclei as would be the case on a silicon particle. In fact, whiskers only allow low directional growth of nuclei from their surface to form Si_3N_4 needles. In this way the nucleation rate would increase at the expense of the growth of these nuclei.

T(ºC)	0% SiCw	15% SiCw	30% SiCw
1340	0.4	0.4	0.4
1365	0.9	0.8	0.3
1390	3.4	1.8	1.6

Table 5.3: Kinetic rate constant k_{II} (%Siconv/min)

Table 5.3 gives the kinetic rate constant (k_{II}) values for the different nitridations. The kinetics of formation of α- and β-Si_3N_4 are reduced by the presence of whiskers.

In addition to the aforementioned argument concerning increased nucleation at the expense of growth, another factor may be contributing to the decrease in reaction rate. Because of the volume expansion during nitridation, new pores for reaction products must be created in the silicon compact to allow for nitrogen diffusion and subsequent reaction. The whisker network, which will not form pores, may hinder the creation of the space required for the reaction to progress.

T(ºC)	0% SiCw	15% SiCw	30% SiCw
1340	1.25	0.9	0.85
1365	1.2	1	0.8
1390	0.5	1.1	1.1

Table 5.4: Kinetic time Δt_{III} (hrs)

Table 5.4 shows that there is a shorter final conversion stage in the nitridation of whisker containing compacts at 1340ºC and 1365ºC than for Si-only compacts. The final period corresponds to the closure of all channels in the nitride layer. Due probably to the difficulty for N_2 to penetrate through the partially converted whisker-containing compact, the final stage of nitridation (and associated weight gain) in the whisker-compacts is reduced.

At 1390ºC, the pattern is reversed and the silicon-only compact stops converting in a shorter time. This is due to local melting in the compact at this temperature. Due to the exothermic reaction ($Si \rightarrow Si_3N_4$) temperatures within the compact may rise above the melting point of silicon and cause melting, producing a faster, uncontrolled reaction. In a pure silicon compact this melting can cause the formation of large pores and small regions of unreacted silicon (see Fig 2.17) and is generally undesirable.

This type of phenomena was not observed in the whisker containing compacts. This may be due to two reasons: firstly, the SiC whisker network may help in reducing any thermal build-up and secondly, because a structural network exists due to the presence of the whiskers, the amount of silicon that can melt and cause large pores is limited to a small amount; in effect only between the whiskers. Therefore, it has been possible to carry out complete nitridation experiments of such whisker compacts even up to 1415ºC (above the silicon melting point).

To summarize, it is believed that the effect of temperature is more important than the effect of whisker content on the kinetics of nitridation. In fact, increasing the temperature up to 1365ºC leads to an acceleration of the removal of silica layer and the evaporation-condensation process. At higher temperature (1390ºC), diffusion in the liquid state occurs due to the presence of molten silicon or $FeSi_2$. In this liquid state, the diffusion is faster, corresponding to rapid nitridation.

The presence of whiskers plays a smaller effect on the kinetics. Since a whisker network exists in the compact, diffusion of nitrogen through the pore channels or creation of the space required for the reaction to progress may be hindered, whereas a surplus of silica available to be converted into SiO gas is present, leading to an important nucleation step during the nitridation. One beneficial effect of the whiskers is to allow nitridation at higher temperatures without excessive melt-out of silicon. There is therefore a compromise between the factors which accelerate or hinder the nitridation kinetics, probably explaining the small effect of whisker additions.

Having discussed the influence of the temperature and whiskers content on the kinetics of Si_3N_4 formation, it is important to note that only the rate of nitridation has been considered. In the following section, the study will focus on the degree of silicon conversion into silicon nitride, as a function of the green density of the compacts and of the whisker content.

5.3 REACTION BONDING

In the previous section (5.2), it was seen that the nitridation kinetics depend more on the temperature than on the whisker content of the compact.

Another parameter that also effects the nitridation process is that of green density (section 2.2.5).

As the nitridation reaction progresses into the silicon, volume expansion occurs and the pores are refilled with nitride. The green density is therefore an important factor in influencing the nitridation mechanism.

5.3.1 EFFECT OF GREEN DENSITY ON THE NITRIDATION MECHANISM

In order to investigate the effect of green density on the nitridation behavior of these composites, experiments were carried out on compacts prepared with varying green densities.

Compacts with relative green densities of between 44 to 70 percent, containing 0% and 18% SiC whiskers, were prepared and nitrided for 22 hours according to the temperature-time program presented in Chapter 4.

The thermogravimetric curve for the pure silicon compacts is presented in figure 5.13.

Initially, the weight gains were fastest in the densest compact and considerably slower in the most porous compact. This stage of the nitridation, whereby the particle surface absorbs nitrogen, corresponds to the beginning of the nucleation period. It is possible that the green density of the samples plays a certain role in this behavior, but it depends more on the surface chemistry of the particles in the different compacts, as seen previously (section 4.1). Nonetheless, it should be pointed out that the induction period in the nitridation of samples with a low density is shorter than for the others. This could be explained by the more

rapid "cleaning" of the larger pores (removal of SiO_2). As this would be resulting in weight loss (SiO_2 solid → SiO_2 gas), the overall weight gain (due to nitridation) would be lower until the oxide was removed and then the weight gain would increase rapidly.

This can be seen at ~9 hrs (~1300ºC) when the rate of nitridation on the lowest density (1.17 g/cm^3) compact increases quite rapidly, to give ~ 40% conversion. This could be the result of the rapid growth of the nitride layer on the external surfaces of the silicon particles, due to the nitrogen's facility to diffuse into the larger pores.

After this however, the conversion rate decreases for the low density compact, fluctuating at the points where the temperature was raised. The overall conversion was less than 80%. As it is most likely that gaseous phases (N, N_2, Si, SiO) are the primary reactants in nitriding, a more open compact (lower density) would be more prone to a "flushing" action from the flowing nitrogen atmosphere around the sample and this may account for the lower conversion. In addition, due to the rapid growth of the nitride layer on the external surface of the silicon particles, some silicon would be trapped inside these particles, which would explain the high Si content found in the final product. On the other hand, if the growth of the nitride layer were important, sintering between particles could occur before complete nitridation. This could lead to the closure of the pores, which would act as barriers to the transport of reactants.

In a dense structure, the progress of the nitridation is slower but results in a higher conversion rate. The final plateau in the thermogravimetric curve (Fig 5.13) is reached later by the denser compact but attains the highest percentage conversion.

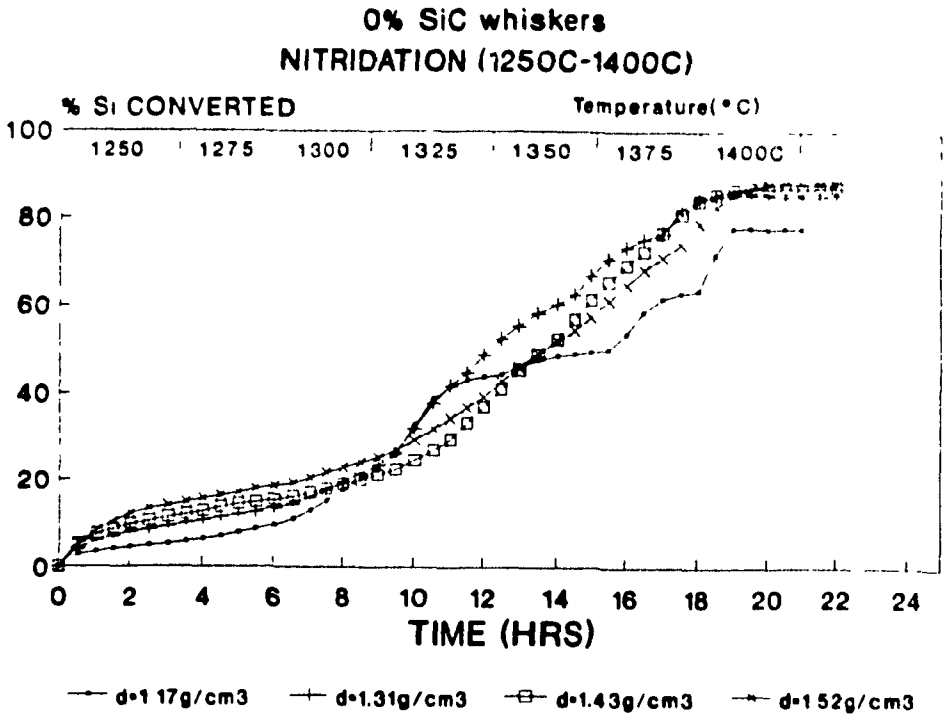

Fig 5.13: %Si converted vs time for sample without whiskers

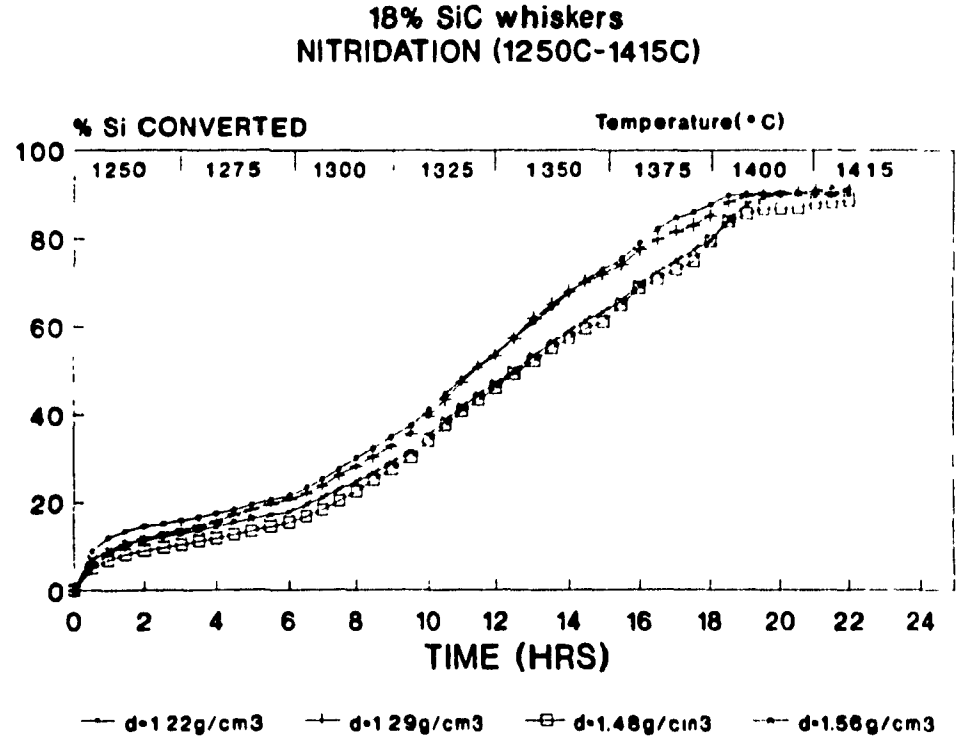

Fig 5.14: %Si converted vs time for sample containing 18 wt% whiskers

5.3.2 EFFECT OF WHISKER CONTENT

Figure 5.14 presents the nitriding behavior of compacts containing whiskers. All the curves have the same appearance, similar to the highest density 0% whiskers compacts. However, the lower density compacts (1.22 g/cm^3 and 1.29 g/cm^3) start faster than the highest density compacts but once started, they appear to follow similar kinetics.

A slightly higher amount of Si_3N_4 is obtained from the lower density samples containing whiskers (Figure 5.15). However at higher green densities (and higher nitrided densities) this difference is negligible.

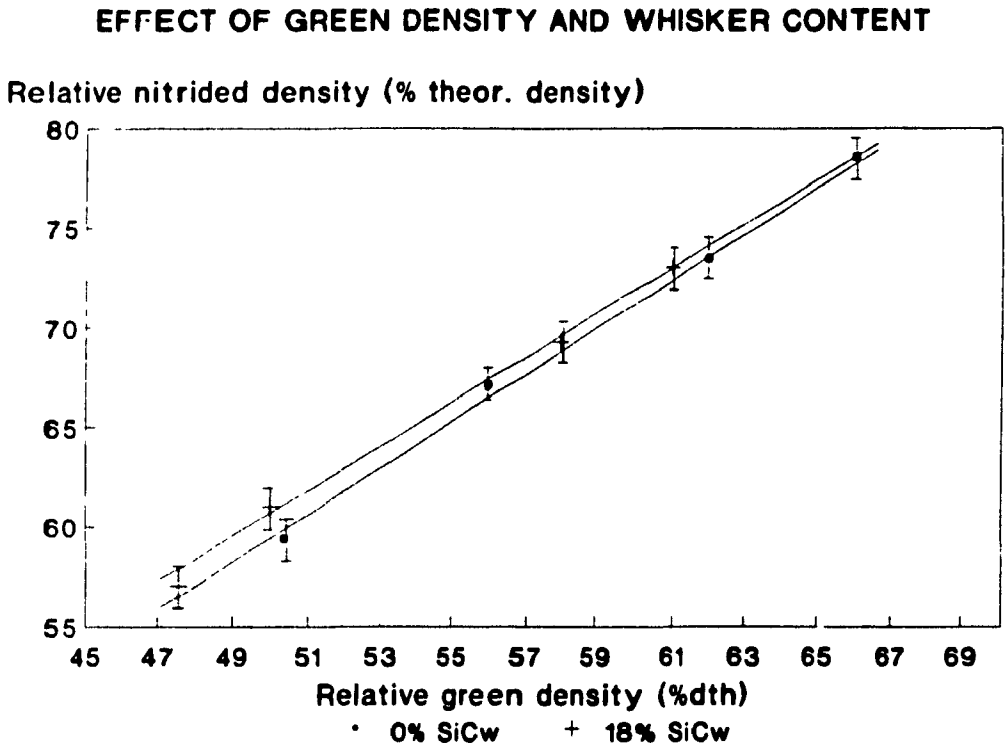

Fig 5.15: Relative nitrided density vs relative green density for samples containing 0 and 18 wt% SiC whiskers

As the green density increases, the nitrided density increases, in accordance with the previous discussion and the literature (43).

X-ray diffraction analysis shows that α-Si_3N_4 is the predominant phase produced (70 percent) in this range of temperatures, and there is no difference in the α/β ratio for samples containing whiskers. An average of 90% Si converted was obtained. More complete conversion might be achieved at a higher temperature, but local overheating and melting of Si was observed when this was attempted, leading to a microstructure with large voids that are associated with poor mechanical properties.

To summarize, it is believed that the effect of green density is more important than the effect of whisker content of the nitridation behavior. A lower percentage of Si_3N_4 has been obtained in the nitridation of low density compacts, possibly due to too fast a rate at the beginning of the nitridation, leading to trapped and unconverted silicon or closure of pores channels before complete nitridation.

No significant effect of whiskers have been noticed. However a slightly higher degree of conversion has been obtained for compacts containing whiskers

5.3.3 MICROSTRUCTURAL EXAMINATION

An analysis of a polished nitrided surface shows a high porosity of ~25 percent. Pores are connected together in the α-Si_3N_4 matte, which is the predominant microconstituent (Figure 5.16).

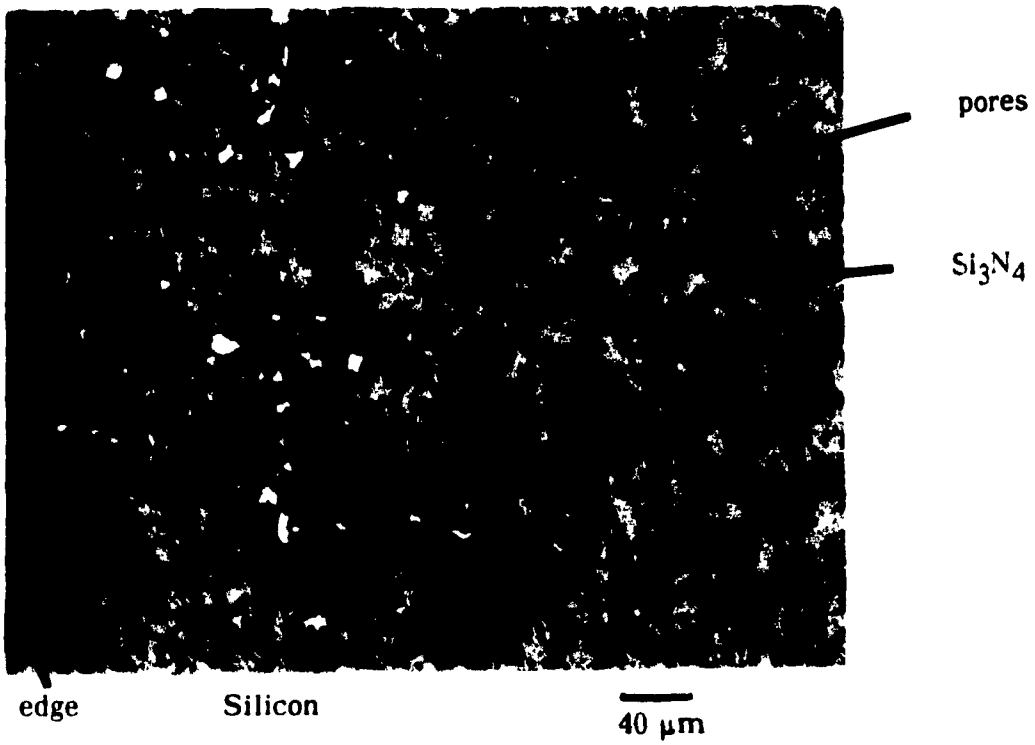

Fig 5.16: Optical micrograph of the edge of a nitrided sample without whiskers

Microstructural observations of samples with different nitrided densities show that an increase in nitrided density is coupled to a decrease in pore size. In fact, the pore size varies from 0.5 to 12µm in a sample containing 21 percent pores whilst at a higher porosity of 33 percent, the largest pore size reaches 40µm. This nitrided porosity distribution reflects more or less the green distribution. This can be explained by the nitridation process, whereby the porosity decreases by approximately 20 percent as the solid's volume increases.

No difference in porosity was observed between the edge and the center of the sample. However, unconverted silicon remains predominantly at the edge of the sample. This may result from the temperature gradient present in the sample; the sample center being hotter than the edge due to the exothermic nature of the reaction and thus more complete conversion of Si to Si_3N_4 at the center compared to the periphery.

That some silicon remains trapped inside the alpha silicon nitride matte can be seen in Figure 5.17.

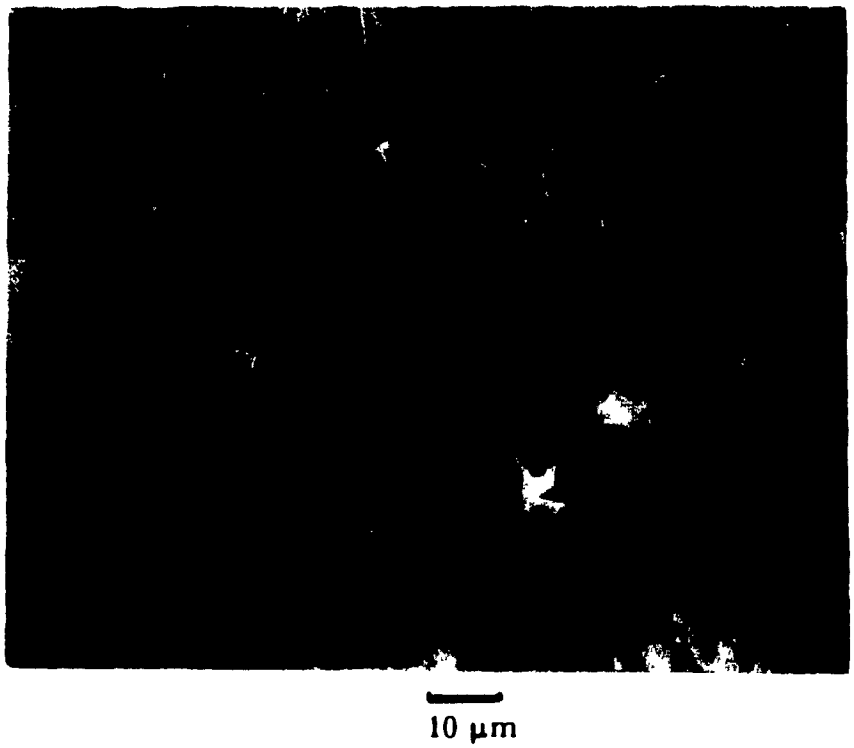

Fig 5.17: Optical micrograph of nitrided sample showing trapped Si (white phase).

At a higher magnification, the microstructural examination shows that the alpha silicon nitride is present as a matte and as needles (Fig 5.18) as described in the literature (31).

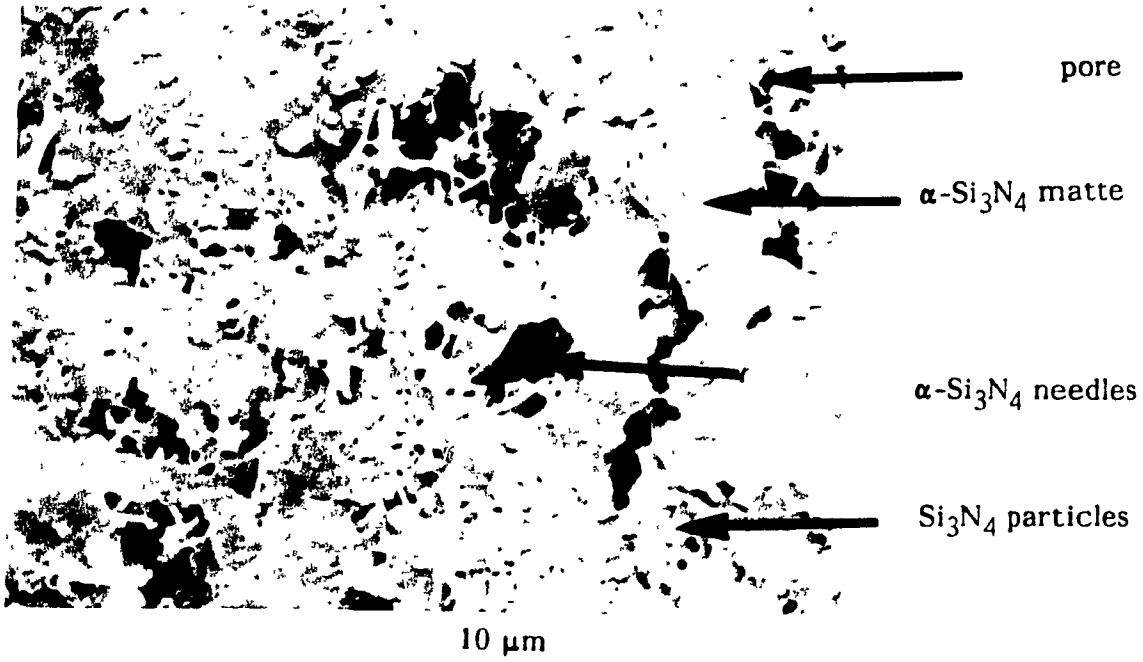

Fig 5.18: Fracture surface of nitrided sample with no whiskers (SEM)

The matte is formed around the large particles and is constituted of fine grains. The pores are filled by α-Si_3N_4 needles that grew from the surface of silicon particles (Fig 5.19).

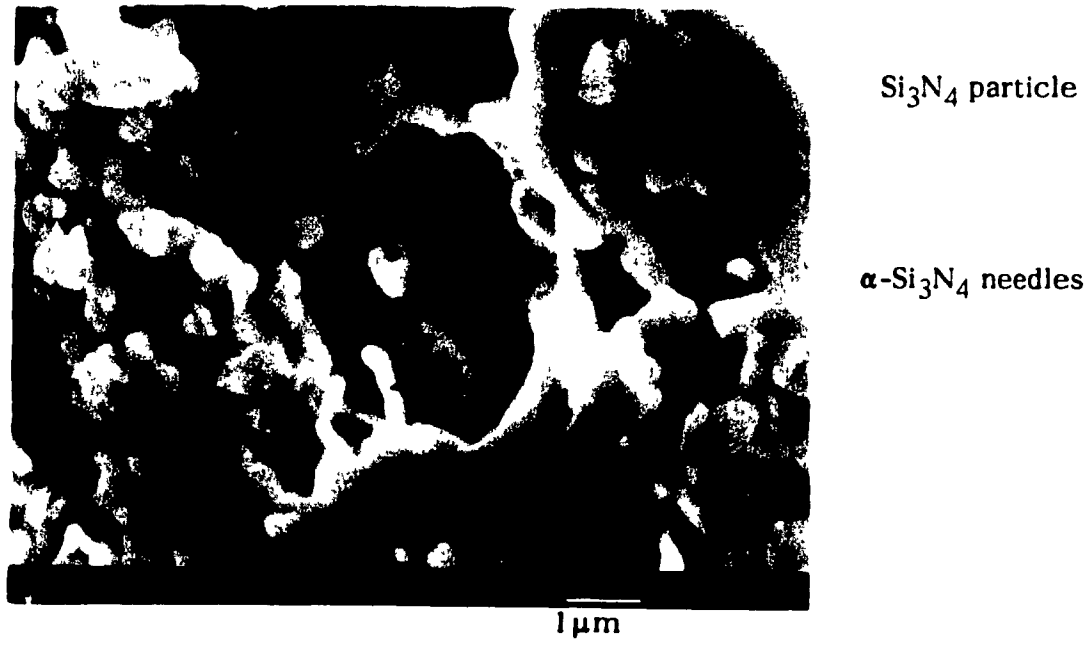

Fig 5.19: α-Si_3N_4 needles in a pore.

Fracture surface of nitrided sample with no whiskers (SEM)

According to the literature (31), alpha needles form by a vapor-liquid-solid mechanism. The beads at the terminus of some needles (Fig 5.20) often contain impurities such as Fe, which can lower the melting temperature of the silicon, thus promoting growth at lower temperature. Silicon vapor is transported to the bead where nitrogen reacts at the solid-liquid interface to form silicon nitride, which then lengthens the needle.

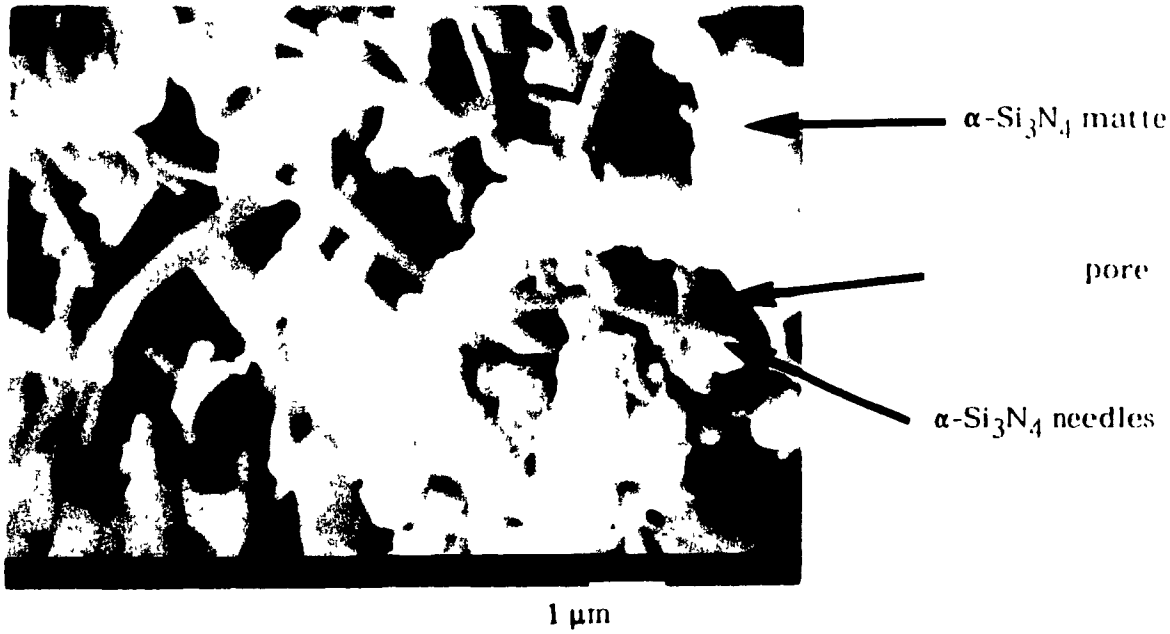

Fig 5.20: Pore filled with α-Si_3N_4 needles
Fracture surface of nitrided sample with no whiskers

Interesting microporosity was observed in the α matte. Circular micropores of less that 1 μm of diameter exist at the border between the particles and the matte (Fig 5.21).

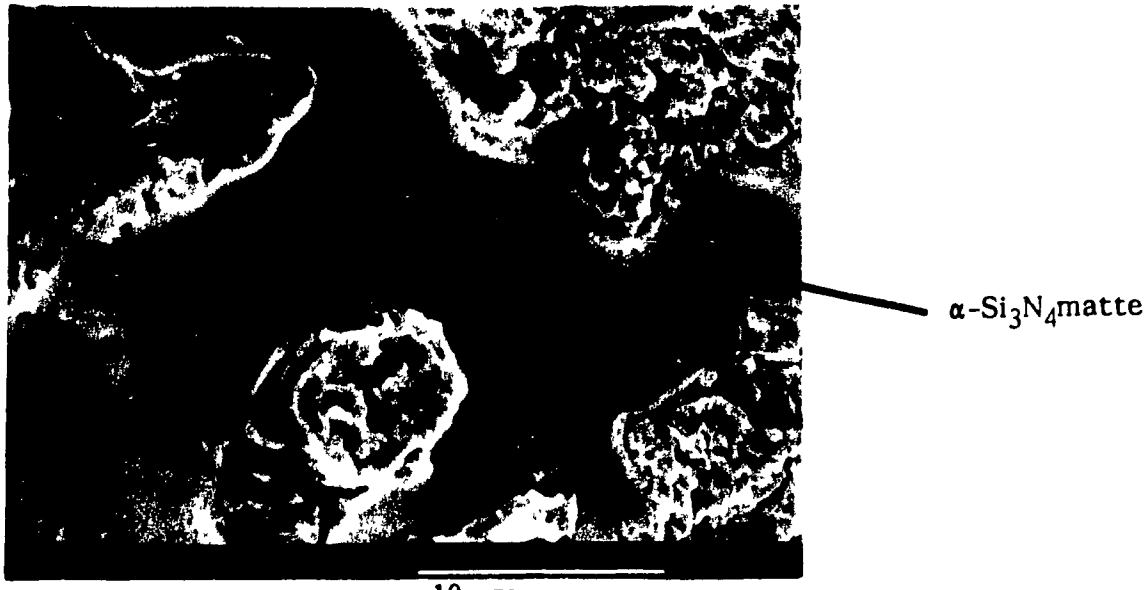

Fig 5.21: α-Si_3N_4 matte around large grains
Fracture surface of nitrided sample with no whiskers

It has been suggested (section 2.2.2), that the α matte is formed from the vapor state; the reaction generates pores where the silicon evaporated. In these newly formed pores, nitrogen reacts with Si or SiO in the gas phase and condensation of silicon nitride partially refills the newly formed pores, but some small pores remain in the α matte (Fig 5.22).

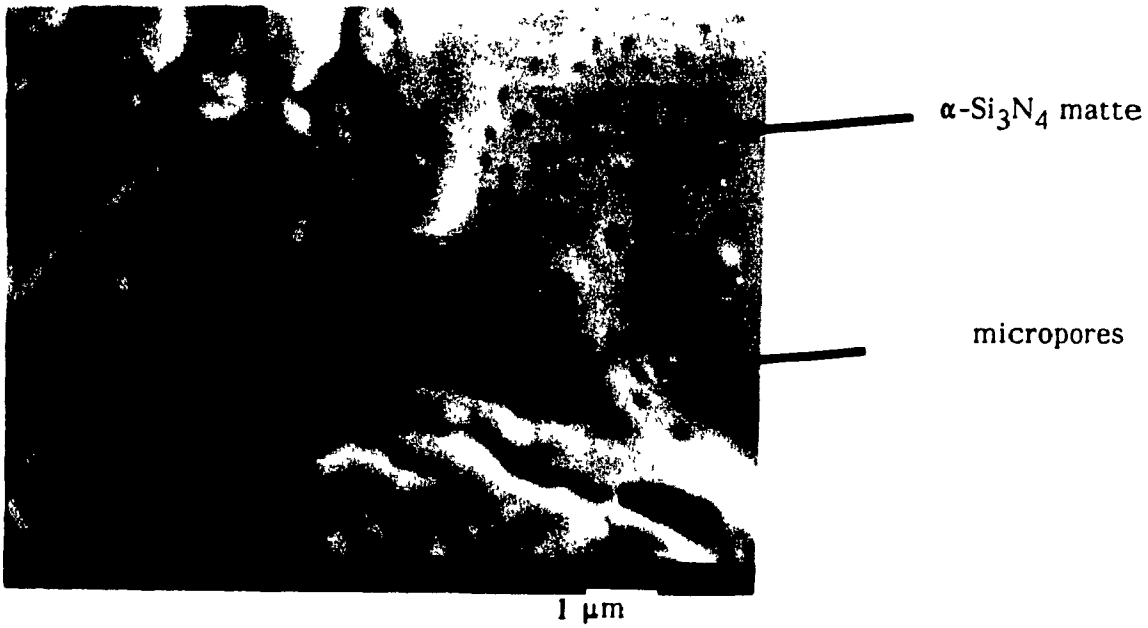

Fig 5.22: Microporosity in the α-Si_3N_4 matte
Fracture surface of nitrided sample with no whiskers

The beta phase is difficult to distinguish from the alpha phase, but it was located by the presence of beta spikes. Figure 5.23 shows beta spikes emerging from the beta phase into a larger pore.

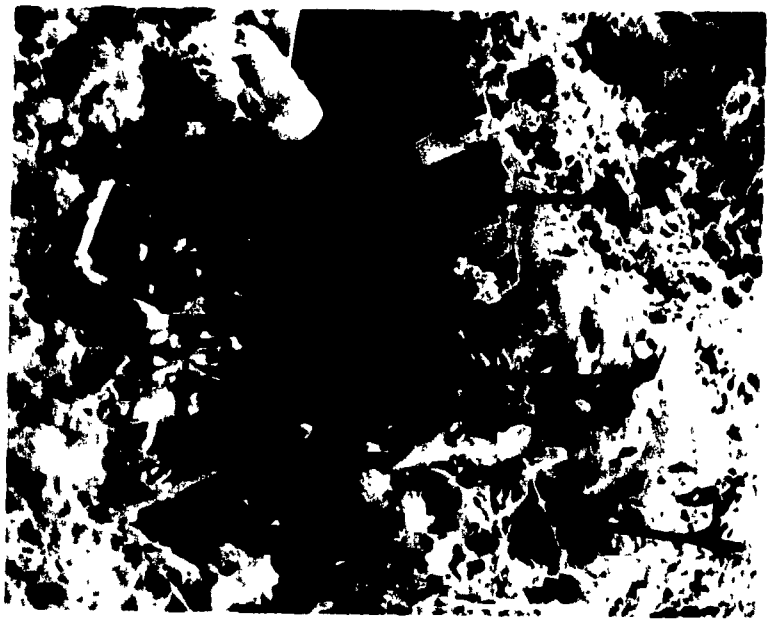

Fig 5.23: β-Si_3N_4 spikes emerging in a pore
Fracture surface of nitrided sample containing 30wt% whiskers

The β spikes have an aspect ratio of 2, which is smaller than that of the alpha needles (25). It is suggested (31) that as such a reaction progresses, the spikes become larger; they coalesce and fuse together, forming a large grained beta phase. The grain size is much larger than the size of the alpha grains. The large pore from which the beta spikes emerge was probably formed when silicon melted and flowed away.

The predominant microconstituents, alpha needles, alpha phase matte and beta spikes, are also observed in nitrided samples containing SiC whiskers. No particular difference was noted. The initial SiC whiskers, completely covered by Si_3N_4 particles, are difficult to distinguish from the rest of the microconstituents (Fig 5.24) even at high magnification in a fracture surface.

Fig 5.24: SiC whisker covered by Si_3N_4 particles
Fracture surface of nitrided sample containing 15 wt% whiskers

Optical observations show that the composite porosity follows the same tendency as the RBSN sample: it decreases by 20 percent during the reaction, and whiskers are no hindrance to the phenomena.

In longitudinal and horizontal sections, whiskers are observed (Fig 5.25)as lighter phases in the RBSN. They appear to be well bonded in the alpha matte. This is likely explained by the growth of the nitride around the acicular structure.

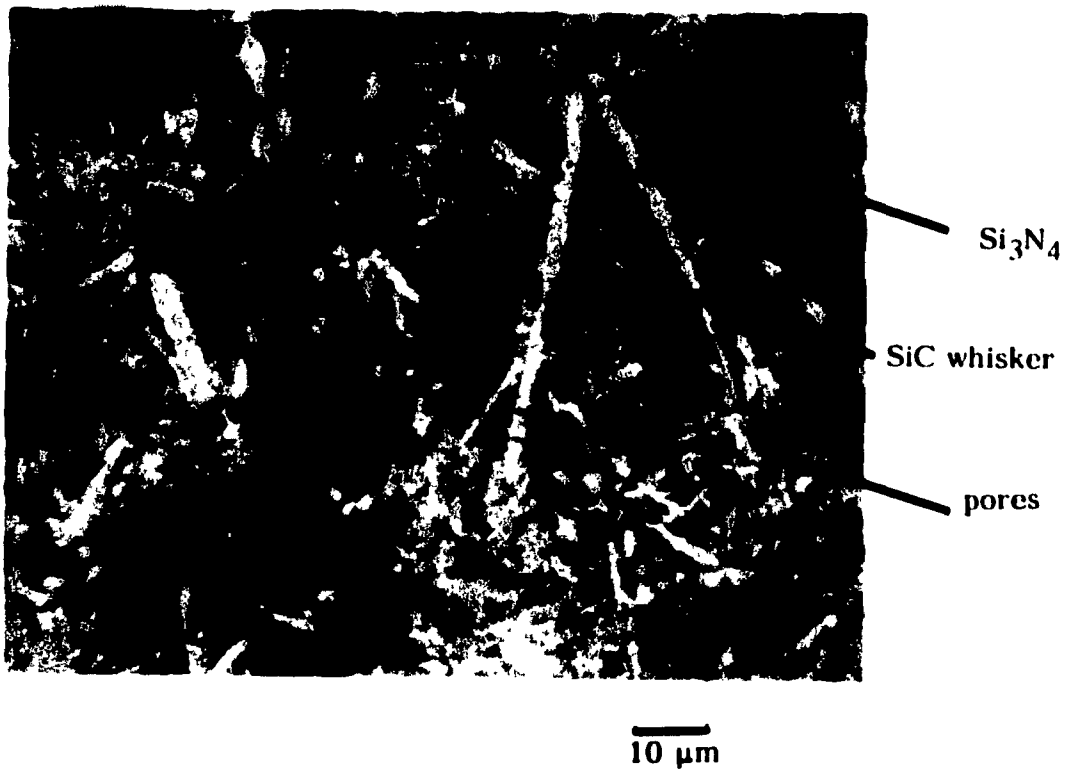

Fig 5.25: Optical micrograph of nitrided sample containing 15 wt% whiskers

This microstructural examination was presented to illustrate the formation mechanism referred to previously, but is also serves in understanding the mechanical properties obtained in bend tests and hardness measurements. The next section will summarize the mechanical characterization of nitrided samples where SiC whiskers are in the proportions of 0, 15 and 30 wt%.

5.3.4 MECHANICAL PROPERTIES

RBSN bars containing various amounts of SiC whiskers (0, 15, 30 wt%) were tested in 4-point bending. The Modulus of Rupture values are shown in Fig 5.26. These values are 120-190 MPa, similar to those given in the literature for commercial RBSN (160 MPa). The samples tested are characterized by almost the same relative density ~72% theoretical. From the results, it is clear that as the whisker content of the sample increases, the strength decreases. With high whisker content, a good dispersion of whiskers in the compact is difficult to obtain even with optimum deflocculation and thus, clumps of whiskers exist in the nitrided sample. These clumps prevent nitridation around the whiskers and therefore they are not completely integrated in the RBSN. In consequence, they act as defects and stress concentrators in the structure, explaining the decrease of MOR with increasing whisker content.

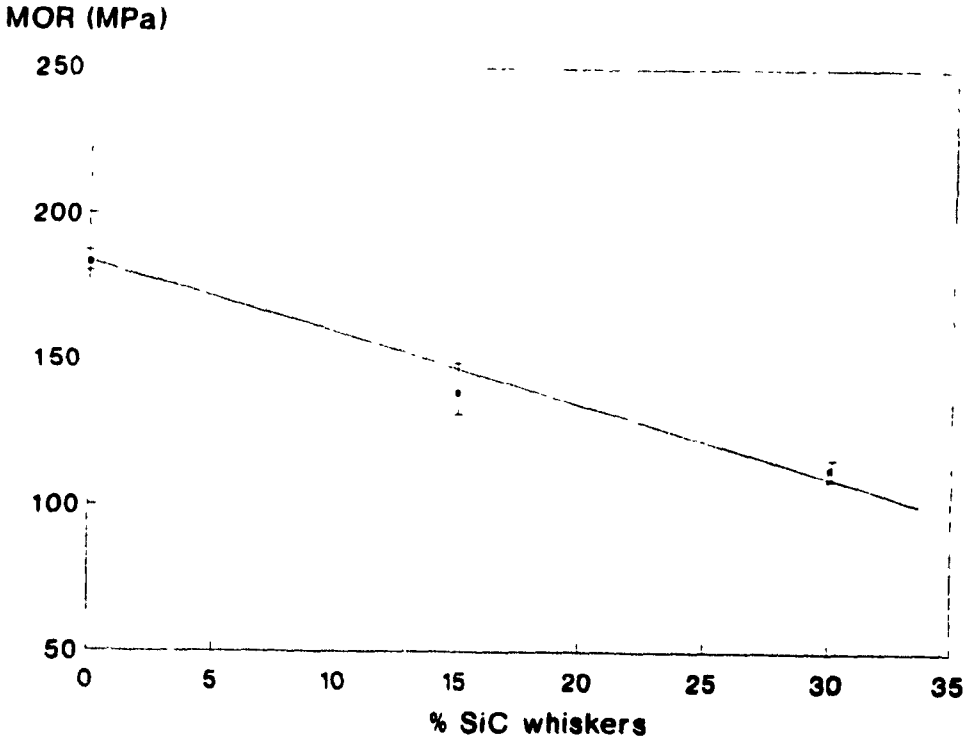

Fig 5.26: Influence of SiC whisker content on MOR

Upon analyzing the fracture surfaces, critical defects were mostly low density areas with large surface pores at the edge of the sample (Fig 5.27).

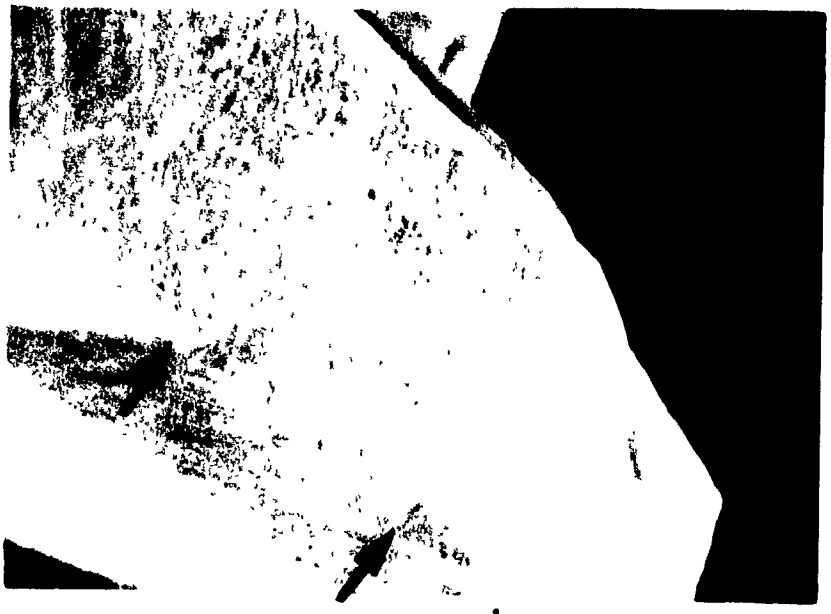

Fig 5.27: Fracture origin of MOR test sample (SEM)

This is due to the non-uniform growth of the nitride during reaction bonding. Figure 5.28 presents a higher magnification picture of the defects at the tensile edge of the bar.

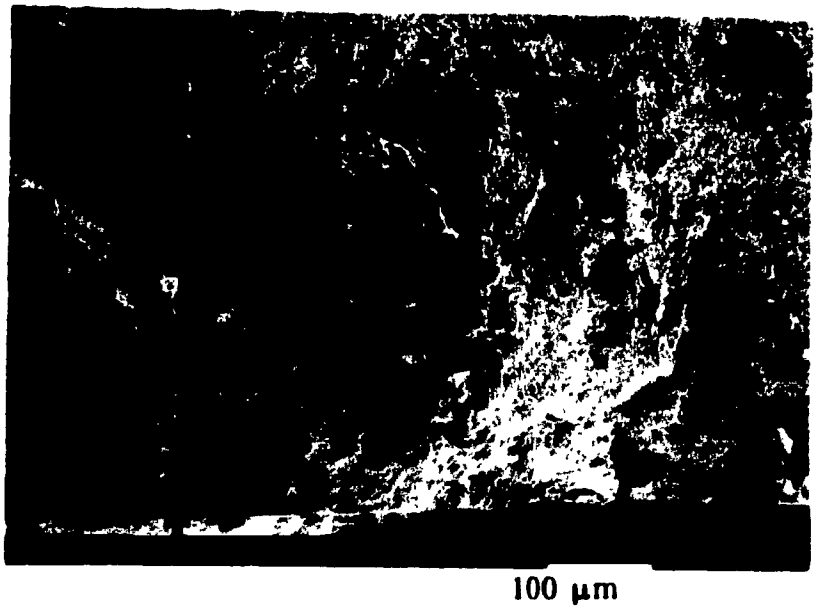

Fig 5.28: Critical defects in a MOR test sample (SEM)

Details of the microstructure show the presence of huge pores containing a large amount of Si_3N_4 needles which are other defects in the structure (Fig 5.29).

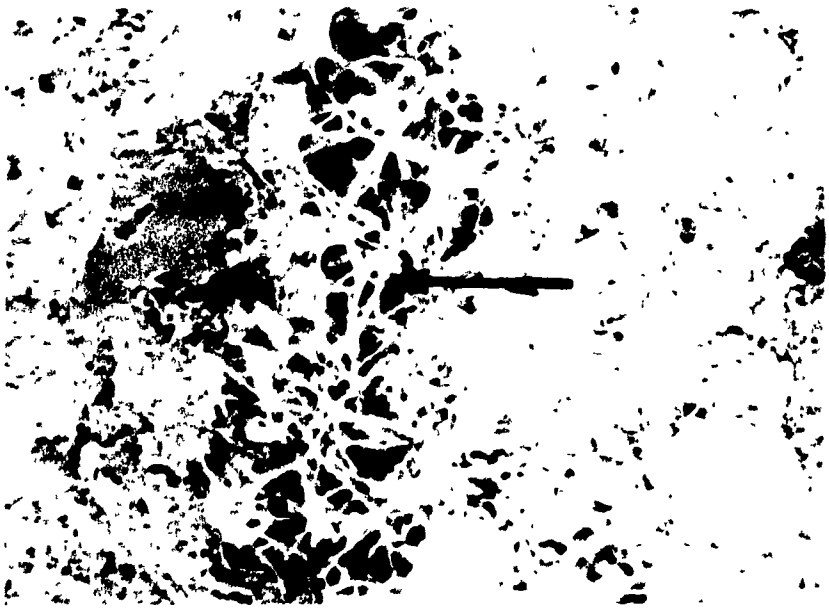

Fig 5.29: Bundle of α-Si_3N_4 needles filling a pore in a low density area (SEM)

As shown by the MOR values and the microstructure analysis, the material is weak due to the porosity through which cracks can quickly thread their way.

In terms of possible toughening by whisker reinforcement, no whisker pull-out or bridging has been observed whereas crack branching occurs as shown in Figure 5.30.

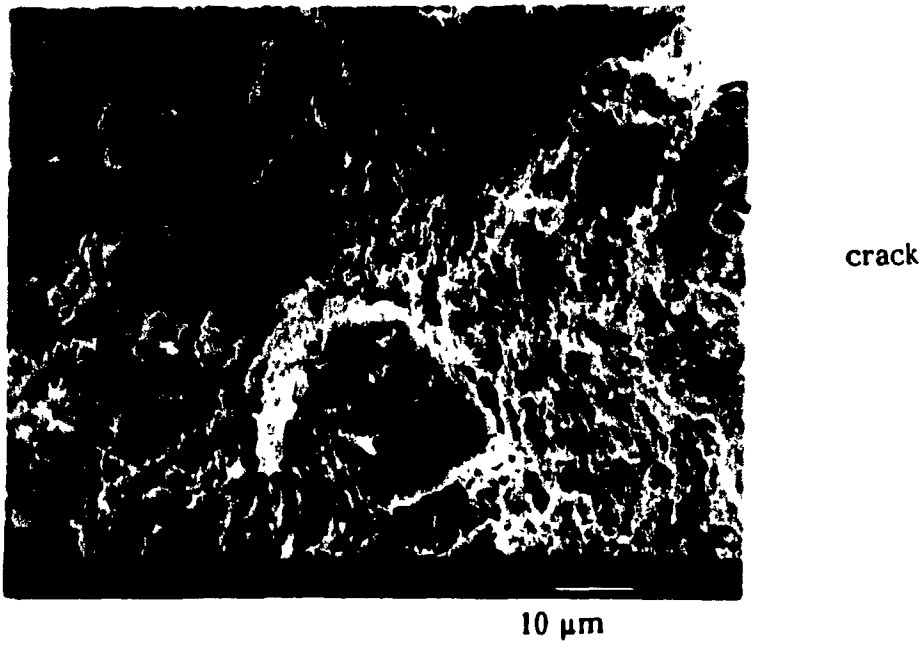

Fig 5.30: Branching of a crack (SEM)

In an attempt to measure toughness as a function of whisker content, microindentation using a Vickers diamond indenter was carried out. Fig 5.31 is a Vickers' indent on a polished surface of the material.

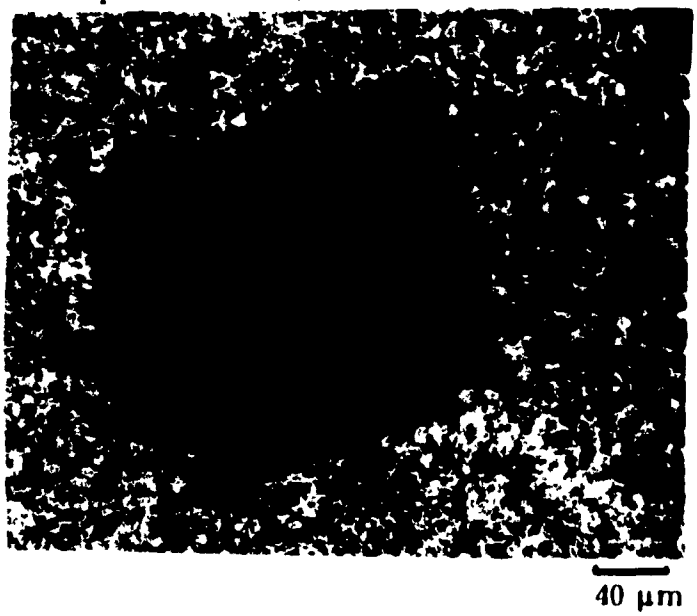

Fig 5.31: Optical micrograph of a Vickers indent

In both materials containing whiskers and those not, cracks are nearly impossible to detect, due to the porosity around the indent, causing crack-blunting. Therefore, only the average values of hardness have been calculated and are presented in Table 5.5.

Sample	Relative Nitrided Density (%)	Vickers Hardness (kg/mm^2)
0%SiCw	67	189±10
	79	426±10
15%SiCw	57	450±10
	73	529±10

Table 5.5: Hardness values for nitrided samples with 0% and 15wt% whiskers

The hardness values measured for samples with no whiskers and with 15% of SiC whiskers both depend strongly on the relative nitrided density. At constant density, samples containing whiskers have a higher hardness than the other samples with no whisker. Fig 5.32 shows a very fine crack propagating through pores and whiskers.

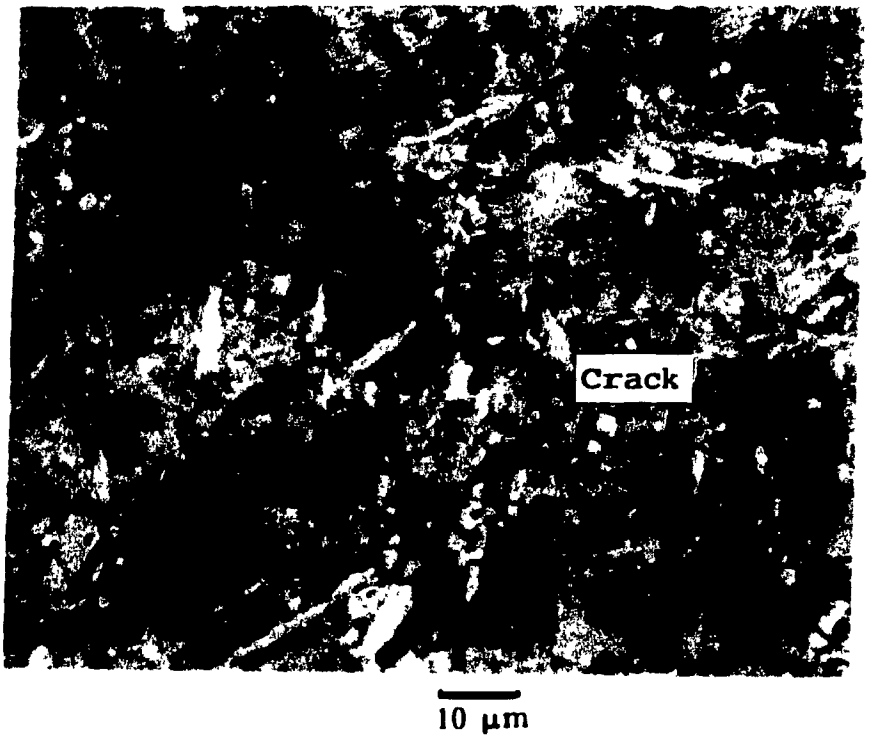

Fig 5.32: Fine crack propagating through pores and SiC whiskers from a Vickers indentation

It is observed that no crack deflection occurs and the crack passes straight through the whiskers. This is possibly due to the good bonding which exists between the deposited Si_3N_4 and the whiskers. In fact, it has been previously suggested that silicon nitride could grow onto the SiC whisker itself and become bonded with the surrounding silicon nitride matte that is forming within the composites.

6 CONCLUSIONS

- The dispersion of the SiC whiskers in the starting Si compact has been controlled by viscosity measurements and pH adjustment of the whisker/powder slip. Deflocculation occurs in the range of pH 4 to 5, corresponding to a minimum viscosity. The viscosity of slurries containing more than 15% whiskers appears to be more sensitive to a change in pH.

- The relative green density of slip cast compacts decreases by only 4% with increasing whisker content up to 20%.

Compacts with relative green densities up to 68% theoretical density have been obtained.

- A kinetic study of nitridation has been carried out using thermogravimetric curves recorded at constant temperature ranging from 1315º to 1390ºC. The effect of temperature and whisker content on the kinetics of nitridation have been studied.

It has been shown that the effect of temperature is more important than the effect of whisker content on the kinetics of nitridation. In fact, increasing the temperature up to 1365ºC leads to an acceleration of the removal of silica layer and the subsequent evaporation-condensation process. At higher temperature (1390ºC), diffusion in the liquid state occurs due to the presence of molten silicon or $FeSi_2$: diffusion is faster, leading to rapid nitridation.

- A temperature-time schedule for complete nitridation of the green compacts has been established, based on the kinetic results: the kinetic curve at a specific temperature has allowed for the determination of the time necessary for each compact to reach the final conversion plateau.

The green density has an important effect on the degree of silicon conversion. High density nitrided samples have been obtained from high green density compacts.

Whisker content does not significantly influence the nitridation.

- Microstructural examination revealed a porosity of ~25% in the nitrided material; the pore size distribution reflecting the green distribution. Six microconstituents have been observed: α-Si_3N_4 matte, α-Si_3N_4 needles and β-Si_3N_4 spikes, unconverted Silicon, porosity and SiC whiskers. The initial SiC whiskers, completely covered by Si_3N_4 particles, have been difficult to distinguish from the rest of the microconstituents.

- Modulus Of Rupture (MOR) decreases with increasing whisker content due to low density regions and the presence of whisker bundles in high whisker content samples.

The low nitrided densities (75% theor. density) can explain the low average MOR value of the pure RBSN. Upon analyzing fracture surfaces, critical defects were mostly low density areas with large surface pores, sometimes filled with α-Si_3N_4 needles, at the edge of the sample.

- No toughness measurement was possible because of the difficulty in observing and measuring the total length of cracks, due to the high porosity. However, the observation of a fine crack segment showed that no crack deflection occurs and the crack passes straight through the SiC whiskers. This is possibly due to the good bonding existing between the nitride and SiC whiskers.

Hardness values revealed a stiffer structure for the nitrided samples containing whiskers but this behavior strongly depends on the nitrided density.

7 SUGGESTED FUTURE WORK

- The particle size of the starting powder could be smaller such that a better packing is obtained. This could lead to a denser green material and hence a higher nitrided density.

- The removal of the silica layer on both Si and SiC whiskers could be carried out by: a) washing the starting powder with a solution of HF acid or

b) a hydrogen pretreatment to evaporate the SiO_2 film according to :

$$SiO_2(s) + H_2(g) \rightarrow SiO(g) + H_2O(g)$$

- Coating of the whiskers to avoid good bonding between SiC whiskers and the nitride, thus allowing crack deflection and bridging, could eventually be investigated (eg Carbon coating).

- Electron microscopy examination could be systematically used to investigate microstructural evolution during reaction bonding after each temperature step. Combined with a kinetic study, a better understanding of the nitriding mechanism could be achieved.

- A more complete study of the strength and toughness of the material and the effect of whisker content could be carried out once denser composites with a better distribution of whiskers are obtained.

REFERENCES

(1) B.H. Kear, E.R. Thomson. Science 208 847 (1980)

(2) R.F. Decker. J. Met. 33 24 (1981)

(3) G. Petzow, J. Lorentz. Umschau 11 340 (1983)

(4) J. Clark, M. Flemings. Pour la science 10 18 (1986)

(5) E.M. Lenoe, J.L.Meglen. Am. Ceram. Bull. 64 271 (1985)

(6) H.B. Probst. Am. Ceram. Bull. 59 206 (1980)

(7) A. Bennet. Mat. Sci & Tech. 2 895 (1986)

(8) D.J. Godfrey. Science of ceramics 12 27 (1986)

(9) H. Deville, F. Wuller. Lieberg's Ann. 104 256 (1857)

(10) A. Sinding-Larsen. Brit. Patent No 7307 (1909)

(11) H. Mehner. Brit. Patent No 88999 (1896)

(12) J.Y. Johnson. Brit. Patent No 15641 (1909)

(13) E.T. Turkdogan, P.M. Billis, V.A. Tippett. J. App. Chem. 8 296 (1958)

(14) D. Hardie, .H. Jack. Nature 179 332 (1957)

(15) N.L. Parr, G.F. Martin, E.R.W. May. Special ceramics p 102, ed.P. Popper, B.C.R.A. (1960)

(16) S. Wild, P. Grieveson, K.H. Jack. Special Ceramics 5 197 (1972)

(17) S. Wild, P. Grieveson, K.H. Jack. Special Ceramics 5 385 (1968)

(18) F.F. Lange. International Metals Review, 247 [1],1

(19) H.F. Priest, F.C. Burns, G.L. Priest, E.C. Skaar. J. Am. Ceram. Soc. 56 395 (1973)

(20) A.J. Edwards, D.P. Elias, M.W. Lindley, A. Atkinson, A.J. Moulson. J. Mat. Sci. 9 516 (1974)

(21) A.J. Moulson. J. Mat. Sci. 14 1017 (1979)

(22) P. Popper, S.N. Ruddlesden. Trans. Brit. Ceram. Soc. 60 603 (1961)

(23) L. Pauling, in "The Nature of the Chemical Bond", 3rd Edn. Cambridge Univ. Press, N.Y. (1960) p98

(24) J.S. Nadeau. Am. Ceram. Bull. 52 170 (1973)

(25) S. Prochazka, R.J.Charles. Am. Ceram. Bull. 52 170 (1973)

(26) S. Prochazka. General Electric Report SRD 74-040 (1973)

(27) J.S. Hirschhorn. Am. Powder Metall. Institute, N.Y. (1969)

(28) M.F. Ashby. Acta Met. 22 276 (1974)

(29) K.H. Jack. . Mat. Sci. 11 1135 (1976)

(30) B.J. Dalgleish, P.L. Pratt. Proc. Brit. Ceram. Soc. 25 295 (1975)

(31) M. Jennings. J. Mat. Sci. 18 951 (1983)

(32) P. Phelke, J.F. Elliott. Trans. Met. Soc. AIME 215 781 (1959)

(33) M. Jennings, J. Edwards, M. Richman. Inorganica Chemica Acta 20 167 (1976)

(34) W. Kaiser, C.D. Thurmond. J. Appl. Phys. 30 427 (1959)

(35) P. Longland, A.J. Moulson. J. Mater. Sci. 13 2279 (1978)

(36) C.M.B. Henderson, D. Taylor. Trans. Brit. Ceram. Soc. 74 49 (1975)

(37) H.M. Jennings, M.H. Richman. J. Mater. Sci. 11 2087 (1976)

(38) J. Mukeiji, S.K. Biswas. J. Am. Ceram. Soc. 64 519 (1982)

(39) H.M. Jennings, S.C. Danforth, M.H. Richman. J. Mater. Sci. 14 1013 (1979)

(40) S.M. Boyer, A.J. Moulson. J. Mater. Sci. 11 1288 (1976)

(41) B.F. Jones, M.W. Lindley. J. Mater. Sci. 11 1288 and 1969 (1976)

(42) M.W. Lindley, D.P. Elias, B.F. Jones, K.C. Pitman. J. Mater. Sci. 14 70 (1979)

(43) A.Atkinson, A.J. Moulson, E.W. Roberts. J. Am. Ceram. Soc. 59 285 (1976)

(44) A. Atkinson, P.J. Leatt, A.J. Moulson, E.W. Roberts. J. Mater. Sci. 9 981 (1974)

(45) B.J. Dalgleish, H,M. Jennings, P.L. Pratt. "Science of ceramics", Weiden, Dtsh Ceram. Ges., 10 369 (1980)

(46) D.R. Messier, P. Wong. J. Am. Ceram. Soc. 56 480 (1973)

(47) H.D. Batha, E.D. Whitney. J. Am. Ceram. Soc. 56 365 (1973)

(48) K. Kijima, S. Shirasaki. J. Chem. Phys. 65 2668 (1976)

(49) B.J. Masters, J.M. Fairfield. Appl. Phys. Lett. 8 280 (1966)

(50) B W. Sheldon, J.S. Haggerty. Ceram. Eng. Sci. Proc. 10 784 (1989)

(51) M. Billy, "Nitrogen ceramics" ERA No 539 CNRS (1976)

(52) W. Ku, O.J. Gregory, H.M. Jennings. J. Am. Ceram Soc. 73 286 (1990)

(53) G.S. Hugues, C. McGreavy, J.H. Merkin. J. Mater. Sci. 15 2345 (1980)

(54) U.R. Evans, "Corrosion and oxidation of metals", Edward Arnold (Publishers) Ltd., London, (1960)

(55) B.F. Jones, M.W. Lindley. Powder Met. Int. 8 32 (1976)

(56) G. Ziegler, J. Heinrich, G. Wotting. J. Mater. Sci. 22 3041 (1987)

(57) H.J. Kleebe, G. Ziegler. J. Physique, FASC.2 Colloque No1 (1986)

(58) H.R. Baumgrtner. Cer. G. T. Demo. Eng. Prog. Rev. Fairbarks and Rice. MCIC Report (1978)

(59) S.A. Siddiqi, A. Hendry. J. Mater. Sci. 20 3230 (1985)

(60) S.M. Boyer, A.J. Moulson. J. Mater. Sci. 13 1637 (1978)

(61) S.M. Boyer, D. Sang, A.J. Moulson. "Nitrogen ceramics" edited by F.L. Riley (Noordhoff, Leyden) 297 (1977)

(62) A.G. Ravesz. J. Non-Crystalline Solids 11 309 (1970)

(63) T.G. Chart. High Temp.-High-Press. 2 461 (1970)

(64) J.A. Mangels. Am. Ceram. Bull. 60 613 (1981)

(65) P.E.D. Morgan. J. mater. Sci. 15 791 (1980)

(66) D.R. Messier, P. Wong, A.E. Ingram. J. Am. Ceram. Soc. 56 171 (1973)

(67) H. Dervisbegovic, F.L. Riley. J. Mater. Sci. 16 1945 (1981)

(68) B.F. Jones, M.W. Lindley. J. Mater. Sci. 10 967 (1975)

(69) J. Heinrich, D. Munz, G. Ziegler. Powder Met. Int. 14 153 (1982)

(70) G. Grathwohl, F. Thummler. J. Mater. Sci. 13 1177 (1978)

(71) J.M. Birch, B. Wilshire. J. Mater. Sci. 13 2627 (1978)

(72) G. Grathwohl, F. Thummler. Ceramung Int. 6 43 (1980)

(73) E. Gugel, M. Kessel. "Ceramics for high performance applications II", Ed. J.J. Burke, E.M. Lenoe, R.N. Katz, Brook Hill Publ. Co. 515 (1978)

(74) J.A. Mangels. "Progress in Nitrogen ceramics", ed. F.L. Riley (Martinus Nijhoff) 231 (1983)

(75) J.M. Birch, B. Wilshire. J. Mat. Sci. 13 2627 (1978)

(76) F. Portz, G. Grathwohl, F. Thummler. Proc. Brit. Ceram. Soc. 31 157 (1981)

(77) A. Giachello, P. Popper. Ceramurgia International 5 (1979)

(78) P.F. Becher, T.N. Tiegs, J. Ogle, W.H. Warwick

(79) R.T. Bhatt. Nasa Technical-Memo. 87085 (1985)

(80) A. Linhtfoot, H.L. Ker, J.S. Haggerty. Ceram. Eng. Sci. Proc. 11 842 (1990)

(81) K.T. Faber, A.G. Evans. Acta Metall. 31 565 (1983)

(82) R.W. Rice. Ceram. Eng. Sci. Proc. 2 661 (1981)

(83) G.H. Campbell, M. Ruhle, B.J. Dalgleish, A.G. Evans. J. Am. Ceram. Soc. 73 521 (1990)

(84) F.F. Lange. Phil. Mag. 22 983 (1970)

(85) A.G. Evans. Phil. Mag. 26 1327 (1972)

(86) R.W. Rice. Ceram. Eng. Sci. Proc. 2 661 (1981)

(87) P.F. Becher, G.C. Wei. J. Am. Ceram. Soc. 67 C-267 (1984)

(88) R.G. Horm. J. Am. Ceram. Soc. 73 1117 (1990)

(89) C.S. Hirtzeland, R. Rajagopalan. Colloidal Phenomena Advanced Topic, Noyes Publ., N.Y. 15 (1985)

(90) A.P. Philipse, A. Vrij. J. Colloid. & Interface Sci. 128 121 (1989)

(91) A.P. Philipse, A. Vrij. J. Chem. Phys. 88 6459 (1988)

(92) K. Chou, L. Lee. J. Am. Ceram. Soc 72 1622 (1989)

(93) A.P. Philipse, C. Bonckamp, H.J. Veringa. J. Am. Ceram. Soc. 73 2720 (1990)

(94) A.J. Whitehead, T.F. Page. Ceram. Eng. Sci. Proc. 10 986 (1989)

(95) G. Morscher, P. Pirouz, A.H. Heuer. J. Am. Ceram. Soc. 73 713 (1990)

(96) T.L. Starr, J.N. Harris, D.L. Mohr. Ceram. Eng. Sci. Proc. 8 985 (1987)

(97) N.D. Corbin, G.A. Rossetti, J. and S.D. Hartein. Ceram. Eng. Sci. Proc. 7 958 (1986)

(98) R. Warren, R. Lundberg, L. Kahlman, R. Pompe, R. Carlsson. Ceram. Bull. 6 330 (1987)

(99) S.T. Buljan, J.. Baldeni, M.L. Hickabee. Am. Ceram. Soc. Bull. 66 347 (1987)

(100) K.G. Nickel, M.J. Hoffmann, P. Greil, G. Petzow. Advanced Ceramic Material 3 557 (1988)

(101) A. Lightfoot, L. Ewart, J. Haggerty, Z. Cai, J. Ritter, S. Nair. Ceram. Eng. Sci. Proc. 12 1265 (1991)

(102) A. Lightfoot, B.W. Sheldon, J.H. Flint, J.S. Haggerty. Ceram. Eng. Sci. Proc. 10 1035 (1989)

(103) "Flexural strength of High Performance Ceramics at ambient temperature". MIL-STD-1942 (MR) 8 (1983)

APPENDIX 4.1

Determination of the thickness of the silica layer around commercial silicon particles.

By oxygen analysis, a total weight percent of 0.5% of oxygen was found.

Since, the molar weights of O and SiO_2 are respectively 16 and 50g, 0.5 wt% of O corresponds to an amount of 0.4 wt% of SiO_2, covering the silicon particles.

Assuming spherical silicon particles, the volume of silicon and silica in a 7μm-diameter commercial Si particle can be calculated as follows:

$V_{Si} = 4/3\ \pi\ r^3$, $V_{SiO2} = 4/3\ \pi\ (R^3-r^3)$

r: radius of Si particle

R: radius of Si particle covered with silica ($R=\phi/2=3.5\mu m$)

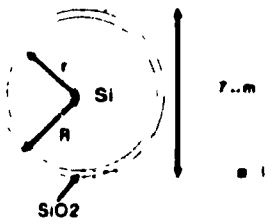

As seen above, $M_{SiO2} = 0.4wt\%\ M_{Si}$ [1]. Therefore, $\rho_{SiO2}\ V_{SiO2} = 4x10^{-3}\ \rho_{Si}\ V_{Si}$. Since $\rho_{SiO2}=2.8g/cm^3$ and $\rho_{Si}=2.32g/cm^3$, equation [1] can be expressed as following:

$$2.8x4/3\pi(R^3-r^3)=4x10^{-3}x2.32x4/3\pi(r^3).$$

Solving this equation gives r = 0.9989 R with R=3.5 μm. The thickness, ℓ, of the silica layer can be calculated as following: $\ell=R-r=0.004\mu m=4nm$.

Therefore, a thickness of ~4nm of silica is covering the commercial Silicon particles used in this research.

APPENDIX 4.2

Plaster mold preparation for slip-casting

To ensure a constant casting rate, the molds were all made using the following standardised procedure.

Plaster of Paris was used in the fabrication of slip casting molds. 100g of plaster was sieved and then added to 70ml of distilled water. After mixing for 3.5 minutes with an impellor, the plaster was cast in different forms, depending on the required shape of the cast samples. Figure 1 presents a plaster mold for test bar samples: the bed of plaster was more than 10 times deeper than the mold depth (see Fig).

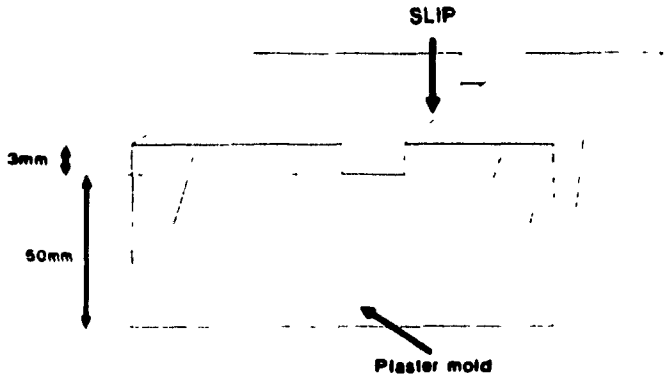

Fig 1: Plaster mold for test bar sample

Thus, with a mold density of $1g/cm^3$, the suction pressure was sufficient to create a pressure gradient, causing the slip casting of the Si/SiC whiskers slurries.